

35e jaargang 2013 nummer 4 issn 1381 - 4842

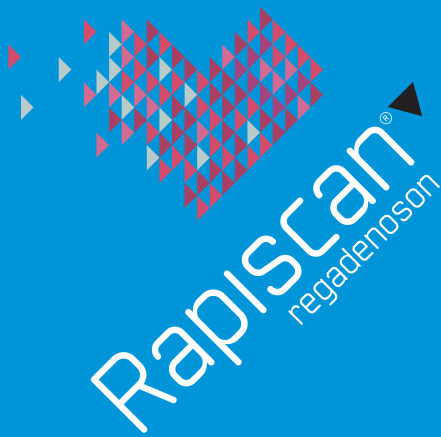
T I J D S C H R I F T

V O O R

N U  L E A I R E

G E N E E S K U N D E

Special issue on multimodality imaging



Rapiscan[®]
regadenoson



IDB Holland by
From Atom to Image

Now this won't take a minute...



Rapiscan is the only standard dose, infusion pump-free, selective coronary vasodilator for use as a pharmacological stress agent for radionuclide myocardial perfusion imaging.

- ▶ Administer Rapiscan as a full 10 sec IV injection
- ▶ Flush immediately with 5 ml saline
- ▶ Deliver radiotracer 10-20 seconds after saline flush

Stress simplified by design

RAPISCAN[®] ▼ (regadenoson)
ABBREVIATED PRESCRIBING INFORMATION

PRESCRIBERS SHOULD READ THE SUMMARY OF PRODUCT CHARACTERISTICS (SPC) Rapiscan vials contain regadenoson (400 microgram solution for injection). Indication: Pharmacological stress agent for radionuclide myocardial perfusion imaging in adult patients which are unable to undergo adequate exercise stress. Dosage and Administration: Each 5 mL vial contains 400 micrograms regadenoson, which is injected over 10 seconds into a peripheral vein followed by 5 mL saline (0.9% sodium chloride) solution flush. The radiopharmaceutical should be administered 10-20 seconds after saline injection. The same catheter may be used for Rapiscan and the radiopharmaceutical. Patients should avoid consumption of any products containing methylxanthines (e.g. caffeine) as well as any medicinal products containing theophylline for at least 12 hours before Rapiscan administration. When possible, dipyrindamole should be withheld for at least two days prior to Rapiscan administration. Contra-indications: Hypersensitivity to active substance or excipients; patients with second or third degree AV block or sinus node dysfunction who do not have a functioning artificial pacemaker; unstable angina that has not been stabilised with medical therapy; severe hypotension; decompensated heart failure. Precautions: Rapiscan has the potential to cause serious and life-threatening reactions. Continuous ECG monitoring should be performed and vital signs monitored at frequent intervals until ECG parameters, heart rate and blood pressure have returned to pre-dose levels. Aminophyl-

line may be administered by slow intravenous injection to attenuate severe and/or persistent adverse reactions to Rapiscan. Fatal cardiac arrest, life-threatening ventricular arrhythmias, and myocardial infarction may result from the ischaemia induced by pharmacologic stress agents like regadenoson. Adenosine receptor agonists including regadenoson can depress the sinoatrial (SA) and AV nodes and may cause first, second or third degree AV block, or sinus bradycardia. Adenosine receptor agonists including regadenoson induce arterial vasodilation and hypotension. The risk of serious hypotension may be higher in patients with autonomic dysfunction, hypovolemia, left main coronary artery stenosis, stenotic valvular heart disease, pericarditis or pericardial effusions, or stenotic carotid artery disease with cerebrovascular insufficiency. Adenosine receptor agonists may cause bronchoconstriction and respiratory compromise. For patients with known or suspected bronchoconstrictive disease, chronic obstructive pulmonary disease (COPD) or asthma, appropriate bronchodilator therapy and resuscitative measures should be available prior to Rapiscan administration. Regadenoson stimulates sympathetic output and may increase the risk of ventricular tachyarrhythmias in patients with a long QT syndrome. This medicinal product contains less than 1 mmol sodium (23 mg) per dose. However, the injection of sodium chloride 9 mg/ml (0.9%) solution given after Rapiscan contains 45 mg of sodium. To be taken into consideration by patients on a controlled sodium diet. Undesirable effects: Adverse reactions in most patients were mild, transient (usually resolving within 30 minutes) and required no medical intervention. Rapiscan may cause myocardial ischaemia, hypotension leading to syncope and transient ischaemic attacks, and SA/AV node block requiring intervention. Aminophylline may be used to attenuate severe or

persistent adverse reactions. Very common adverse events reported were dyspnoea, headache, flushing, chest pain, electrocardiogram ST changes, gastrointestinal discomfort, and dizziness. Common adverse events reported were paraesthesia, hypoesthesia, dysgeusia, angina pectoris, atrioventricular block, tachycardia, palpitations, other ECG abnormalities including electrocardiogram QT corrected interval prolonged, hypotension, throat tightness, throat irritation, cough, vomiting, nausea, oral discomfort, back, neck or jaw pain, pain in extremity, musculoskeletal discomfort, hyperhidrosis, malaise, and asthenia. See SPC for details of other undesirable effects. Presentation: One carton contains a single vial of Rapiscan (400 micrograms regadenoson in 5mL solution for injection). Price: Please see your local distributor. ATC code: C01EB21. Legal Classification: UR. Marketing authorization holder: Rapiscan Pharma Solutions EU Ltd, Regent's Place, 338 Euston Road, London, NW1 3BT, United Kingdom. Marketing authorization number: EU/1/10/643/001 Date of preparation: April 2012.

IDB Holland is the exclusive distributor in The Netherlands

IDB Holland bv	Phone: +31 (0)13 507 9558
Weverstraat 17	Fax: +31 (0)13 507 9912
5111 PV Baarle-Nassau	E-mail: sales@idb-holland.com
The Netherlands	Internet: www.idb-holland.com

Date of preparation: April 2012 RPS EU 12-009

For more information please visit www.rapiscan-mpi.com

Rapiscan is a registered trademark of Rapiscan Pharma Solutions EU Ltd ©2012 Rapiscan Pharma Solutions EU Ltd. All rights reserved RPS EU 12-010

Integration of small animal SPECT and PET with other imaging modalities <i>P.E.B. Vaissier, Msc</i>	1136
Integrated PET/MRI in preclinical studies State of the art <i>F. Brunotte, MD</i>	1144
Methodological aspects of PET/MR imaging <i>M. Yaqub, PhD</i>	1153
Towards multiparametric medical imaging with PET/MRI: current clinical status <i>D.E. Oprea-Lager, MD</i>	1160
Combining radioactivity with fluorescence: the first clinical experiences using hybrid tracers <i>B.M.F. Winkel, BSc</i>	1173
The use of SPECT/CT in daily practice <i>B.L.F. van Eck-Smit, MD PhD</i>	1184
COURSES & CONFERENCES	1194

Multimodality imaging

More than ten years ago, we both were trainees in Nuclear Medicine. During that period, we only spent three months at the department of Radiology in the Academic Medical Center. We learned some things about conventional radiology, about MR techniques, and we were also scheduled to report on whole-body CT scans for a few weeks while being supervised by a radiologist. At that time, we couldn't predict multimodality imaging would develop so fastly into clinical practice. However, a lot has changed in the last decade. Nowadays, in many hospitals PET/CT and SPECT/CT systems are available for routine clinical studies. This is the case not only for The Netherlands but also for Europe, USA and most developed countries. Also, recently PET/MRI systems as well hybrid tracers became available for clinical studies. In addition, in the field of preclinical imaging, multimodality imaging is now the state-of-the-art. The aim of this special issue is to learn our readers more about multimodality imaging and hybrid tracers. Vaissier and colleagues as well as Brunotte and co-workers will provide an update on the challenges and breakthroughs on the integration of small animal SPECT and PET with other imaging modalities including PET/MRI. Then Yaqub and colleagues will discuss the methodological aspects of combined PET/MRI, concentrating on the performance of this system for clinical studies. The current clinical status of PET/MRI has been reviewed by Oprea and co-workers. Winkel and colleagues present a fascinating historical overview of radio- and fluorescence-guidance techniques and the evolution of these technologies into an integrated hybrid approach. Moreover, the current clinical applications of hybrid imaging techniques are outlined, focusing on the first clinical studies in patients undergoing a sentinel lymph node procedure. Finally, van Eck describes some typical examples of the additional clinical value of integrated SPECT/CT versus SPECT alone. In light of the developments of the last decade it is likely that if we, in ten years from now, will look back and reflect on the current time, we will probably be amazed by the speed of clinical implementation of the, now sometimes seemingly futuristic, issues described in this special issue of our Journal. Therefore, to have our readers be a little better prepared for the future than the editors of this special issue were ten years ago, we hope that this edition of our Journal gives a glance at the (near) future.

Jan Booij and Hein Verberne

Editors-in-chief of this special issue



Cover: Integrated ¹⁸F-FDG PET/CT in a patient with liver metastases from colon cancer.

Integration of small animal SPECT and PET with other imaging modalities

P.E.B. Vaissier, Msc¹, C.Wu, PhD^{1,2} F.J. Beekman, PhD^{1,2}

¹Section Radiation, Detection & Medical Imaging, Delft University of Technology, Delft, the Netherlands

²MILabs B.V., Utrecht, the Netherlands

Abstract

Vaissier PEB, Wu C, Beekman FJ. Integration of small animal SPECT and PET with other imaging modalities.

Single Photon Emission Computed Tomography (SPECT) and Positron Emission Tomography (PET) imaging of small experimental animals is used to quantitatively and visually assess the distribution of radioactive biological markers (tracers) *in vivo* in order to e.g. study animal models of disease and test new pharmaceuticals. While SPECT and PET provide information about molecular mechanisms through detection of gamma-rays that are emitted when the tracer decays, other imaging modalities use radio-waves (Magnetic Resonance Imaging; MRI), near-infrared/visible light (Optical Imaging; OI) or X-rays (X-ray Computed Tomography; CT) to obtain anatomical and/or functional information of living subjects. Since each modality has unique qualities, e.g. in terms of spatial- and temporal resolutions and abilities to measure structure and function, they are often combined: e.g. CT or MRI images can be used as an anatomical reference for locating tracer uptake, or can be used for attenuation correction of emission tomography images. An increasing effort is being spent on hardware integration of different imaging modalities. In this work we discuss the methods, limitations and challenges of multimodality integration in the development of preclinical dual- triple- and quadruple modality systems that include SPECT and/or PET.

Tijdschr Nucl Geneesk 2013; 35(4):1136-1142

Introduction

In preclinical research, *in vivo* imaging techniques are used for non-invasive assessment of structure and function in small animals in e.g. studies of disease and to test new pharmaceuticals. Each imaging modality that is currently available has its strengths and weaknesses in terms of e.g. spatial- and temporal resolutions, sensitivity, abilities to measure structure and function and the availability of suitable contrast agents or tracers for the task at hand (1). Combining images from different imaging modalities can be very useful, as different modalities often provide highly complementary information. For instance, spatially registered SPECT and CT or PET and CT images enable anatomical

localization and accurate quantification of uptake of radioactive tracer molecules, particles or cells. To achieve good spatial registration, much effort is being spent on integrating different modalities. Nice review papers about multimodality imaging include the ones from Cherry, Townsend and Beyer (2-6). These papers mostly focus on clinical dual-modality imaging, however in this work we only focus on preclinical multimodality imaging, including systems that integrate more than two modalities. The integration of preclinical imaging modalities can be as simple as a click-over bed that can be taken from one scanner to the other. This *side-by-side* integration of imaging modalities requires suitable mechanical interfaces to smoothly disconnect the bed from one scanner and (preferably) reproducibly mount the bed to another scanner. Multimodal fiducial markers attached to the bed or a pre-measured transformation matrix can then be used to automatically fuse the images (7-9). This approach allows for different systems to be used at the same time and allows for replacement or addition of individual modalities. A drawback that comes with *side-by-side* integration is that an animal may shift on the bed during (manual) transportation between scanners if the animal is not properly fixed to the bed, which may introduce image registration errors. Moreover, the animal must be kept under controlled anaesthesia in between scans, which might become problematic if the animal bed is disconnected to be moved between scanners. To overcome these issues, systems have been developed that integrate multiple modalities on a single platform (figure 1a).

Most of these systems achieve integration by placing the modalities in a *back-to-back (in line)* configuration, which is also commonly applied in clinical hybrid imaging instruments. In this configuration, modalities are placed in close proximity of each other and the animal is automatically transferred on a bed from one subsystem to the other along the common axis of the subsystems. The main advantage of *in line* integration is that the animal can be scanned without having to be manually transferred from one system to the other, thereby reducing the chance of animal movement and making it easier to keep the animal under controlled anaesthesia. Moreover, these solutions mostly offer a single control interface, which makes operating the scanners easier, rather than having to learn how to operate several separate scanners.

A clear disadvantage can be that the throughput on individual scanners is suboptimal since only one modality can be used at each given point in time. In addition, SPECT and PET systems

usually have detectors with photomultiplier tubes (PMTs) that are highly sensitive to magnetic fields. These systems can therefore only be safely combined *in line* with lower-field MRI systems which may result in long MRI acquisition times. MR-compatible SPECT hardware will likely overcome these issues in the future.

Instead of *in line* integration, imaging systems can also be integrated on a single gantry. An example of a preclinical system where both SPECT and CT are integrated on the same gantry is the Siemens Inveon SPECT/CT scanner (figure 1b). Drawback of such a system is that the number of (SPECT) detectors that can be integrated is limited by the space required for the CT's X-ray source and detector. In attempts to perform simultaneous SPECT-MRI and PET-MRI, SPECT and PET inserts for MRI scanners have been developed (10-14).

Full integration of modalities is achieved when the detectors of a system are optimized such that they can detect radiation signals from different modalities. The images that are obtained with such systems are inherently aligned in space and time. An example of such integration is the VECTor⁺ system which can perform simultaneous SPECT and PET imaging (see the next section on the integration of SPECT with PET). Table 1 gives an overview of some commercially available preclinical multimodality imaging systems.

Integrating SPECT with PET

Preclinical SPECT systems are most times based on the use of pinholes that magnify projections of the radionuclide distribution on detectors that would otherwise not have been able to resolve the small details within such animals: reconstructed spatial resolutions of these systems can reach

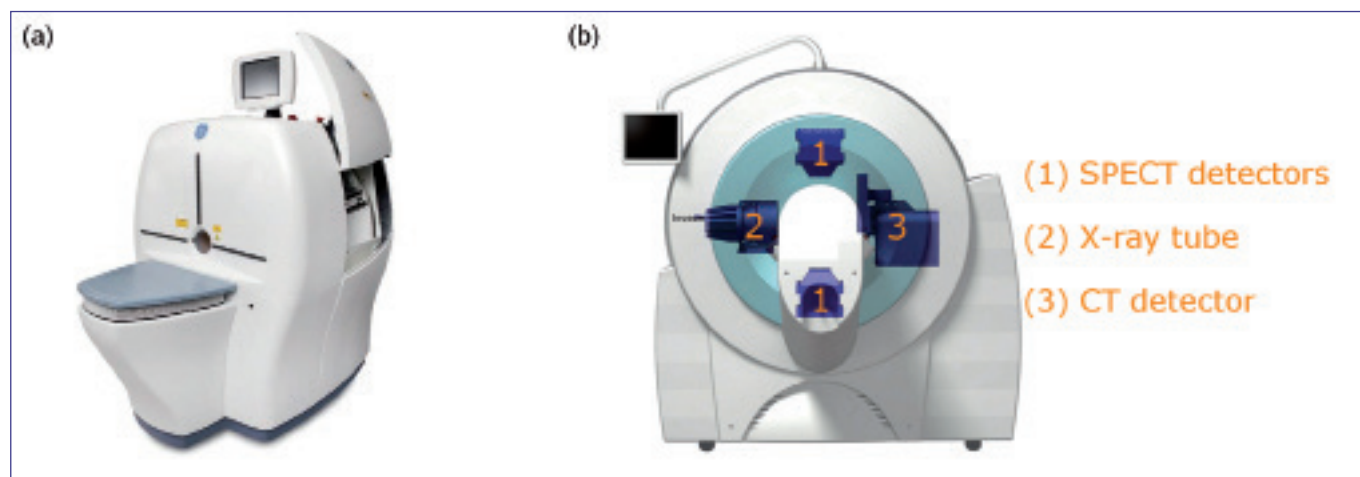


Figure 1. (a) The Triumph system is the world's first preclinical tri-modality imaging system as it combines SPECT, PET and CT on a single platform. Image courtesy of TriFoil Imaging. (b) Integrated SPECT/CT system with SPECT and CT subsystems attached to same gantry. Image courtesy of Siemens Healthcare.

Table 1. Overview of some commercially available multimodality systems

	MRI	OI	CT	SPECT	PET
Bruker Albira	no	no	yes	yes	yes
Mediso nanoSPECT/CT	no	no	yes	yes	no
Mediso nanoPET/CT	no	no	yes	no	yes
Mediso nanoSPECT/MRI	yes	no	no	yes	no
Mediso nanoPET/MRI	yes	no	no	no	yes
MILabs USPECT+/CT/MRI/OI	yes	yes	yes	yes	no
MILabs VECTor+/CT/MRI/OI	yes	yes	yes	yes*	yes*
Siemens Inveon	no	no	yes	yes	yes
TriFoil Triumph II	no	no	yes	yes	yes

*simultaneous SPECT/PET imaging possible

well below half a millimetre (15, 16). Some commercial multimodality systems that can perform SPECT use a number of rotating gamma detectors and collimators to acquire complete sampling of the subject, which is required for image reconstruction, while other systems use a stationary setup and a focussing multi-pinhole geometry to readily obtain a high sensitivity and complete data within the focal region that is seen by all pinholes. For this reason, stationary SPECT allows for fast dynamic imaging (17).

Coincidence PET systems apply electronic collimation to reconstruct a line-of-response from each detected pair of anti-parallel 511 keV photons that are formed when a positron (emitted by the radioactive tracer) annihilates with an electron in the tissue. From these lines-of-response images of the tracer distribution can be reconstructed. The absence of physical collimators is a major reason why coincidence PET has a higher sensitivity than SPECT. State-of-the-art preclinical coincidence PET can achieve spatial resolutions of about 1 mm.

Imaging platforms that can perform both SPECT and PET can take advantage of the entire complement of available SPECT and PET tracers. Most commercial systems that are capable

of SPECT-PET imaging have an *in line* configuration of a pinhole SPECT subsystem with a coincidence PET subsystem and can therefore only perform sequential SPECT-PET imaging. Another recent approach to combined SPECT-PET is to physically collimate the 511 keV annihilation (PET) photons by clusters of focussed pinholes on a SPECT platform (pinhole PET (18, 19)). This form of collimation can offer sub-mm spatial resolution (figure 2a) but relatively low sensitivity compared to coincidence PET. However, resolution and image quality in coincidence PET are limited by a number of physical factors (table 2) that are not prominent in pinhole PET and in a number of imaging situations pinhole PET imaging results in better resolution than coincidence PET.

A major difference between a pinhole SPECT/PET system over an *in line* combination of a (pinhole) SPECT subsystem with a coincidence PET subsystem is that a pinhole SPECT/PET system allows for simultaneous SPECT-PET imaging which may open up new possibilities for multiple functional studies (figure 2b).

Integrating SPECT and PET with CT

Combining SPECT and PET with CT can provide an anatomical context of biological processes (e.g. figure 3 (20)) and can

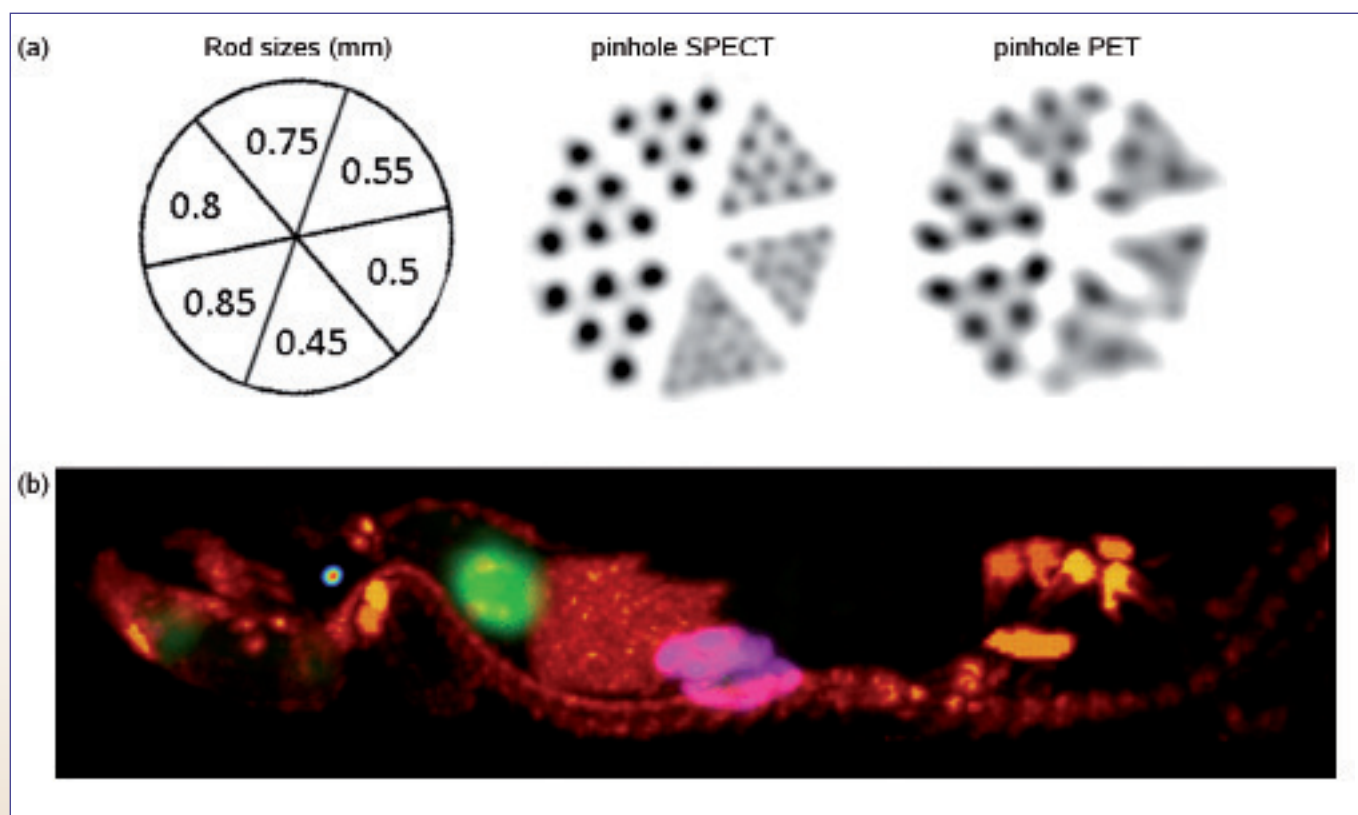


Figure 2. Simultaneous PET and SPECT isotope imaging with VECTOR: (a) SPECT and PET reconstructions of a Jaszczak phantom containing 16 MBq ^{99m}Tc and 24 MBq ^{18}F at the start of the scan (scan time was 60 min). For SPECT the 0.5 mm rods can still be distinguished, for PET the 0.75 mm rods. (b) Quadruple SPECT and PET isotope imaging showing a maximum-intensity-projection of a 60 minute total body mouse scan with 100 MBq ^{99m}Tc -HDP (red), 35 MBq ^{18}F -FDG (green), 19 MBq ^{111}In -pentetreotide (magenta) and 5 MBq ^{123}I -Nal (rainbow). Images courtesy of MILabs B.V.

Table 2. Differences in imaging physics between coincidence PET and pinhole PET.

	coincidence PET	pinhole PET
detector resolution and DOI	issue	small issue
non-collinearity	issue	no issue
random coincidences	issue	no issue
coincidence losses	issue	no issue
positron range	issue	issue

also improve the quantitative accuracy of SPECT and PET data through improved attenuation correction that is enabled by CT. CT systems used in small-animal imaging usually consist of a microfocus X-ray tube. The typical focal-spot size is less than 50 μm and reaches down to only a few μm in some systems. Reconstruction resolutions of well below 100 μm are achievable with such X-ray tubes in combination with accurate design of mechanics. The maximum voltage of the X-ray tubes in preclinical CT systems varies among vendors, but usually the actual working voltage for imaging small animals is less than 80 kVp (i.e. 80 keV maximum X-ray energy). In contrast, the energy of photons used in PET is much higher (511 keV). This has enabled the design of PET/CT systems that can perform simultaneous PET and CT scanning in order to prevent image registration errors due to changes in the position of the animal which may occur in the case of sequential scanning: e.g. a system that consists of a single-gantry with separate PET and CT detectors (21) or even with the same detectors (22). In some commercial preclinical multimodality systems that incorporate CT, the CT subsystem is integrated *in line* with the other modalities, while in other systems the SPECT and CT subsystems are mounted on the same rotating gantry (e.g. figure 1b).

Since CT measures radiodensity of the scanned object, CT data can be converted into attenuation maps which can be used for attenuation correction of SPECT or PET images (23-26). This undoubtedly strengthens the power of emission tomography since applications such as pharmacokinetic investigations can benefit from the accurate quantification of tracer distributions.

Integrating SPECT and PET with MRI

Since CT imaging uses ionizing radiation which may influence animal welfare and study outcome (27,28), a development towards integrating SPECT and PET with MRI, which offers a high-resolution, non-ionizing method for anatomical imaging of small animals with excellent soft tissue contrast, has commenced. To illustrate the use of CT and MRI images as an anatomical reference for locating tracer uptake in emission tomography images, figure 4a shows fused SPECT, CT and MRI images.

Initial MRI-compatible PET inserts were developed in the mid-1990s (10, 14). These systems used long optical fibre

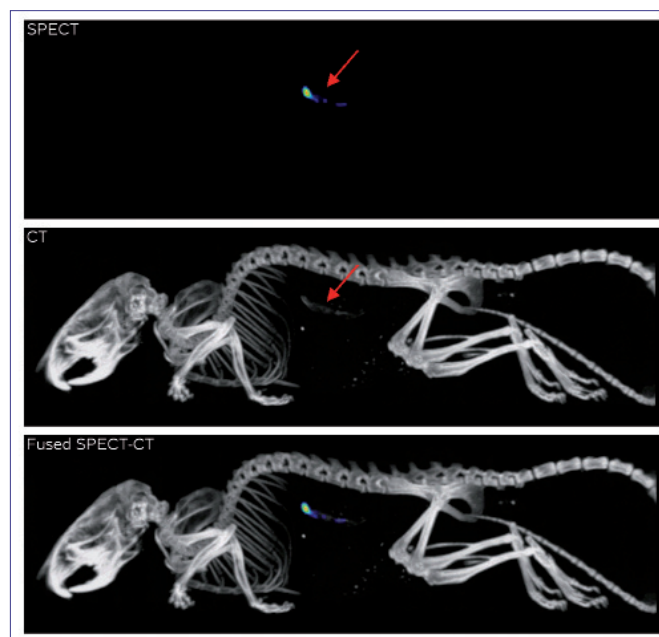


Figure 3. Example of SPECT/CT imaging: holmium-166 acetylacetonate microspheres ($^{166}\text{HoAcAcMS}$) are used for treatment of kidney tumours (for details see reference 20). ^{166}Ho emits high-energy beta particles suitable for anticancer therapy and the simultaneously emitted gamma rays (81 keV) allow for SPECT imaging. Moreover, nonradioactive holmium-165 can be visualised by CT. Arrows indicate the presence of the microspheres in the kidney area in the SPECT and CT images. The fused SPECT/CT image clearly shows agreement between the SPECT and CT signals. Images courtesy of W. Bult, University Medical Centre Utrecht, the Netherlands.

connections between the scintillator elements inside the MRI and the PMTs that were placed outside the MRI to effectively eliminate the interference of the magnetic field with the PMTs. More recently, MR-compatible PET inserts that are based on solid-state detectors have been developed and applied for *in vivo* studies (29, 30).

The development of SPECT/MRI systems started much later: the first combined SPECT/MRI platform was proposed in 2007. In this set-up a single pinhole SPECT system was used next to a 0.1T magnet (31). Similar *in line* set-ups are proposed by Mediso in which the SPECT or PET subsystem is combined with a 1T MRI subsystem. Other *side-by-side* solutions are provided by MILabs (figure 4b,c). Figure 4c shows a solution with a robotic rotation/translation stage that automatically transfers the animal between the MRI (available with field strengths of 1.5T or 3T) and up to three other modalities (SPECT/PET/CT). This set-up functions as if the MRI system is integrated *in line* with the other modalities, while preventing interference between the MRI and the other modalities. In attempts to perform simultaneous SPECT/MRI, SPECT inserts for MRI systems have been developed by using a stationary detector configuration and MRI-compatible

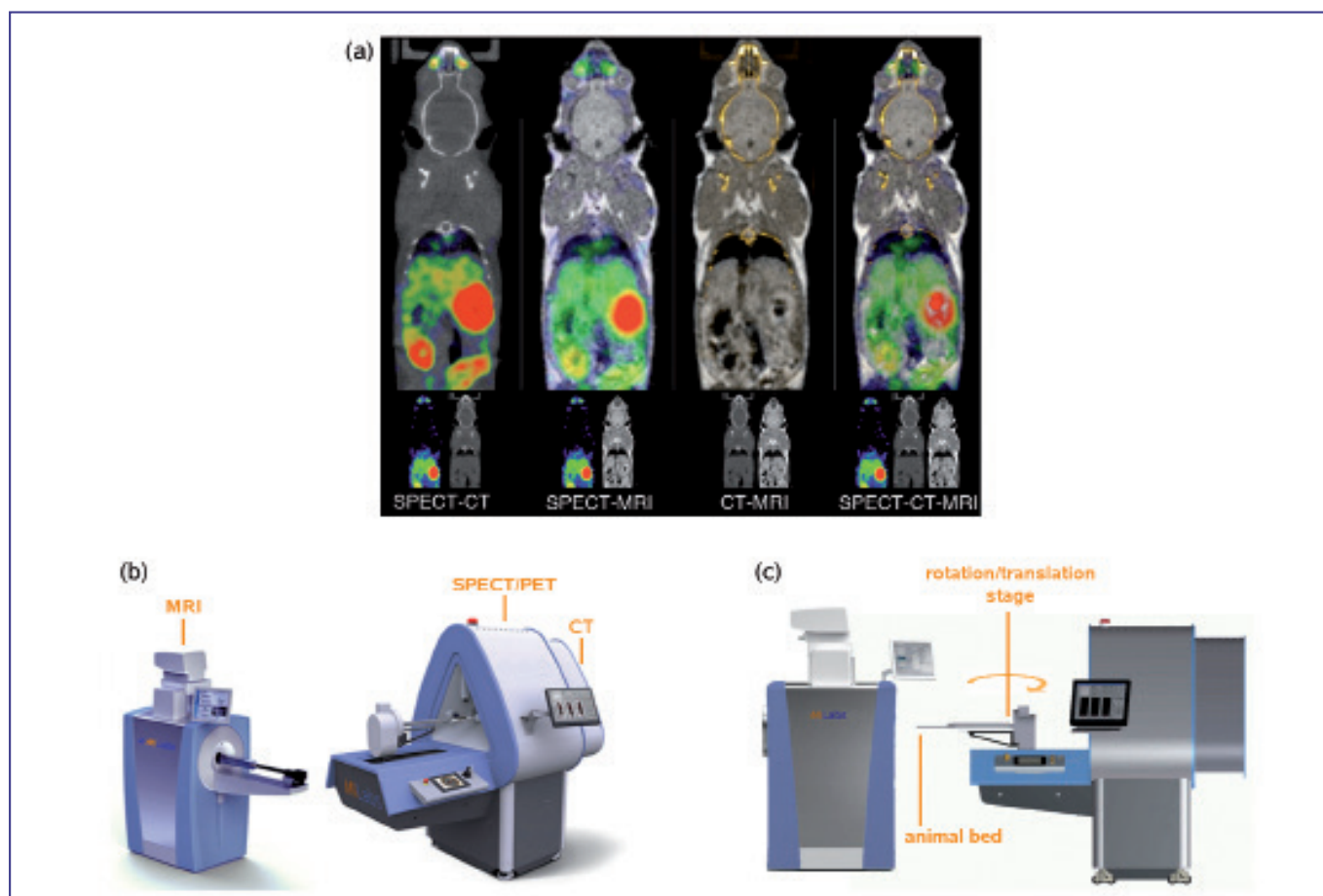


Figure 4. (a) Fusion display of an in vivo mouse multimodality study, combining SPECT, CT and MRI. Image (a) reprinted from (4), Copyright (2013), with permission from Elsevier. (b) Side-by-side solution to imaging with MRI and other modalities. (c) Another solution uses a stage that automatically transfers the animal between the MRI and other modalities thereby preventing interference between the MRI and the other modalities. Images (b,c) courtesy of MILabs B.V.

collimators and detectors (11, 13). The number of pinholes that can be integrated is relatively low compared to modern stand-alone multi-pinhole SPECT systems, which results in relatively low sensitivity. Due to the limited bore-size of MRI systems, pinhole magnification is also relatively low, which results in compromised image resolution. Very high-resolution MR-compatible detectors are required to enable performance comparable to that of modern stand-alone SPECT with traditional detectors and high pinhole magnification factors (32). However, today these detectors are costly and hard to acquire at an industrial-quality-level.

In contrast to CT, a potential limitation of MRI is that it does not readily provide adequate information for attenuation correction of SPECT and PET images, since it is a challenge to e.g. distinguish between bone and air. However, since the non-uniformity of attenuation or the high accuracy of attenuation maps do not play a critical role in small-animal emission tomography (33), MRI-derived attenuation maps may be sufficient for some studies.

Integrating SPECT and PET with OI

Optical techniques allow for in vivo imaging of cellular and molecular processes. OI systems generally consist of a black box in which a bioluminescent or fluorescent small animal is placed and images of the optical signal are acquired by a (CCD) camera. A number of prototype instruments for small animal PET/OI have been developed (34, 35). Furthermore, an OI system that can be docked in line to a SPECT/PET/CT platform is currently being developed (figure 5). This set-up allows for all combinations of SPECT/PET/CT/OI on a single platform.

Conclusions and perspectives

Preclinical multimodality imaging can be very useful, as different modalities can provide highly complementary or enhanced information for scientific researchers. Today, most commercial systems that can perform SPECT/PET imaging can only acquire the SPECT and PET data sequentially. However, a recently developed high-energy pinhole collimation technique enables simultaneous SPECT/PET

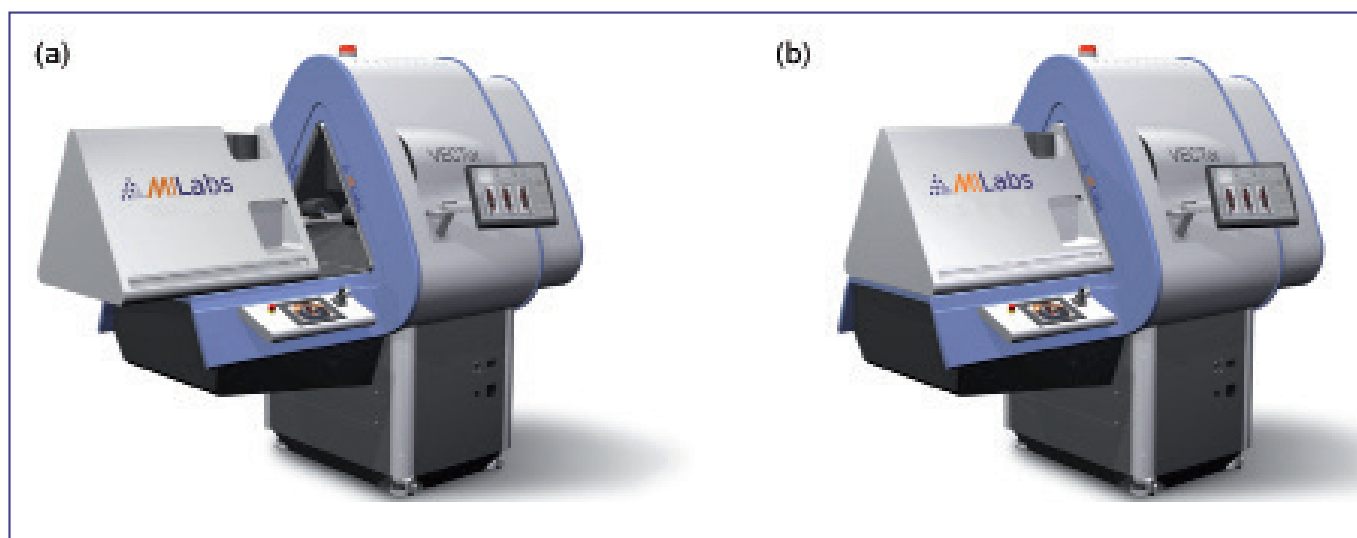


Figure 5. Conceptual impression of an optical imaging system that is docked to a SPECT/PET/CT system. In (a) the optical imaging box is open and the rodent can be prepared for scanning. In (b) the box is closed (i.e. light-tight) and SPECT/PET/CT/OI can be performed. Image courtesy of MILabs B.V.

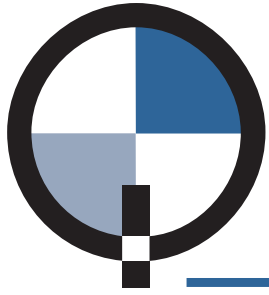
imaging with sub-half-mm SPECT and sub-mm PET resolution. This enables to exploit the entire complement of SPECT and PET tracers in a single scan and may therefore open up new possibilities for multiple functional studies. CT mostly provides anatomical reference images for SPECT and PET images but can also be used for attenuation correction of SPECT and PET data. However, CT uses ionizing radiation which may influence animal welfare or even study results, although new developments in small animal CT (e.g. better reconstruction software (36-38) and improved scan protocols (28)) should lead to higher image quality at lower doses. MRI does not use ionizing radiation and can offer detailed anatomical images of soft tissues, which is compatible with longitudinal multimodality studies. Since stand-alone use of MRI and SPECT or PET systems gives rise to challenges regarding e.g. image registration and prolonged anaesthesia, highly integrated SPECT/MRI and PET/MRI systems are desirable. However, these systems are still in a very early stage of development and the feasibility of highly integrated SPECT/MRI and PET/MRI strongly depends on technologies that enable minimal compromises to the performance of the individual modalities.

E-mail address for correspondence: P.E.B. Vaissier@tudelft.nl

References

1. Seevinck PR, Seppenwoolde JH, de Wit TC, et al. Factors affecting the sensitivity and detection limits of MRI, CT, and SPECT for Multimodal diagnostic and therapeutic agents. *Anticancer Agents Med Chem.* 2007;7:317-34
2. Townsend DW. Multimodality imaging of structure and function. *Phys Med Biol.* 2008;53:R1-R39
3. Cherry SR. Multimodality in vivo imaging systems: twice the power or double the trouble? *Annu Rev Biomed Eng.* 2006;8:35-62
4. Beyer T, Townsend DW, Czernin J, Freudenberg LS. The future of hybrid imaging-part 2: PET/CT. *Insights Imaging* 2:225-34
5. Beyer T, Freudenberg LS, Townsend DW, Czernin J. The future of hybrid imaging-part 1: hybrid imaging technologies and SPECT/CT. *Insights Imaging* 2:161-9
6. Beyer T, Freudenberg LS, Czernin J, Townsend DW. The future of hybrid imaging-part 3: PET/MR, small-animal imaging and beyond. *Insights Imaging* 2:235-46
7. Dillenseger JP, Guillaud B, Goetz C, et al. Coregistration of datasets from a micro-SPECT/CT and a preclinical 1.5 T MRI. *Nucl Instrum Methods Phys Res A.* 2013;702:144-7
8. Chow PL, Stout DB, Komisopoulou E, et al. A method of image registration for small animal, multi-modality imaging. *Phys Med Biol.* 2006;51:379-90
9. Ji C, Van der Have F, Gratama van Andel H, et al. Accurate Coregistration between Ultra-High-Resolution Micro-SPECT and Circular Cone-Beam Micro-CT Scanners. *Int J Biomed Imaging.* 2010;2010:12
10. Cherry SR, Shao YP, Siegel S, et al. Optical fiber readout of scintillator arrays using a multi-channel PMT: A high resolution PET detector for animal imaging. *IEEE Trans Nucl Sci.* 1996;43:1932-7
11. Meier D, Wagenaar DJ, Chen S, et al. A SPECT camera for combined MRI and SPECT for small animals. *Nucl Instrum Methods Phys Res A.* 2011;652:731-4
12. Pichler B, Lorenz E, Mirzoyan R, et al. Performance test of a LSO-APD PET module in a 9.4 Tesla magnet. 1997 IEEE Nuclear Science Symposium - Conference Record, Vols 1 & 2. 1998:1237-9
13. Tan JW, Cai LA, Meng LJ. A Prototype of the MRI-Compatible Ultra-High Resolution SPECT for in Vivo Mice Brain Imaging. 2009 IEEE Nuclear Science Symposium Conference Record, Vols 1-5. 2009:2800-5
14. Christensen NL, Hammer BE, Heil BG, et al. Positron Emission

- Tomography within a Magnetic-Field Using Photomultiplier Tubes and Lightguides. *Phys Med Biol.* 1995;40:691-7
15. Beekman F, van der Have F. The pinhole: gateway to ultra-high-resolution three-dimensional radionuclide imaging. *Eur J Nucl Med Mol Imaging.* 2007;34:151-61
 16. van der Have F, Vastenhouw B, Ramakers RM, et al. U-SPECT-II: An Ultra-High-Resolution Device for Molecular Small-Animal Imaging. *J Nucl Med.* 2009;50:599-605
 17. Vaissier PEB, Goorden MC, Vastenhouw B, et al. Fast Spiral SPECT with Stationary gamma-Cameras and Focusing Pinholes. *J Nucl Med.* 2012;53:1292-9
 18. Goorden MC, Beekman FJ. High-resolution tomography of positron emitters with clustered pinhole SPECT. *Phys Med Biol.* 2010;55:1265-77
 19. Goorden MC, van der Have F, Kreuger R, et al. VECTor: A Preclinical Imaging System for Simultaneous Submillimeter SPECT and PET. *J Nucl Med.* 2013;54:306-12
 20. Bult W, Kroeze SG, Elschot M, et al. Intratumoral administration of holmium-166 acetylacetonate microspheres: antitumor efficacy and feasibility of multimodality imaging in renal cancer. *PLoS One.* 2013;8:e52178
 21. Goertzen AL, Meadors AK, Silverman RW, Cherry SR. Simultaneous molecular and anatomical imaging of the mouse in vivo. *Phys Med Biol.* 2002;47:4315-28
 22. Fontaine R, Belanger F, Cadorette J, et al. Architecture of a dual-modality, high-resolution, fully digital positron emission tomography/computed tomography (PET/CT) scanner for small animal imaging. *IEEE Trans Nucl Sci.* 2005;52:691-6
 23. Zaidi H, Hasegawa B. Determination of the attenuation map in emission tomography. *J Nucl Med.* 2003;44:291-315
 24. Wu C, de Jong JR, van Andel HAG, et al. Quantitative multi-pinhole small-animal SPECT: uniform versus non-uniform Chang attenuation correction. *Phys Med Biol.* 2011;56:N183-N93
 25. Hwang AB, Hasegawa BH. Attenuation correction for small animal SPECT imaging using x-ray CT data. *Med Phys* 2005;32:2799-804
 26. Ay MR, Shirmohammad M, Sarkar S, et al. Comparative Assessment of Energy-Mapping Approaches in CT-Based Attenuation Correction for PET. *Mol Imaging Biol.* 2011;13:187-98
 27. Kersemans V, Thompson J, Cornelissen B, et al. Micro-CT for anatomic referencing in PET and SPECT: radiation dose, biologic damage, and image quality. *J Nucl Med.* 2011;52:1827-33
 28. Willekens I, Buls N, Lahoutte T, et al. Evaluation of the radiation dose in micro-CT with optimization of the scan protocol. *Contrast Media Mol Imaging.* 2010;5:201-7
 29. Catana C, Procissi D, Wu YB, et al. Simultaneous in vivo positron emission tomography and magnetic resonance imaging. *Proc Natl Acad Sci U S A.* 2008;105:3705-10
 30. Judenhofer MS, Wehrl HF, Newport DF, et al. Simultaneous PET-MRI: a new approach for functional and morphological imaging. *Nat Med.* 2008;14:459-65
 31. Breton E, Choquet P, Goetz C, et al. Dual SPECT/MR imaging in small animal. *Nucl Instrum Methods Phys Res A.* 2007;571:446-8
 32. Rentmeester MCM, van der Have F, Beekman FJ. Optimizing multi-pinhole SPECT geometries using an analytical model. *Phys Med Biol.* 2007;52:2567-81
 33. Wu C, van Andel HA, Laverman P, et al. Effects of attenuation map accuracy on attenuation-corrected micro-SPECT images. *EJNMMI Res.* 2013;3:7
 34. Vu NT, Silverman RW, Chatziioannou AF. Preliminary performance of optical PET (OPET) detectors for the detection of visible light photons. *Nucl Instrum Methods Phys Res A.* 2006;569:563-6
 35. Li CQ, Yang YF, Mitchell GS, et al. Simultaneous PET and Multispectral 3-Dimensional Fluorescence Optical Tomography Imaging System. *J Nucl Med.* 2011;52:1268-75
 36. De Man B, Nuyts J, Dupont P, et al. An iterative maximum-likelihood polychromatic algorithm for CT. *IEEE Trans Med Imaging.* 2001;20:999-1008
 37. Nuyts J, De Man B, Fessler JA, et al. Modelling the physics in the iterative reconstruction for transmission computed tomography. *Phys Med Biol.* 2013;58:R63-R96
 38. Ritschl L, Sawall S, Knaup M, et al. Iterative 4D cardiac micro-CT image reconstruction using an adaptive spatio-temporal sparsity prior. *Phys Med Biol.* 2012;57:1517-25 



2QUART BV MEDICAL

**Een nieuw bedrijf in de markt van Nucleaire Geneeskunde.
Wij zijn Technetium sponsor van de NVNG en vertegenwoordigen sinds kort
Comecer Spa en Scintomics GmbH.**



COMECERGROUP

Comecer SpA levert:

- Diverse LAF kasten voor PET- en Single Photon isotopen
- Radiochemie kasten voor NM lab en research
- Meubel inrichting voor Medische laboratoria
- Volautomatische dispensing systemen
- Stralings afscherming accessoires
- Speciaal maatwerk voor unieke projecten

Comecer producten onderscheiden zich ondermeer door gebruik van hoogwaardige kwaliteitsmaterialen en automatisering van processen.

Voor meer informatie: www.comecer.com



SCINTOMICS

Scintomics GmbH levert:

- Labeling modules
- Geïntegreerde HPLC unit
- Volautomatisch dispensing systeem
- Gebruiksklare GMP disposable cassette & reagens labelings kits (FDG, FET, FMC, FLT, FMISO, Fluoride, Ga-/Lu- γ -peptides...)
- Innovatieve en exclusieve introductie van PET Radiopharmca (Pentixafor (CXCR4), TRAP (RGD)₃,...)
- Advies (samenwerking) voor ontwikkeling van unieke labelingen processen.

Scintomics producten onderscheiden zich door het compacte ontwerp van de modules, betrouwbaarheid, flexibiliteit in labeling processen en scherpe prijsstelling.

Voor meer informatie: www.scintomics.com en/of info@scintomics.com

2Quart Medical BV wenst u allen een stralend 2014

Integrated PET/MRI in preclinical studies

State of the art

F. Brunotte, MD^{1,2,3}, H. Haas, PhD⁴, B. Collin, PharmD, PhD^{2,5}, A. Oudot, PhD², S. Bricq, PhD¹, A. Lalande, PhD^{1,3}, X. Tizon, PhD⁶, J.M. Vrigneaud, PhD², P.M. Walker, PhD^{1,3}

¹ Laboratory of Electronics, Computer Science and Image, UMR CNRS 6306, University of Burgundy, Dijon, France

² Cancer Center Georges-François Leclerc, Dijon, France

³ University Hospital, Dijon, France

⁴ Bioscan Molecular Imaging France, a TriFoil Imaging company, Dijon, France

⁵ Institute of Molecular Chemistry of the University of Burgundy, UMR CNRS 6302, University of Burgundy, Dijon, France

⁶ Oncodesign Biotechnology, Dijon, France

Abstract

Brunotte F, Haas H, Collin B, Oudot A, Bricq S, Lalande A, Tizon X, Vrigneaud JM, Walker PM. Integrated PET/MRI in preclinical studies. State of the art. The exquisite tissue contrast of magnetic resonance imaging (MRI), the absence of ionising radiation and the opportunity to obtain new molecular and functional data have strengthened the enthusiasm for coupling MRI rather than computed tomography (CT) to positron emission tomography (PET). When reviewing the current literature one might be surprised by the almost unlimited diversity of what is placed under the name of PET/MRI in the articles. The magnetic field is varying from 0.3 Tesla (T) to 9.4 T, the size of the bore varies also from the wide bore of clinical scanners to volumes limited to a few tens of mL. Many preclinical studies are performed using separate PET and MRI scanners. Sometimes PET and the magnet are in line or sequential. More rarely, fully integrated PET/MRI scanners are used. In that case, mutual interference between PET and MRI has required innovative designs. Initially, the conventional photomultipliers had been installed outside the magnet using long optical fibres. They have now been replaced by avalanche photodiodes (APD), and in the near future silicon photomultipliers (SiPM) could provide an alternative. Tumours and neurological and cardiovascular disorders have been the most studied conditions. Many issues remain to be resolved such as image registration, attenuation correction and animal monitoring. Friendly consoles integrating the control of both imaging modalities also need to be developed.

Tijdschr Nucl Geneesk 2013; 35(4):1144-1152

Introduction

The idea of multimodal imaging techniques is not new (1). Nowadays, the coupling of positron emission tomography (PET) and computed tomography (CT) is the standard in clinical

practice (2) and more recently the integration of single photon emission computed tomography (SPECT) and CT is becoming more and more available (3). These imaging techniques have proven to be extremely effective in diagnosing a variety of diseases (4). Tissue characterisation has been improved by combining the specificity of radiopharmaceuticals and the 3D imaging capabilities of modern CT scanners. Although straightforward, coupling of PET and CT has two serious drawbacks: X-ray exposure contributes to an increased patient irradiation dose and CT tissue characterisation is limited. Magnetic resonance imaging (MRI) has demonstrated a much more convincing ability to provide tissue characterisation through measurement of key parameters such as relaxation times T1 and T2, apparent diffusion coefficient (ADC), tissue perfusion and spectroscopy. One very prolific application has been dynamic contrast-enhanced magnetic resonance imaging (DCE-MRI) of tumours, which has permitted an accurate monitoring of tumour perfusion in response to anti-angiogenic treatments (5).

Garlick *et al* described under the name of PANDA (PET and NMR dual acquisition) in isolated, perfused rat hearts in 1997 (6). LSO crystals were inserted in a 9.4 T magnet with a bundle of optical fibres towards external photomultipliers. Fifteen years later the integration of MRI and PET has generated considerable enthusiasm in the clinical field (7) since nuclear medicine specialists are in need of several requirements that MRI can offer: (i) reduction of the radiation exposure of the patients, especially in case of repeated examinations and in paediatrics, (ii) improvement of soft tissue characterisation by simple addition of the advantages of both techniques and finally (iii) the access to additional physiological parameters that could be derived only by combining both approaches. All these advantages could make PET/MRI a tool of importance especially when focusing on a given organ with the aim of monitoring the effect of a treatment.

In animals many of the rationale retained for clinical studies also apply. The animal irradiation due to CT images can be as high as

several tenths of grays (8). Therefore, reduction of the ionising radiation exposition is also an issue in animal studies especially when studies are repeated. Translational research from animal to human requires the same type of imaging. It is now well recognised that imaging can reduce the duration of drug development and the attrition rate of newly developed drugs (9). The availability of PET/MRI both in preclinical and clinical studies will boost this multimodal imaging technique as a key tool in pharmacological research. Nowadays, integrated PET and MRI is developing in a parallel manner in the preclinical and clinical fields and any improvement achieved finds quickly application in the other field, thus making PET/MRI a truly translational imaging modality.

General design of integrated PET/MR scanner

In recent years, the acquisition of PET and MR images of the same animal has been realised using different imaging strategies. So far, most studies have been performed on separate scanners with subsequent registration of the images, but new and more integrated systems are now available.

1. Separate scanners

In developing multimodality systems, the idea of separate systems makes sense since it offers the possibility to perform sequential studies using various imaging modalities (10), the only requirement being the design of the animal handling cell in which the animal is positioned and which has to fit the different modalities. This enables to use sequentially any combination

of imaging modalities (optical, SPECT, PET, MRI). Another advantage of this approach is to allow the use of the scanners for different experiments at the same time. Regarding PET/MRI, this might be also an advantage by allowing the use of magnets with different field strengths in combination with the same PET scanner. It also allows MRI to be performed outside of the area dedicated to radioactivity handling.

The University of Burgundy and Bioscan, Inc., jointly developed parallel imaging in Phase I of the IMAPI (Integrated Magnetic resonance and PET in Preclinical Imaging) project in the framework of the 'invest for the future' program of the French government (11). The installation in a room accredited for the use of radioactivity of a PET/CT and a MRI system allows easy switching from one system to the other (figure 1). The system configuration allows the use of both scanners at their optimal performances due to the lack of interference between both scanners. However, the system has two major drawbacks: firstly, it is impossible to position the animal in a reproducible manner that makes the use of registration software mandatory, and secondly, simultaneous acquisition is obviously impossible.

To meet the objectives of the project a special animal handling cell with a new miniature gating and acquisition module has been developed. This animal cell can be easily moved from one scanner and docked to the other scanner and vice versa. Data is transmitted through a small bi-directional high-speed optical communication device whereas the module is supplied

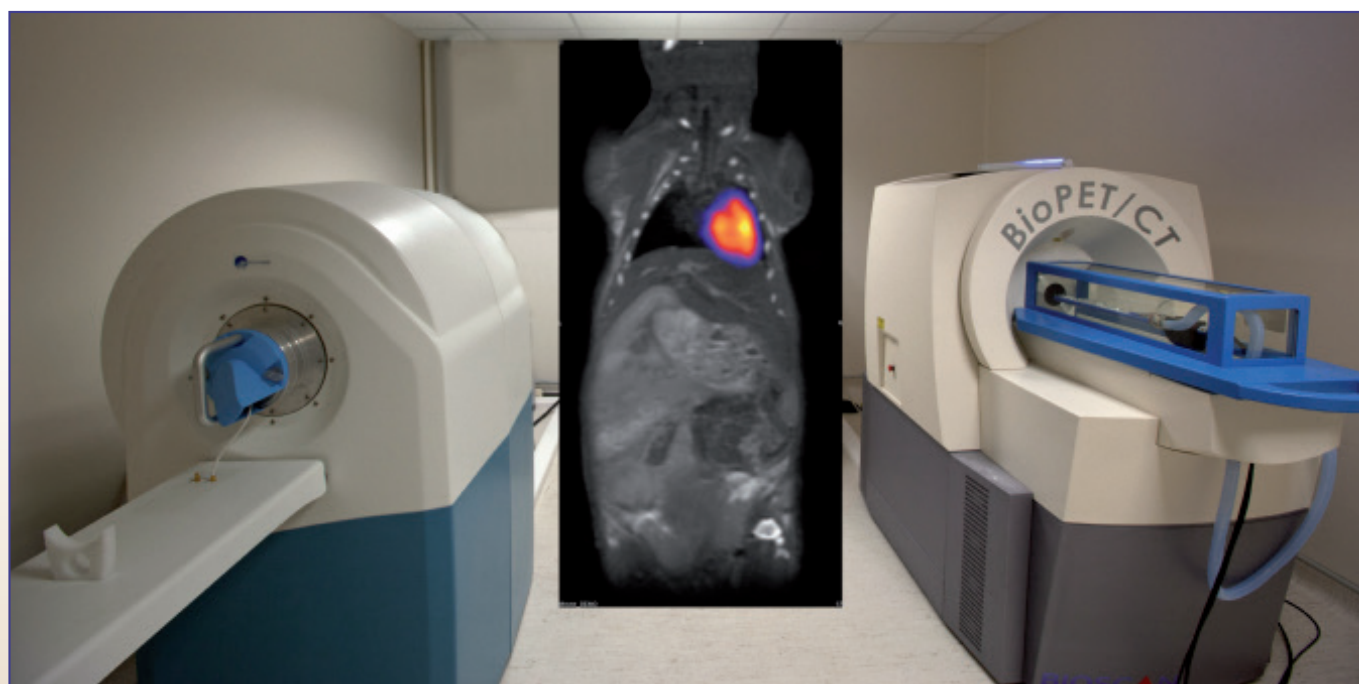


Figure 1. IMAPI Phase I: Two separate imaging systems installed in the preclinical imaging room. On the right, the PET/CT system with the universal animal handling cell and on the left the MRI 3.0T system with the identical animal cell completely inside the magnet bore.

with standard compatible animal sensors for ECG and respiratory gating.

In several studies, clinical scanners have been used for preclinical imaging with some success (12, 13). These studies usually belong to the 'separate imaging' modality and have the advantage of allowing the choice of different magnetic fields for MRI acquisitions.

2. In-line (or sequential) PET/MRI

Several companies are marketing systems consisting in existing PET scanners installed in the vicinity of a magnet. The bores of both systems are aligned in order to allow a smooth displacement of the animal between both scanners as shown in figure 2. Philips is using a similar configuration in clinical nuclear medicine (13, 14). Among the strong disadvantages, the effect of the magnetic field even outside the magnet might be significant. Of course it is impossible to use such systems for independent, parallel experiments.

3. Fully integrated PET/MRI scanners

Although cost-effective and efficient for a preclinical lab, permitting the use of magnets of different fields, both system configurations, parallel and in-line, do not allow for simultaneous acquisition of PET and MR images. Yet, a fully integrated PET/MRI scanner is the most promising technology (15, 16). Moreover, the animal is studied in the same position and under the same physiological conditions for both techniques. One of the strong points of the technique is the possibility of reducing the total examination time and consequently the duration of



Figure 2. IMAPPI Phase II: One integrated in-line PET/MR imaging system with the PET ring mounted in front of the MRI and the MR-compatible motorised conveyance system with the animal cell positioned inside the scanner.

the anaesthesia. Two designs of the integrated scanner are possible: a fully integrated PET ring inside the MRI scanner or a removable PET insert. Many teams found removable inserts useful in order to benefit from the possible separate use of both imaging techniques.

What is the ideal magnetic field for MRI coupled with PET?

One important question is the choice of the magnetic field to be used. This is a key question for those wishing to move towards that technology. The magnet size, its weight and costs increase rapidly with the size of the bore and the main magnetic field (B_0). In order to get the best possible signal to noise ratio, a high field of 7 T or more is preferable. High field magnets with strong gradients offer an unprecedented spatial resolution. When performing magnetic resonance spectroscopy (MRS), the spectral resolution is better and smaller voxels can be studied. For that reason, most of the preclinical magnets installed in the world belong to that category. Unfortunately, since many of these magnets have not been installed in areas dedicated to handling of radioactive substances, it appears often difficult to use them as part of a PET/MRI project.

High field magnets may have limitations. The first is the limited possible translation to clinical imaging. In the foreseeable future, clinical imaging will be mainly performed at magnetic field strengths of 1.5 T and 3 T, and these will remain the highest fields used in routine MRI. Since the behaviour of MRI contrast agents depends on the field strength of the magnet, it could be interesting to stay at field strengths similar to those used in human imaging situations. Most of the encountered artefacts, including PET/MRI mutual interference increase with the magnetic field intensity. For these reasons, other groups have developed scanners at fields as low as 0.3 T (17). Imaging at low fields has some advantages due to a better tissue contrast with or without contrast agents. Low field magnets have the advantage of low weight, transportability and even bench top imaging. Hence, they are easy to install in areas dedicated and licensed for the use of radioactive sources. The bore is usually limited in size, allowing imaging of small rodents typically mice and rats, and the magnetic field is relatively low (between 0.3 T and 3 T) with a limited image quality, requiring long acquisition times and limited temporal resolution thus reducing the dynamic acquisition capability of these magnets.

When considering the integration of a PET detector inside the bore of a magnet, additional requirements apply, since the PET detector ring will reduce the available space for the animal, monitoring devices, the installation of gas supply and intravenous lines. The minimal bore diameter of the magnet cannot be less than 30 cm if mice or rats are imaged.

PET technology compatible with magnetic fields

Acquiring simultaneously PET and MRI datasets is technically very demanding due to mutual interactions between magnetic fields and the electronics of the PET detectors. Coincidence detection in PET requires scintillation crystals, light amplification,

electric wiring and some X-ray shielding. Interactions between the magnetic field and these electronic devices require new approaches, which have been developed in the late 1990's. The nature of the best PET scintillation crystals has been debated, but it has been shown that sodium iodide, cesium iodide, lutetium orthosilicate (LSO), or lutetium-yttrium oxyorthosilicate (LYSO) cause limited MRI artefacts. Due to the presence of gadolinium in the LGSO and GSO crystals, causing MRI artefacts (18), LSO (19) and LYSO (20) seem to be the preferred crystals for PET/MRI. Since conventional photomultipliers cannot be used in a magnetic field without severe artefacts, long light guides of 2 m with light amplification outside the magnet (3 T) have been used (21). In another approach a split magnet of 1 T has been used to allow the magnetic-sensitive components to be placed outside the magnet (22). Some groups have pursued this approach using shortened light fibres and PSMTs (Position Sensitive Photomultiplier Tubes) (16).

Since conventional photomultipliers are extremely sensitive to magnetic fields, two other approaches have been used: avalanche photodiodes (APD) and silicon photomultipliers (SiPM). APDs have been proposed in 1997 by Pichler *et al* as compatible with magnetic fields as high as 9.4 T (23).

The SiPM is a relatively new photodetector (24) consisting of a Geiger-mode avalanche (G-APD) photodiode described in the nineties (25). These photodetectors have also been named avalanche photodiodes based on MRS (Metal Resistor-Semiconductor) (26, 27), multipixel photon counter (MPPC) or solid-state photon counter (SSPC). They are now referred to as SiPM. Systems for imaging small animals based on LGSO crystals and SiPMs have been developed (28, 29). It has been suggested that a SiPM with 50 μm pixels gives the best results for developing high-resolution PET (30). SiPMs combine the advantages of conventional photomultipliers and APDs with high gain, high signal to noise, excellent timing properties and insensitivity to magnetic fields (31). Nevertheless, interference between PET and MRI may persist (32). A fully digital implementation of a SiPM has been developed, simplifying the overall PET detector design while reducing the sensitivity to temperature variations and electronic noise susceptibility (33). Regarding the way PET crystals and coils are installed in the magnet, PET scanners have been configured differently across the different research groups. As mentioned earlier, a split magnet has been proposed by the group at Cambridge with a PET scanner installed between the two halves of the MRI (22). Field cycled MRI has been used with a PET detector based on conventional photomultipliers. In that case, PET acquisition occurs only when the 0.3 T magnetic field is switched off (34).

The key issue of inserting a PET detector into a magnet is the mutual interference between PET and MRI. PET detectors and electronics can decrease the homogeneity of the main magnetic field (B_0) and of the radiofrequency (RF) field (B_1) induced by the coils. The presence of PET detectors can make the coil

tuning difficult. RF radiations and noise can be emitted by the PET detector and picked up by the receiver coil. On the other hand, eddy currents can be induced in the PET detector by switching the MR gradients used for MRI.

When inserting a PET detector inside a magnet, one question arises regarding the respective position of the RF coils and the PET detector. Different solutions have been proposed. Yoon *et al* have placed the RF coil inside the PET ring (35). When the RF coils are inside the PET detectors, the PET detectors are outside the field of view of the MR and thus will create less artifacts. Other designs of integrated PET/MRI have been proposed and sometimes, scintillator, diodes and analogue electronics have been installed inside the RF coils and thus in the MR field of view (36). In animal imaging, the issue of the field of view is of lesser importance than in humans where omitting the patient's arms in the field of view of MRI is a significant limitation for attenuation correction in PET (37). The presence of coils inside the PET field of view can induce attenuation artefacts that are difficult to take into account as MR coils are not visible on MR images (38).

Other key issues of PET/MRI in preclinical imaging

Besides the design of the PET/MRI system, many other issues have to be addressed in order to establish integrated PET/MRI as a tool for routine preclinical imaging. The recording of the physiological signals inside the magnet is mandatory for MR imaging of anatomical structures concerned with respiratory and cardiac motion. MR compatibility is obviously the most demanding requirement for ECG and respiratory monitoring devices which should be optimised for high magnetic fields and gradients. Other devices such as blood samplers are also very important (39). After selecting the best MR-compatible PET hardware, the MRI scanner has to be optimised for image quality. The design of the MR gradients, RF coils and acquisition sequences has to be carefully optimised to avoid artefacts. In most studies the consoles for PET and MRI acquisition control are different, making the experiments somewhat tedious. So an important objective is the design of one unique user-friendly console for controlling both tasks of PET and MRI. New adapted software to analyse acquired data also has to be developed. Firstly, software for registration of PET and MRI data sets without the use of CT is required (figure 3). CT produces irradiation that is not negligible even in small animals and it would not make sense to use CT in PET/MRI studies. Several studies have been reported regarding registration of MRI and PET (40-42). Bagci *et al* have described PET/MRI co-segmentation of breast cancer xenografts implanted in mice (43). Registration might not be limited to parallel or in-line imaging modalities since movement of the animal is still possible even in a fully integrated PET/MRI scanner. Secondly, software needs to be developed for attenuation correction. Despite the limited size of rodents, attenuation correction is preferable even in mice (44, 45). Attenuation correction using CT scans is straightforward. However, using MR requires

converting anatomical information obtained from MRI into an attenuation map that can be used for attenuation correction (46). Most of the work has been done in the clinical setting or in relatively large animals like rabbits (12), whereas in preclinical studies MR attenuation correction is still a topic of research. Several methods have been suggested. It is possible to convert maps obtained by 3- or 4-class tissue segmentation into attenuation maps (47). Atlases might also be used (48). After registration of the acquired data with an atlas, attenuation correction is performed according to the attenuation maps of the atlas. Another method is to obtain images of bone using ultra short echo times (UTE) (49). One interesting method has been proposed for the brain which consists of performing an additional PET with ^{18}F -NaF permitting a clear identification of the skull with a low uptake in the brain (50). As mentioned before, the correction of the attenuation induced by MR coils is another important challenge. Another field of interest in PET/MR imaging is the development of MR-based motion correction for PET (51). In animals the advantages of MRI to correct motion in PET have been shown in rabbits and monkeys (52).

An adapted quality control of PET as well as MRI is an important requirement including the separate control of image quality obtained both by PET and MRI, and the study of the effects of their mutual interference. It is of course mandatory that the PET scanners, to be inserted in a magnet, reach a performance similar to that of the best stand-alone PET scanners (53-55). Fluids adapted to phantoms have been proposed for PET/MRI (56).

Biological studies involving PET/MR acquisitions

1. Tumour imaging

Most of the studies coupling MRI and PET have been carried out in tumour-bearing animals. Many radiopharmaceuticals have proven useful in investigating experimental tumours. ^{18}F -FDG has been, by far, the most widely used radiopharmaceutical. The overexpression of the glucose transporter membrane transporter (GLUT1) in many cancer cells makes ^{18}F -FDG an ideal tracer (57). Modifications of ^{18}F -FDG uptake in response to treatment had been shown in the 1990s of the 20th century (58) and were confirmed in many animal models (59). Nowadays, ^{18}F -FDG is used daily in the clinical setting as a surrogate marker

of pathological response and of survival (60). Most of the clinical and preclinical studies have been performed using PET or PET/CT. Using MRI instead of CT reduces the irradiation of the animals and its potential effects on the biology of the tumour. More importantly, MRI provides high resolution and high contrast anatomical and functional imaging. It is in particular very easy to differentiate central necrosis from surrounding viable tumour, to analyse perfusion, water diffusion which is related to cellular density, and to assess the concentration of metabolites detected by magnetic resonance spectroscopy.

It has been shown that simultaneous PET/MRI of tumours can yield images of the biodistribution of ^{18}F -FDG or of a radiolabelled anti-carcino-embryonal-antigen (CEA) antibody along with MRI, including ADC mapping (61). One of the interests of coupling MRI and PET is to benefit from DCE-MRI, which is a well validated technique in exploring tumour perfusion and vascular permeability (62). Tumour uptake of ^{18}F -fluoromisonidazole (^{18}F -Fmiso) and DCE-MRI have been compared in prostate cancer of the rat (63) by performing PET and MRI sequentially and registering the images with the aid of positioning moulds (64). PET/MRI experiments have also allowed the comparison of total choline concentration at H-MRS performed in a 3 T clinical magnet and ^{18}F -fluoromethylcholine uptake at PET in rat rhabdomyosarcoma (65). The authors suggest a complementary role of both techniques rather than redundancy. Magnetic resonance spectroscopic imaging of hyperpolarised ^{13}C -pyruvate metabolism has also been compared to ^{18}F -FDG uptake in hepatocellular carcinoma bearing rats (66). Coupling MRI and PET has been useful in the evaluation of the effects of radiofrequency on VX2 tumours in rabbits (67).

Many authors have proposed nanoparticles as multifunctional platforms allowing multimodal imaging, particularly PET/MR imaging. Iron oxide nanoparticles have been encapsulated in human serum albumin and labelled with ^{64}Cu -DOTA and Cy5.5 dye, thus being detectable by PET, MRI and near infrared fluorescence (NIRF) (68). Nanoparticles are very flexible platforms and can be used in PET/MR imaging of specific biological target such as tumour $\alpha_v\beta_3$ integrin using Arginine-Glycine-Aspartic (RGD) conjugated nanoparticles (69). This kind



Figure 3. FDG-PET, MRI and co-registered PET/MRI of a mouse bearing a PC3 prostate tumour.

of approach paves the way towards theranostics as proposed by Yang *et al* with nanoparticles RGD-functionalised and conjugated with doxorubicin (70). Recently, liposomes functionalised by octreotide and labelled by gadolinium (Gd) and ^{89}Zr have shown affinity for tumours expressing sstr2 receptor as demonstrated in mice by MRI at 4.7 T and PET (71).

2. Brain imaging

Brain imaging might benefit enormously from coupling both imaging modalities. MRI benefits from an unsurpassed resolution and tissue contrast for brain study. Moreover, MRI has the ability to assess oxygenation using the blood oxygen level dependent (BOLD) effect, perfusion from the ADC measurements and neuronal viability from n-acetyl aspartate (NAA) concentration measurements using spectroscopy. On the other hand, the sensitivity of PET permits an accurate study of receptors such as serotonin 5-HT_{1A} receptor imaging co-registered with rat and mouse MRI templates (72). Combining PET and MRI is very promising in the field of brain metabolism and perfusion studies. MRI has been proved useful to provide anatomical localisation as in FDG-PET studies of brain metabolism coregistered with MRI at 4.7 T (73). Cerebral blood flow was studied by Watabe *et al* using ^{15}O PET registered with separately acquired brain MRI at 0.3 T (74). PET provides a gold standard for MRI to validate imaging protocols as in the study of Bos *et al* comparing arterial spin labelling at 7 T and biodistribution to ^{68}Ga or ^{64}Cu -labelled microspheres (75).

Brain tumours have benefited from the excellent spatial resolution and tissue characterisation provided by MRI combining, T1-, T2-weighted images, ADC imaging and spectroscopy. On the other hand, PET studies of brain tumours allow the use of many radiopharmaceuticals, which have been proved to be efficient in studying brain tumours. Coupling MRI, MRS and PET would probably improve the comprehensive study of brain tumours and the subsequent follow-up of the effects of new targeted drugs. Belloli *et al* investigated a preclinical model of glioblastoma multiforme (76). In that study, gadolinium enhanced MRI was acquired in a 3 T clinical magnet to assess tumour morphology and growth separately from brain PET using ^{18}F -FAZA to assess hypoxia and ^{18}F -FDG to assess brain metabolism. Many other tracers have been investigated in preclinical models such as choline, thymidine or amino-acids. Two tumour phenotypes of glioblastoma (angiogenic and infiltrative) have been studied by co-registered 7 T MRI and PET performed separately, showing that ^{11}C -methionine (MET) accumulation was more specific of angiogenic glioblastoma in comparison with infiltrative glioblastoma than ^{18}F -fluorothymidine (FLT) (77).

3. Cardiovascular imaging

In the field of cardiovascular diseases, MRI combined with PET will be an important tool since X-ray attenuation is similar for blood, the myocardium and vessel walls. Therefore, using CT, these different tissues are not distinguishable without

injection of an iodine-based contrast agent. MRI has the unique advantage of showing spontaneous contrast between blood, myocardium and vessel wall. Moreover, dynamic imaging is possible, allowing visualisation of heart and vessel motion without contrast agent. MRI makes it easy to combine cardiovascular dynamics with PET study of tracer uptake. This has been proved useful for studying vulnerable plaques and differentiate myocardial scar from myocardium with residual viability.

Stegger *et al* have shown that left ventricular volumes of mice can be measured either using MRI at 6.3 T or ^{18}F -FDG-PET (78). Results were similar except for a slight overestimation of left ventricular diastolic volume by PET. Both techniques permitted adequate triggering at heart rates over 500 beats/min. Quantification of regional myocardial oxygenation by MRI has been validated by PET in dogs (79). Using a clinical 1.5 T MRI scanner and a dedicated PET, it has been shown that the myocardial defect of ^{18}F -FDG uptake correlated with late enhancement observed with gadolinium MRI (80). Feasibility of imaging heart mouse with simultaneous PET/MRI was demonstrated at 7 T (81), but myocardial uptake was lower than with high resolution PET. PET/MRI of the heart is also promising in the field of regenerative therapy based on stem cells PET. It has been shown that PET and MRI at 4.7 T were able to follow stem cells labelled with both superparamagnetic iron oxides (SPIO) and a PET tracer (82). PET/MRI of the heart can also be used for early stem cell engraftment in predicting late cardiac functional recovery (83).

PET combined with MRI has been used to study vascular diseases as these two techniques are particularly complementary. MRI allows the anatomical imaging of the vessels and of the atherosclerotic plaques. Angiogenesis in the vessel wall can be delineated using DCE-MRI and inflammation can be outlined by ^{18}F -FDG-PET (84). USPIO can demonstrate the presence of macrophages in the inflammatory wall of the vessels. Nanoparticles labelled with ^{89}Zr have been imaged by PET and anatomically localised using 7 T MRI (85). In another study of atherosclerotic rabbits in a clinical sequential PET/MRI scanner at 3 T, it has been suggested that ^{18}F -FDG was superior to USPIO to assess the effects of atorvastatin (86). PET/MR imaging has been proposed to assess the effect of pioglitazone (87). True simultaneous PET/MRI of intra-arterial thrombus was achieved in the rat at 3 T using a fibrin-targeted probe labelled with gadolinium and ^{64}Cu (88). Especially for the assessment of aortic aneurisms the future of multimodal imaging seems bright (89).

Conclusion

Many of the experimental approaches described in this review have been performed with separate PET and MRI. This separate approach fulfils most of the demands on the coupling of both technologies like irradiation reduction and anatomical co-localisation of images. Nevertheless, the most

interesting perspectives are probably those where the addition of both techniques allows access to new fields of physiological investigation. A very elegant example is shown in the study of Frullano *et al* who described a smart PET/MRI agent, made of a gadolinium chelate labelled with ^{18}F , enabling direct quantification of pH value in vivo (90). In their approach, the MR probe had a relaxivity dependant on the pH and PET permitted absolute quantification of the concentration of the molecular probe. These two simultaneous measurements allowed for adequate pH measurement.

There is no doubt that coupling magnetic resonance imaging and PET will offer an unprecedented comprehensive study of metabolism in many diseases. Scanners integrating PET and MRI offer the brightest perspective to the addition of both modalities. Nevertheless most of the available studies rely on separate instruments. For the foreseeable next five years, it is obvious that all the different approaches will coexist. Before deciding on the acquisition of PET and MRI in a preclinical laboratory, the research objectives should be carefully defined. One may suggest that flexible instruments including a removable insert usable as a standalone PET would be the best compromise for those unable to afford the purchase of several scanners. Imaging of animals larger than rats and mice is also an issue often requiring the use of clinical scanners. Nevertheless the tremendous potential of PET/MRI as a tool for translation from preclinical models to the clinic will probably assure the success of integrated PET/MRI scanners. This might be reinforced by the advent of multimodal molecular probes.

Email-address for correspondence: hein.haas@trifoilimaging.com

Acknowledgement: This work was supported by a French Government grant managed by the French National Research Agency (ANR) under the program 'Investissements d'Avenir' (with reference ANR- 10-EQPX-05-01/IMAPPI Equipex) and by the Fondation de Coopération Scientifique Bourgogne Franche-Comté.

References

- Beyer T, Townsend DW, Brun T, et al. A combined PET/CT scanner for clinical oncology. *J Nucl Med*. 2000;41:1369-79
- Beyer T, Townsend DW. Putting 'clear' into nuclear medicine: a decade of PET/CT development. *Eur J Nucl Med Mol Imaging*. 2006;33:857-61
- Mariani G, Bruselli L, Kuwert T, et al. A review on the clinical uses of SPECT/CT. *Eur J Nucl Med Mol Imaging*. 2010;37:1959-85
- Bockisch A, Freudenberg LS, Schmidt D, Kuwert T. Hybrid imaging by SPECT/CT and PET/CT: proven outcomes in cancer imaging. *Semin Nucl Med*. 2009;39:276-89
- Jackson A, O'Connor JP, Parker GJ, Jayson GC. Imaging tumor vascular heterogeneity and angiogenesis using dynamic contrast-enhanced magnetic resonance imaging. *Clinical Cancer Research*. 2007;13:3449-59
- Garlick PB, Marsden PK, Cave AC, et al. PET and NMR dual acquisition (PANDA): applications to isolated, perfused rat hearts. *NMR Biomed*. 1997;10:138-42
- Jadvar H, Colletti PM. Competitive advantage of PET/MRI. *Eur J Radiol*. 2013
- Kerseman V, Thompson J, Cornelissen B, et al. Micro-CT for anatomic referencing in PET and SPECT: radiation dose, biologic damage, and image quality. *J Nucl Med*. 2011;52:1827-33
- Fernandes E, Barbosa Z, Clemente G, Alves F, Abrunhosa AJ. Positron emitting tracers in pre-clinical drug development. *Curr Radiopharm*. 2012;5:90-8
- James ML, Gambhir SS. A molecular imaging primer: modalities, imaging agents, and applications. *Physiological Reviews*. 2012;92:897-965
- Butler D. French research wins huge cash boost. *Nature*. 2009;462:838
- Bini J, Izquierdo-Garcia D, Mateo J, et al. Preclinical evaluation of MR attenuation correction versus CT attenuation correction on a sequential whole-body MR/PET scanner. *Invest Radiol*. 2013;48:313-22
- Nagy K, Toth M, Major P, et al. Performance Evaluation of the Small-Animal nanoScan PET/MRI System. *J Nucl Med*. 2013
- Zaidi H, Ojha N, Morich M, et al. Design and performance evaluation of a whole-body Ingenuity TF PET-MRI system. *Phys Med Biol*. 2011;56:3091-106
- Judenhofer MS, Cherry SR. Applications for preclinical PET/MRI. *Semin Nucl Med*. 2013;43:19-29
- Vaska P, Cao T. The state of instrumentation for combined positron emission tomography and magnetic resonance imaging. *Semin Nucl Med*. 2013;43:11-8
- Tatsumi M, Yamamoto S, Imaizumi M, et al. Simultaneous PET/MR body imaging in rats: initial experiences with an integrated PET/MRI scanner. *Ann Nucl Med*. 2012
- Yamamoto S, Kuroda K, Senda M. Scintillator selection for MR-compatible gamma detectors. *Nuclear Science, IEEE Transactions on*. 2003;50:1683-5
- Ziegler SI, Pichler BJ, Boening G, et al. A prototype high-resolution animal positron tomograph with avalanche photodiode arrays and LSO crystals. *European Journal of Nuclear Medicine*. 2001;28:136-43
- Spanoudaki VC, Mann AB, Otte AN, et al. Use of single photon counting detector arrays in combined PET/MR: Characterization of LYSO-SiPM detector modules and comparison with a LSO-APD detector. *Journal of Instrumentation*. 2007;2:P12002
- Raylman RR, Majewski S, Velan SS, et al. Simultaneous acquisition of magnetic resonance spectroscopy (MRS) data and positron emission tomography (PET) images with a prototype MR-compatible, small animal PET imager. *J Magn Reson*. 2007;186:305-10
- Hawkes RC, Fryer TD, Siegel S, Ansorge RE, Carpenter TA. Preliminary evaluation of a combined microPET-MR system. *Technol Cancer Res Treat*. 2010;9:53-60
- Pichler B, Lorenz E, Mirzoyan R, et al. Performance test of a LSO-APD PET module in a 9.4 Tesla magnet. *Nuclear Science Symposium, 1997. IEEE*. 1997;2:1237-9 vol.1232

24. Golovin V, Saveliev V. Novel type of avalanche photodetector with Geiger mode operation. *Nuclear Instruments and Methods in Physics Research Section A: Accelerators, Spectrometers, Detectors and Associated Equipment*. 2004;518:560-4
25. Bisello D, Gotra Y, Jejer V, et al. Silicon avalanche detectors with negative feedback as detectors for high energy physics. *Nuclear Instruments and Methods in Physics Research Section A: Accelerators, Spectrometers, Detectors and Associated Equipment*. 1995;367:212-4
26. Akindinov AV, Martemianov AN, Polozov PA, Golovin VM, Grigoriev EA. New results on MRS APDs. *Nuclear Instruments and Methods in Physics Research Section A: Accelerators, Spectrometers, Detectors and Associated Equipment*. 1997;387:231-4
27. Saveliev V, Golovin V. Silicon avalanche photodiodes on the base of metal-resistor-semiconductor (MRS) structures. *Nuclear Instruments and Methods in Physics Research Section A: Accelerators, Spectrometers, Detectors and Associated Equipment*. 2000;442:223-9
28. Yamamoto S, Imaizumi M, Watabe T, et al. Development of a Si-PM-based high-resolution PET system for small animals. *Phys Med Biol*. 2010;55:5817-31
29. Kwon SI, Lee JS, Yoon HS, et al. Development of small-animal PET prototype using silicon photomultiplier (SiPM): initial results of phantom and animal imaging studies. *J Nucl Med*. 2011;52:572-9
30. Yamamoto S, Watabe H, Hatazawa J. Performance comparison of Si-PM-based block detectors with different pixel sizes for an ultrahigh-resolution small-animal PET system. *Phys Med Biol*. 2011;56:N227-36
31. Roncali E, Cherry SR. Application of silicon photomultipliers to positron emission tomography. *Ann Biomed Eng*. 2011;39:1358-77
32. Yamamoto S, Watabe H, Kanai Y, et al. Interference between PET and MRI sub-systems in a silicon-photomultiplier-based PET/MRI system. *Phys Med Biol*. 2011;56:4147-59
33. Frach T, Prescher G, Degenhardt C, Zwaans B. The digital silicon photomultiplier - System architecture and performance evaluation. *Nuclear Science Symposium Conference Record (NSS/MIC)*, 2010 IEEE. 2010:1722-7
34. Bindseil GA, Gilbert KM, Scholl TJ, Handler WB, Chronik BA. First image from a combined positron emission tomography and field-cycled MRI system. *Magn Reson Med*. 2011;66:301-5
35. Yoon HS, Ko GB, Kwon SI, et al. Initial results of simultaneous PET/MRI experiments with an MRI-compatible silicon photomultiplier PET scanner. *J Nucl Med*. 2012;53:608-14
36. Slaters RB, Farahani K, Shao Y, et al. A study of artefacts in simultaneous PET and MR imaging using a prototype MR compatible PET scanner. *Phys Med Biol*. 1999;44:2015-27
37. Delso G, Martinez-Moller A, Bundschuh RA, Nekolla SG, Ziegler SI. The effect of limited MR field of view in MR/PET attenuation correction. *Med Phys*. 2010;37:2804-12
38. Delso G, Martinez-Moller A, Bundschuh RA, et al. Evaluation of the attenuation properties of MR equipment for its use in a whole-body PET/MR scanner. *Phys Med Biol*. 2010;55:4361-74
39. Breuer J, Grazioso R, Zhang N, Schmand M, Wienhard K. Evaluation of an MR-compatible blood sampler for PET. *Phys Med Biol*. 2010;55:5883-93
40. Rowland DJ, Garbow JR, Laforest R, Snyder AZ. Registration of (18F)FDG microPET and small-animal MRI. *Nucl Med Biol*. 2005;32:567-72
41. Fei B, Wang H, Muzic RF Jr, et al. Deformable and rigid registration of MRI and microPET images for photodynamic therapy of cancer in mice. *Med Phys*. 2006;33:753-60
42. Ng TS, Procissi D, Wu Y, Jacobs RE. A robust coregistration method for in vivo studies using a first generation simultaneous PET/MR scanner. *Med Phys*. 2010;37:1995-2003
43. Bagci U, Kramer-Marek G, Mollura DJ. Automated computer quantification of breast cancer in small-animal models using PET-guided MR image co-segmentation. *EJNMMI Res*. 2013;3:49
44. Chow PL, Rannou FR, Chatziioannou AF. Attenuation correction for small animal PET tomographs. *Phys Med Biol*. 2005;50:1837-50
45. El Ali HH, Bodholdt RP, Jørgensen JT, Myschetzky R, Kjaer A. Importance of Attenuation Correction (AC) for Small Animal PET Imaging. *Diagnostics*. 2012;2:42-51
46. Hofmann M, Pichler B, Scholkopf B, Beyer T. Towards quantitative PET/MRI: a review of MR-based attenuation correction techniques. *Eur J Nucl Med Mol Imaging*. 2009;36 Suppl 1:S93-104
47. Berker Y, Franke J, Salomon A, et al. MRI-based attenuation correction for hybrid PET/MRI systems: a 4-class tissue segmentation technique using a combined ultrashort-echo-time/ Dixon MRI sequence. *J Nucl Med*. 2012;53:796-804
48. Dogdas B, Stout D, Chatziioannou AF, Leahy RM. Digimouse: a 3D whole body mouse atlas from CT and cryosection data. *Phys Med Biol*. 2007;52:577-87
49. Keereman V, Fierens Y, Broux T, et al. MRI-based attenuation correction for PET/MRI using ultrashort echo time sequences. *J Nucl Med*. 2010;51:812-8
50. Buitter HJ, van Velden FH, Leysen JE, et al. Reproducible Analysis of Rat Brain PET Studies Using an Additional ((18)F)NaF Scan and an MR-Based ROI Template. *Int J Mol Imaging*. 2012;2012:580717
51. Ouyang J, Li Q, El Fakhri G. Magnetic resonance-based motion correction for positron emission tomography imaging. *Semin Nucl Med*. 2013;43:60-7
52. Chun SY, Reese TG, Ouyang J, et al. MRI-based nonrigid motion correction in simultaneous PET/MRI. *J Nucl Med*. 2012;53:1284-91
53. Chatziioannou AF, Cherry SR, Shao Y, et al. Performance evaluation of microPET: a high-resolution lutetium oxyorthosilicate PET scanner for animal imaging. *J Nucl Med*. 1999;40:1164-75
54. Goertzen AL, Bao Q, Bergeron M, et al. NEMA NU 4-2008 comparison of preclinical PET imaging systems. *J Nucl Med*. 2012;53:1300-9
55. Wang Y, Seidel J, Tsui BM, Vaquero JJ, Pomper MG. Performance evaluation of the GE healthcare eXplore VISTA dual-ring small-animal PET scanner. *J Nucl Med*. 2006;47:1891-1900
56. Ziegler S, Braun H, Ritt P, et al. Systematic Evaluation of Phantom Fluids for Simultaneous PET/MR Hybrid Imaging. *J Nucl Med*. 2013;54:1464-71
57. Shaw RJ. Glucose metabolism and cancer. *Current Opinion in Cell Biology*. 2006;18:598-608
58. Yoshioka T, Takahashi H, Oikawa H, et al. Influence of chemotherapy on FDG uptake by human cancer xenografts in nude mice. *J Nucl Med*. 1997;38:714-7

59. Cullinane C, Dorow DS, Kansara M, et al. An in vivo tumor model exploiting metabolic response as a biomarker for targeted drug development. *Cancer Research*. 2005;65:9633-6
60. Weber WA. Assessing tumor response to therapy. *J Nucl Med*. 2009;50 Suppl 1:1s-10s
61. Ng TS, Bading JR, Park R, et al. Quantitative, simultaneous PET/MRI for intratumoral imaging with an MRI-compatible PET scanner. *J Nucl Med*. 2012;53:1102-9
62. Barnes SL, Whisenant JG, Loveless ME, Yankeelov TE. Practical Dynamic Contrast Enhanced MRI in Small Animal Models of Cancer: Data Acquisition, Data Analysis, and Interpretation. *Pharmaceutics*. 2012;4:442-78
63. Cho H, Ackerstaff E, Carlin S, et al. Noninvasive multimodality imaging of the tumor microenvironment: registered dynamic magnetic resonance imaging and positron emission tomography studies of a preclinical tumor model of tumor hypoxia. *Neoplasia*. 2009;11:247-59, 242p following 259
64. Zanzonico P, Campa J, Polycarpe-Holman D, et al. Animal-specific positioning molds for registration of repeat imaging studies: comparative microPET imaging of F18-labeled fluoro-deoxyglucose and fluoro-misonidazole in rodent tumors. *Nucl Med Biol*. 2006;33:65-70
65. Rommel D, Bol A, Abarca-Quinones J, et al. Rodent rhabdomyosarcoma: comparison between total choline concentration at H-MRS and (18F)-fluoromethylcholine uptake at PET using accurate methods for collecting data. *Mol Imaging Biol*. 2010;12:415-23
66. Menzel MI, Farrell EV, Janich MA, et al. Multimodal assessment of in vivo metabolism with hyperpolarized (1-13C)MR spectroscopy and 18F-FDG PET imaging in hepatocellular carcinoma tumor-bearing rats. *J Nucl Med*. 2013;54:1113-9
67. Ohira T, Okuma T, Matsuoka T, et al. FDG-MicroPET and diffusion-weighted MR image evaluation of early changes after radiofrequency ablation in implanted VX2 tumors in rabbits. *Cardiovascular and Interventional Radiology*. 2009;32:114-20
68. Xie J, Chen K, Huang J, et al. PET/NIRF/MRI triple functional iron oxide nanoparticles. *Biomaterials*. 2010;31:3016-22
69. Lee HY, Li Z, Chen K, et al. PET/MRI dual-modality tumor imaging using arginine-glycine-aspartic (RGD)-conjugated radiolabeled iron oxide nanoparticles. *J Nucl Med*. 2008;49:1371-9
70. Yang X, Hong H, Grailer JJ, et al. cRGD-functionalized, DOX-conjugated, and 64Cu-labeled superparamagnetic iron oxide nanoparticles for targeted anticancer drug delivery and PET/MR imaging. *Biomaterials*. 2011;32:4151-60
71. Abou DS, Thorek DL, Ramos NN, et al. (89)Zr-labeled paramagnetic octreotide-liposomes for PET-MR imaging of cancer. *Pharm Res*. 2013;30:878-88
72. Saigal N, Bajwa AK, Faheem SS, et al. Evaluation of serotonin 5-HT(1A) receptors in rodent models using ((1)(8)F)mefway PET. *Synapse*. 2013;67:596-608
73. Shultz SR, Cardamone L, Liu YR, et al. Can structural or functional changes following traumatic brain injury in the rat predict epileptic outcome? *Epilepsia*. 2013;54:1240-50
74. Watabe T, Shimosegawa E, Watabe H, et al. Quantitative evaluation of cerebral blood flow and oxygen metabolism in normal anesthetized rats: 15O-labeled gas inhalation PET with MRI Fusion. *J Nucl Med*. 2013;54:283-90
75. Bos A, Bergmann R, Strobel K, et al. Cerebral blood flow quantification in the rat: a direct comparison of arterial spin labeling MRI with radioactive microsphere PET. *EJNMMI Res*. 2012;2:47
76. Belloli S, Brioschi A, Politi LS, et al. Characterization of biological features of a rat F98 GBM model: A PET-MRI study with ((18)F)FAZA and ((18)F)FDG. *Nucl Med Biol*. 2013;40:831-40
77. Viel T, Talasila KM, Monfared P, et al. Analysis of the growth dynamics of angiogenesis-dependent and -independent experimental glioblastomas by multimodal small-animal PET and MRI. *J Nucl Med*. 2012;53:1135-45
78. Stegger L, Heijman E, Schafers KP, et al. Quantification of left ventricular volumes and ejection fraction in mice using PET, compared with MRI. *J Nucl Med*. 2009;50:132-8
79. McCommis KS, Goldstein TA, Abendschein DR, et al. Quantification of regional myocardial oxygenation by magnetic resonance imaging: validation with positron emission tomography. *Circ Cardiovasc Imaging*. 2010;3:41-6
80. Higuchi T, Nekolla SG, Jankaukas A, et al. Characterization of normal and infarcted rat myocardium using a combination of small-animal PET and clinical MRI. *J Nucl Med*. 2007;48:288-94
81. Buscher K, Judenhofer MS, Kuhlmann MT, et al. Isochronous assessment of cardiac metabolism and function in mice using hybrid PET/MRI. *J Nucl Med*. 2010;51:1277-84
82. Qiao H, Zhang H, Zheng Y, et al. Embryonic stem cell grafting in normal and infarcted myocardium: serial assessment with MR imaging and PET dual detection. *Radiology*. 2009;250:821-9
83. Liu J, Narsinh KH, Lan F, et al. Early stem cell engraftment predicts late cardiac functional recovery: preclinical insights from molecular imaging. *Circ Cardiovasc Imaging*. 2012;5:481-90
84. Calcagno C, Cornily JC, Hyafil F, et al. Detection of neovessels in atherosclerotic plaques of rabbits using dynamic contrast enhanced MRI and 18F-FDG PET. *Arteriosclerosis, Thrombosis, and Vascular Biology*. 2008;28:1311-7
85. Majmudar MD, Yoo J, Keliher EJ, et al. Polymeric nanoparticle PET/MR imaging allows macrophage detection in atherosclerotic plaques. *Circ Res*. 2013;112:755-61
86. Millon A, Dickson SD, Klink A, et al. Monitoring plaque inflammation in atherosclerotic rabbits with an iron oxide (P904) and (18)F-FDG using a combined PET/MR scanner. *Atherosclerosis*. 2013;228:339-45
87. Vucic E, Dickson SD, Calcagno C, et al. Pioglitazone modulates vascular inflammation in atherosclerotic rabbits noninvasive assessment with FDG-PET-CT and dynamic contrast-enhanced MR imaging. *JACC Cardiovasc Imaging*. 2011;4:1100-9
88. Uppal R, Catana C, Ay I, et al. Bimodal thrombus imaging: simultaneous PET/MR imaging with a fibrin-targeted dual PET/MR probe—feasibility study in rat model. *Radiology*. 2011;258:812-20
89. Ramaswamy AK, Hamilton M 2nd, Joshi RV, et al. Molecular imaging of experimental abdominal aortic aneurysms. *ScientificWorldJournal*. 2013;2013:973150
90. Frullano L, Catana C, Benner T, Sherry AD, Caravan P. Bimodal MR-PET agent for quantitative pH imaging. *Angewandte Chemie International Ed In English*. 2010;49:2382-4 

Methodological aspects of PET/MR imaging

M. Yaqub, PhD¹, D.E. Oprea-Lager, MD¹, M.B.M. Hofman, PhD², R. Boellaard, PhD¹

¹Department of Radiology & Nuclear Medicine, VU University Medical Centre, Amsterdam

²Department of Physics & Medical Technology, VU University Medical Centre, Amsterdam

Abstract

Yaqub M, Oprea-Lager DE, Hofman MBM, Boellaard R. Methodological aspects of PET/MR imaging.

This paper discusses the methodological aspects of combined position emission tomography (PET) and magnetic resonance imaging (MRI). A short introduction of integrated PET/MRI systems will be given followed by a discussion on methodological aspects of combined PET/MR imaging with a main focus on PET performance. Finally, first (clinical) experiences with the Philips Ingenuity PET/MRI at the VU University Medical Center will be presented. **Tijdschr Nucl Geneesk 2013; 35(4):1153-1159**

Introduction

Position emission tomography (PET) allows for *in vivo* imaging and quantification of tissue function (1). PET is an important imaging modality in oncology and, apart from its diagnostic use, it can be used to study (changes in) physiology and measure the impact of a drug on (molecular) tumor response (2). It is also intensively used to investigate neurodegenerative processes in the brain (3-7). PET is an extremely sensitive imaging modality for which only small amounts of radiolabelled molecules (tracers, ~nM) need to be injected. The measurement of the tracer distribution in the body allows for quantitative assessment of tissue function without affecting the underlying physiology. PET is used to quantify perfusion, metabolism, enzyme activity, receptor density, neurotransmitter release and drug tumor targeting. Although PET provides valuable pharmacokinetic, metabolic and/or molecular information, its anatomical detail is limited due to the low resolution (6-7 mm). Furthermore, tracer distribution does not necessarily coincide with anatomical boundaries or structures. Therefore, combining molecular and anatomical information can provide complementary information, thereby enhancing the diagnostic accuracy. Structural imaging can be performed using e.g. computed tomography (CT) or magnetic resonance imaging (MRI).

MRI is used in clinical practice because of its high soft tissue contrast. The MRI signal intensity can be attributed to proton density. MRI allows the acquisition of various relaxation parameters, such as T1, T2, each providing specific soft tissue contrasts. Moreover MRI has a high spatial resolution and may provide information on specific metabolic processes *in vivo* using techniques such as MR spectroscopy (MRS).

Over the past decade multimodality imaging systems have been introduced, with the purpose of directly combining the specific information that each modality can provide. The combination of PET with CT, for example, resulted in improved diagnostic accuracy by an improved localisation of the functional processes. However, for specific anatomical locations, such as head and neck or brain, CT images may suffer from poor soft tissue contrast in comparison with MRI. Finally, the use of CT results in additional radiation exposure to the patients. This aspect may be relevant in the case of longitudinal studies with young adults with a long life expectancy (e.g. lymphoma).

Recently, clinical whole body PET/MRI systems have been introduced to combine PET molecular imaging with MRI soft tissue contrast and diagnostic information (8, 9). Systems were designed in such a manner that the image quality and quantitative accuracy of the PET in the PET/MRI systems were comparable to that of the current PET/CT systems. However, replacement of the CT with MRI data resulted in loss of accuracy of the attenuation correction of PET data. For example, MRI based attenuation correction (MR-AC) ignores bone, assumes uniform attenuation coefficients in lungs and suffers from MRI truncation due to relatively small transaxial field of view. These all result in quantitative biases in the reconstructed PET images. In the following sections we will discuss in detail the methodological aspects of combined PET/MR imaging.

Current design of PET/MRI systems

Combining PET and MRI systems into a single multimodality system needed a careful design of several hardware components. The MRI requires well-controlled and uniform magnetic and radio frequency (RF) fields (9). Therefore, any unshielded additional electronic hardware can affect the accuracy and quality of MR images. Furthermore, (PET) electronic hardware could breakdown or stop working correctly inside strong magnetic and RF fields. In particular, photo-multiplier tubes (PMTs), which are needed to convert and amplify signals from scintillation crystals into electronic signals (1), do not function properly in, or near, strong magnetic fields.

Integrating PET PMTs within an MRI has proven to be a difficult task requiring vendors to either opt for avalanche photodiodes (LSO-APDs, (10)) or physically separate the PET and MRI units. The performance of APDs, used to replace PMTs, is not affected by strong magnetic fields. However, the tradeoff is that APDs have a poorer timing resolution than PMTs. Thus, the PET/MRI systems, where the PET detectors are based on APDs, do

not have time-of-flight capabilities (TF, (11)). PMTs can only be used if the PET unit is placed sufficiently far away from the MRI unit such that the magnetic field strength at the position of the PET unit is very low. Future PET systems may contain new detectors, such as silicon photon multipliers (SiPM) (12, 13). These detectors are not sensitive to the magnetic field and have excellent timing resolution, making them suitable to generate TF information, while being integrated inside the MRI system.

Currently, three commercial whole body PET/MRI imaging systems are available (table I). General Electric (GE) has built a tri-modality PET/CT + MRI system (tri-modality, Discovery PET/CT 690 (14) & 3T Discovery MRI 750). To this end, the PET/CT and MRI units were placed in two adjacent rooms. A special patient table was designed that can be moved from the PET/CT to the MRI unit (and vice versa) without changing the patient position on the imaging bed. In principle, the system allows for the acquisition of PET, CT and MRI data that are inherently aligned/fused. Clearly, the downside of this design is that it requires (interactive) movement of the imaging bed and patient between PET/CT and MRI, potentially increasing the radiation dose to the technologists. Moreover, patient motion may occur during transport. The main advantage is that both systems can be operated independently and that PET attenuation correction is not hampered by limitations of MRI based attenuation correction. Furthermore, information from three different imaging modalities can be combined and visualised without the need for dedicated image registration software. The patient is scanned in the same position and posture on all three modalities and images are thus inherently co-registered. Siemens has built a fully integrated PET/MRI system (Siemens 3T Biograph mMR, (8)). This system is the only PET/MRI that allows for true simultaneous PET and MRI acquisitions, which ensures the best co-registration of both image datasets and minimises the 'dead time' in clinical

workflows. The PET system is equipped with APD based detectors and, consequently, the PET/MRI system does not have TF functionality.

Philips has built a sequential PET/MRI (Ingenuity TF PET/MRI, (9)) system with a rotating table, moving the patient from the MRI to the PET without changing patient position. The PET is placed at a ~3 m distance from the actively shielded MRI. Therefore, it was possible to use conventional PET technology based on PMTs. Consequently, the PET unit is hardware and performance wise comparable to that of a regular Philips Gemini PET/CT (15).

Technical PET performance of commercially available systems

Nowadays commercially available clinical PET/MRI systems have a high-end MRI unit which is generally not limited by the presence of a PET system. A detailed analysis of MRI performance issues in integrated/combined PET/MRI systems is beyond the scope of this review.

In order to assess PET performance and image quality, both NEMA NU-2 performance tests (16) and assessments of attenuation correction have been studied. NEMA NU-2 describes a series of (phantom) experiments to evaluate PET scanner performance characteristics, such as resolution, sensitivity, scatter fraction, count rate performance, count rate correction accuracy and image quality. Table II provides an overview of some NEMA NU-2 performance evaluation results as published for the various systems. In general, no large differences in performance are observed between the various listed systems. It can also be concluded that NEMA NU-2 performance characteristics of PET/MRI systems are comparable to those usually observed on the clinical whole body PET/CT systems. The only exception is the slow timing resolution of the Siemens Biograph mMR, which is the consequence of using APDs (and therefore no TF), as explained before.

Table I. Overview of some functionality on various commercially available whole body PET/MRI systems.

functionality	Siemens	Philips	GE
simultaneity of PET and MRI scans	+ (integrated)	-/+ (in-line)	- (sequential)
overall examination time	+ (integrated)	-/+ (in-line)	- (sequential)
PET attenuation correction	-/+ (MRAC)	-/+ (MRAC)	+ (CT based)
overall radiation dose of examination	-/+ (PET)	-/+ (PET)	- (PET & CT)
time-of-flight	- (APD)	+ (PMT)	+ (PMT)
use of non MRI compatible devices near PET gantry (blood sampling, shielding)	- (same gantry)	-/+ (3m distance)	+ (separate room)

+ = optimal, +/- = possible with known issues, - = not optimal

MRI based PET attenuation correction

Apart from the tri-modality system of GE, PET attenuation correction factors need to be derived from the MRI data collected during a PET/MRI examination. To this end, dedicated (fast) MRI sequences, such as DIXON (17) or atMR (18), are applied to obtain an image of tissue distribution. As MRI primarily measures proton density rather than attenuation coefficients, these MR images cannot be directly used to obtain 511 keV attenuation coefficients. Typically, the MR images collected for attenuation correction (MR-AC) are first segmented into various tissue classes, such as soft tissue (fat and/or water), lungs and air. Next, predefined attenuation coefficients are assigned to these tissue classes in order to derive an attenuation map for subsequent correction of the PET emission data during reconstruction. There are several limitations associated with the current MRI based attenuation correction (for both systems). A summary and review can be found in (19). In short, the limitations of MR-AC are:

1. The MRI has a limited transaxial FOV, which can result in MRI truncation artefacts and therefore in incomplete attenuation maps (figure 1). Some methods have been developed to compensate for truncation artefacts. For example, the outer contour of the patient may first be estimated from a non-attenuation corrected PET image and missing information in the MR-AC attenuation image can then be filled in using the patient outer contour (20). The method, however, does not always provide satisfactory results, as can be seen in figure 1c.
2. Bones are not visible on MRI data and attenuation coefficients are simply set to that of soft tissue (figure 1). Additional ultra short echo-time (UTE) MRI sequences may be applied to visualise bones but these sequences are not yet routinely available on clinical systems (21).
3. Performance of MRI in the thorax is usually limited. In order to obtain attenuation coefficients for the lungs, they are first segmented from the dedicated MR-AC scan and subsequently a uniform attenuation coefficient value is assigned to all voxels indicated as lungs. This approach has several limitations. First of all, in reality attenuation is not uniform across the lungs and, secondly, incorrect or failing lung segmentation causes large attenuation correction artefacts. An example of such an artefact can be seen in figure 2.
4. Patient imaging table (no MRI signal) and MRI coils (used to collect data) are not visible in the MR-AC image. Consequently, attenuation from these structures can not be derived from the MRI data. Predefined attenuation maps (templates) for the patient imaging table and fixed (non-flexible) coils are usually added to the patient attenuation map prior to the PET reconstruction. These

Table II. Overview of NEMA NU-2 2007 performance characteristics for commercially available whole body PET/MRI systems (8,9,14). Gemini TF PET/CT NEMA NU2-2001 results were included for comparison (15).

PET gantry characteristics and NEMA NU-2 performances	Philips Gemini PET/CT	Philips Ingenuity PET/MRI	GE PET/CT Discovery 690 (used in tri-modality setup)	Siemens Biograph mMR
PET FOV axial (cm)	18	18	15.7	25.8
PET FOV transaxial (cm)	57.6	57.6	50-70	59.4
MRI or CT FOV transaxial (for attenuation)	CT	45	CT	50
average spatial resolution @ 1 cm off center (mm FWHM)	4.8	4.7	4.7	4.3
average spatial resolution @ 10 cm off center (mm FWHM)	5.1	5.1	5.3	5.5
timing resolution (ps)	585	525	544	2930
energy resolution (FWHM %)	11.5	12	12.4	11.5
sensitivity (average 0 & 10 cm) (cps / kBq)	6.6	7.1	7.5	14.4
max NECR (kcps) @ (kBq/mL)	125 @ 17.4	88.5 @ 13.7	139.1 @ 29.0	184 @ 23.1
scatter fraction @ NECR peak (%)	27	26	37	37.9

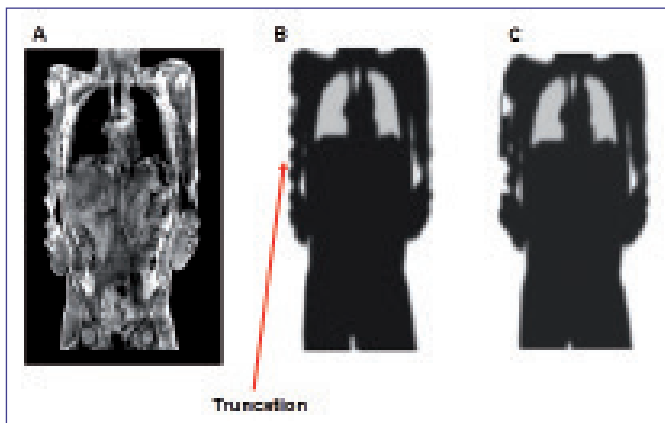


Figure 1. Truncation artefacts and absence of bone attenuation coefficients: (a) MRI scan used for attenuation correction purposes (MR-AC); (b) Attenuation map derived from the MR-AC and (c) attenuation map derived from MR-AC, including truncation correction.

templates are based on CT or PET transmission scans of the patient imaging table or MRI coils. However, the templates used during reconstruction can be mis-aligned with the actual coil position or not represent the actual attenuation of the used coils. The latter may occur when the coil used during template generation is not identical with the (newer) coils used on the PET/MRI system (figure 3).

New improved attenuation correction methods are still under development (21,22) and are part of future research (23). Moreover, despite the possible limitations of MR-AC, a good correspondence between PET/CT versus PET/MRI image quality and quantification is observed (21), but a careful inspection of the MRI based attenuation map is warranted in order to rule out severe attenuation artefacts. Similar to PET/CT studies, it is particularly important for PET/MRI studies to inspect the attenuation map as well as both AC-PET and NAC-PET images.

First (clinical) experiences with the Philips Ingenuity PET/MRI at the VU University Medical Center

The VUmc has recently purchased a Philips TF Ingenuity PET/MRI system, which is the first clinical whole body PET/MRI system in the Benelux. The system consists of a full ring PET system and a 3 Tesla MRI (figure 4). Details and performance characteristics have been described by Zaidi et al (9). The department of Radiology & Nuclear Medicine of the VUmc also has two Philips PET/CT systems. One of these systems (the Philips Gemini TF PET/CT) contains (nearly) identical PET hardware and reconstruction software. The only difference between PET/CT and PET/MRI examinations and consequently PET image quality would therefore be caused by the quality of the CT versus MRI based attenuation correction. The hybrid PET/CT and PET/MRI systems supplied by the same vendor, both equipped with a similar PET gantry, provide

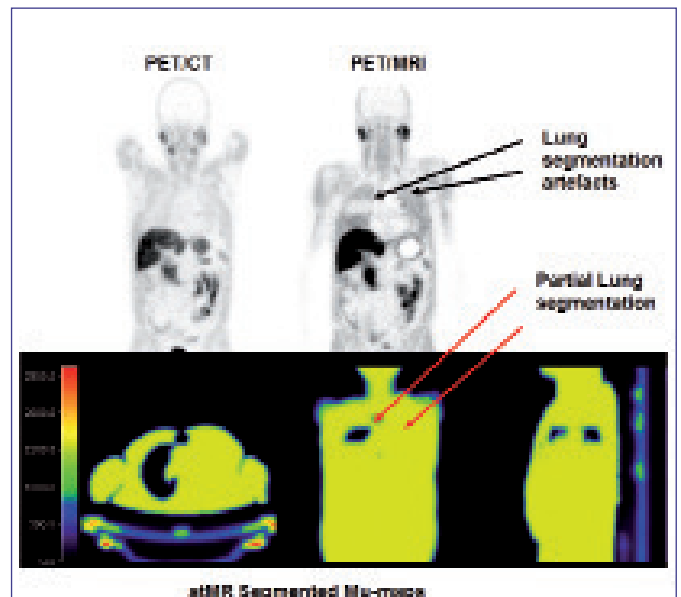


Figure 2. Impact of incorrect lung segmentation. AC-PET using CT based attenuation correction (top row, left figure). AC-PET using MRI based attenuation correction showing artificially increased uptake in the majority part of the lungs (top row, right figure) and corresponding MRI based attenuation map with incorrect lung segmentation. The incorrect lung segmentation resulted in overestimated lung activity concentration in the reconstructed PET/MRI study (top row, right figure).

therefore a unique opportunity to directly compare PET/CT and PET/MRI image quality and to evaluate the effects of using MRI versus CT based attenuation correction. Therefore, an image quality and quantitative performance comparison study was performed with two phantoms (i.e. NEMA NU-2 2007 image quality phantom and a brain phantom) (24) and ^{18}F -fluoromethylcholine (^{18}F -FCH) clinical WB PET studies (25).

The initial experiments revealed that calibration accuracy and image uniformities were comparable between the PET/MRI and the PET/CT systems (within ~5%). However, PET/MRI studies with additional MRI coils showed PET image artefacts (up to 15%) due to missing templates and/or use of metal objects within the coils which were not fully compensated in the atMR templates (figure 3). Standard uptake value (SUV) or contrast recoveries in the NEMA NU-2 2007 image quality phantom were comparable on both systems and met the EANM/EARL requirements. Contrast recovery in the brain phantom was only slightly (5%) lower in the PET/MRI compared to PET/CT, possibly due to limitations in the experimental atMR. In short, initial experimental experiences at VUmc confirmed that basic PET performance characteristics of the Philips PET/CT and PET/MRI systems are similar.

After completing experimental validations and evaluations, a first clinical comparison study was performed. To this end, ^{18}F -FCH PET/MRI and PET/CT whole body studies were performed for restaging in patients with histologically

proven prostate cancer (PCa). This tracer was selected due to minimal changes in uptake and distribution at 30 to 90 min post injection (p.i.) and therefore comparable tracer distributions between sequential PET/CT and PET/MRI may be expected. Six patients (mean age 64 ± 7 years) with relapsing PCa were included. Patients were initially examined using the

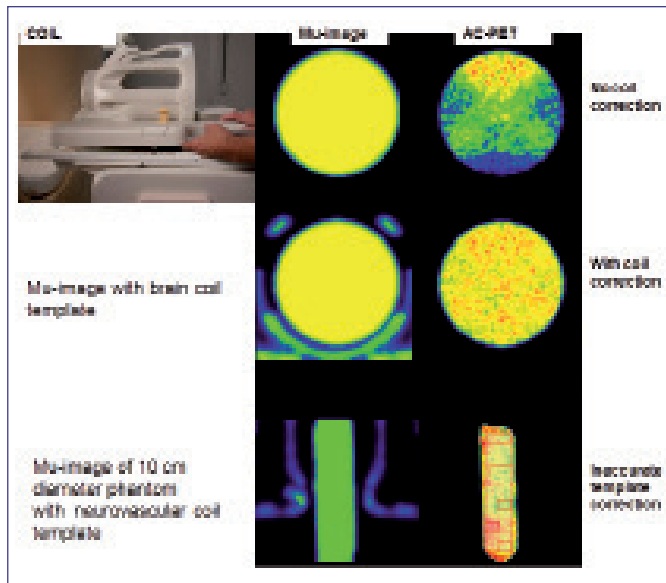


Figure 3. Attenuation artefacts in the reconstructed PET scans of uniformly filled cylindrical phantoms. AC-PET non-uniformity due to missing attenuation template of the MRI coil in the attenuation map (top row). AC-PET became uniform after including the attenuation template of the MRI coil in the attenuation map (middle row). AC-PET non-uniformities due to incorrect or misaligned neurovascular MRI coil template (bottom row).

Philips Gemini TF PET/CT system (30 min p.i., ~ 350 MBq) and subsequently studied using the Philips Ingenuity TF PET/MRI (~ 90 min p.i.). Typical PET/CT and PET/MRI images in one patient are shown in figure 5 and illustrate that (visual) PET image quality for both modalities are comparable. Quantitative evaluation of lesional maximum SUVs derived from PET/MRI and PET/CT showed a good agreement of $6\% \pm 28\%$ ($R^2=0.80$, slope=1.04, figure 6). In normal tissues, PET/MRI SUVs were, however, $17\% \pm 9\%$ lower than those seen in PET/CT. The largest quantitative deviations (up to -40%) were found in the lungs. Two out of the six patients showed severe artefacts in the thorax region in the PET/MRI images, which were caused by incorrect lung segmentation in the MRI attenuation map (figure 2). For clinical use of PET/MRI it is therefore essential that readers are able to interpret both attenuation and non-attenuation corrected images to avoid incorrect conclusions from severe attenuation correction artefacts. The first step in the review process should be the inspection of the attenuation image.

Summary

At present, two integrated commercial PET/MRI systems are available. The Siemens 3T Biograph mMR is fully integrated and allows for the simultaneous acquisition of both PET and MRI data. In order to place the PET within the MRI, PET detectors based on APDs were used, thereby sacrificing TF capability of PET. The Philips Ingenuity TF PET/MRI is designed as an in-line sequential system, allowing the acquisition of both PET and MRI data in a single imaging session, but not truly simultaneously. Moreover, state-of-the-art PET technology could still be used, thereby guaranteeing similar PET performance to the current TF PET/CT systems. Both PET/MRI



Figure 4. Philips Ingenuity TF PET/MRI (left figure) and Gemini TF PET/CT at the VUmc (right figure).

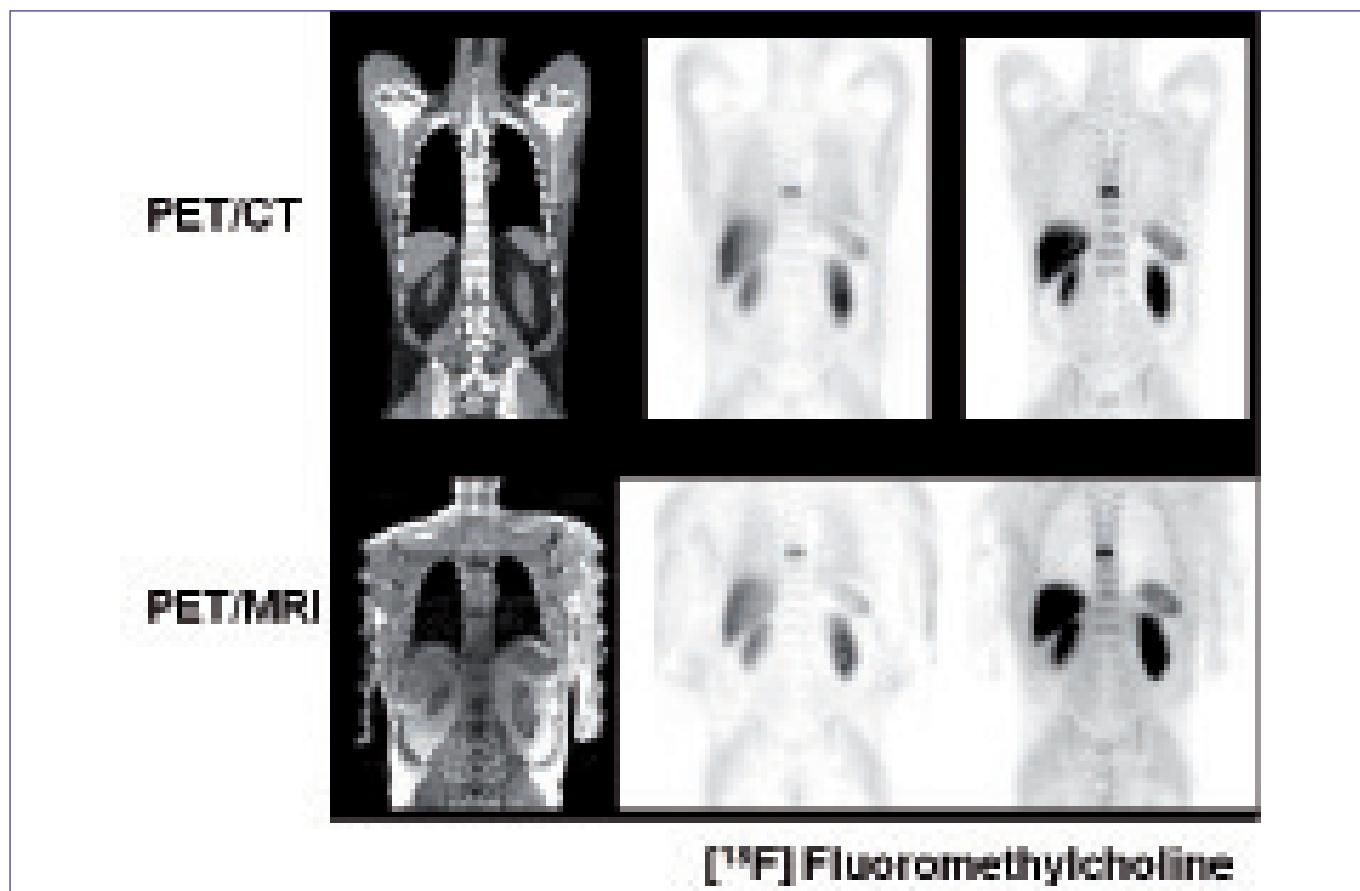


Figure 5. Typical PET/CT and PET/MRI images for ^{18}F -fluoromethylcholine studies illustrating comparable PET image quality for both modalities.

systems have PET and MRI performance characteristics that are comparable to their equivalent PET/CT and MRI counterparts (apart from TF performance for the Siemens mMR). Initial clinical evaluations have shown that PET/(MRI) image quality is equivalent to that of PET/CT studies and sufficient for visual interpretation, providing readers inspect the attenuation maps as well as AC-PET and NAC-PET images. Regardless of the system being used, attenuation correction of PET data needs to be derived from MRI. As MRI data do not represent attenuation coefficients and various attenuating materials (patient imaging table, MRI coils) are not visible in the MR image, MRI based attenuation correction is challenging and frequently (~10-20% of cases) suffers from large artefacts. Therefore, future research focuses on solving the limitations of the current MR-AC methodology in order to enhance the quantitative accuracy of PET/MRI studies.

E-mail address for correspondence: r.boellaard@vumc.nl

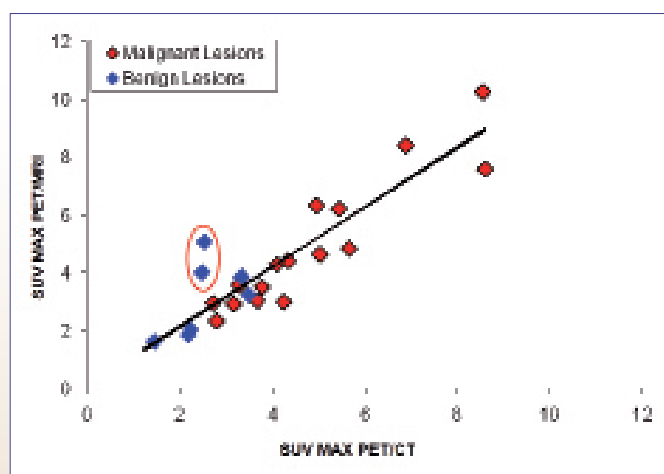


Figure 6. ^{18}F -fluoromethylcholine lesional SUV_{max} derived from PET images acquired using the Ingenuity TF PET/MRI versus Gemini TF PET/CT. For two lesions (indicated within the red circle) SUVs seen on PET/MRI were substantially higher than those seen on PET/CT, which was explained by severe MRI based attenuation artefacts in the lungs, as shown before in figure 2.

References

1. Ter Pogossian MM, Phelps ME, Hoffman EJ, Mullani NA. A positron-emission transaxial tomograph for nuclear imaging (PETT). *Radiology*. 1975;114:19:89-98
2. Weber WA. Assessing tumor response to therapy. *J Nucl Med*. 2009;50 Suppl 1:1S-10S
3. Schuitemaker A, van der Doef TF, Boellaard R, et al. Microglial activation in healthy aging. *Neurobiol Aging*. 2012;33:1067-77
4. Tolboom N, Yaqub M, van der Flier WM, et al. Detection of Alzheimer Pathology In Vivo Using Both 11C-PIB and 18F-FDDNP PET. *J Nucl Med*. 2009;50:191-7
5. Van Berckel BN, Bossong MG, Boellaard R, et al. Microglia activation in recent-onset schizophrenia: a quantitative (R)-[11C] PK11195 positron emission tomography study. *Biol Psychiatry*. 2008;64:820-2
6. Van Berckel BN, Ossenkuppele R, Tolboom N, et al. Longitudinal Amyloid Imaging Using 11C-PiB: Methodologic Considerations. *J Nucl Med*. 2013;54:1570-6
7. Yaqub M, Boellaard R, van Berckel BN, et al. Quantification of dopamine transporter binding using [18F]FP-beta-CIT and positron emission tomography. *J Cereb Blood Flow Metab*. 2007;27:1397-406
8. Delso G, Furst S, Jakoby B, et al. Performance measurements of the Siemens mMR integrated whole-body PET/MR scanner. *J Nucl Med*. 2011;52:1914-22
9. Zaidi H, Ojha N, Morich M, et al. Design and performance evaluation of a whole-body Ingenuity TF PET-MRI system. *Phys Med Biol*. 2011;56:3091-106
10. Pichler BJ, Judenhofer MS, Catana C, et al. Performance test of an LSO-APD detector in a 7-T MRI scanner for simultaneous PET/MRI. *J Nucl Med*. 2006;47:639-47
11. Surti S, Scheuermann J, El FG, et al. Impact of time-of-flight PET on whole-body oncologic studies: a human observer lesion detection and localization study. *J Nucl Med*. 2011;52:712-9
12. Levin C, Glover G, Deller T, et al. Prototype time-of-flight PET ring integrated with a 3T MRI system for simultaneous whole-body PET/MR imaging [abstract]. *J Nucl Med*. 2013;(54 (Supplement 2)):148
13. Schaart DR, van Dam HT, Seifert S, et al. A novel, SiPM-array-based, monolithic scintillator detector for PET. *Phys Med Biol*. 2009;54:3501-12
14. Bettinardi V, Presotto L, Rapisarda E, et al. Physical performance of the new hybrid PETCT Discovery-690. *Med Phys*. 2011;38:5394-411
15. Surti S, Kuhn A, Werner ME, et al. Performance of Philips Gemini TF PET/CT scanner with special consideration for its time-of-flight imaging capabilities. *J Nucl Med*. 2007;48:471-80
16. Rosslyn VA. NEMA Standards Publication NU2-2007: Performance Measurements of Positron Emission Tomographs. NEMA; 2007
17. Martinez-Moller A, Souvatzoglou M, Delso G, et al. Tissue classification as a potential approach for attenuation correction in whole-body PET/MRI: evaluation with PET/CT data. *J Nucl Med*. 2009;50:520-6
18. Hu Z, Ojha N, Resnick SM, et al. MR-based attenuation correction for a whole-body sequential PET/MR system [abstract]. *Proc IEEE Med Imaging Conf*. 2009;3508-12.
19. Andersen FL, Ladefoged CN, Beyer T, et al. Combined PET/MR imaging in neurology: MR-based attenuation correction implies a strong spatial bias when ignoring bone. *Neuroimage*. 2013;84C:206-16
20. Delso G, Martinez-Moller A, Bundschuh RA, Nekolla SG, Ziegler SI. The effect of limited MR field of view in MR/PET attenuation correction. *Med Phys*. 2010;37:2804-12
21. Bezrukov I, Mantlik F, Schmidt H, Scholkopf B, Pichler BJ. MR-Based PET attenuation correction for PET/MR imaging. *Semin Nucl Med*. 2013;43:45-59
22. Hofmann M, Bezrukov I, Mantlik F, et al. MRI-based attenuation correction for whole-body PET/MRI: quantitative evaluation of segmentation- and atlas-based methods. *J Nucl Med*. 2011;52:1392-9
23. Boellaard R, Hoekstra OS, Pieters - van den Bos I, Hofman M, Lammertsma AA. Accurate whole body PET/MR quantification using TF and MLAA reconstruction [abstract]. *J Nucl Med*. 2013;54(suppl2):46P
24. Yaqub M, Horstman P, Oprea-Lager DE, et al. Imaging performance of Ingenuity TF PET/MR versus Gemini TF PET/CT [abstract]. *Eur J Nucl Med Mol Imaging*. 2013;40 (suppl2):S86
25. Oprea-Lager DE, Yaqub M, Jongsma F, et al. Comparison of image quality and quantification between Philips Ingenuity TF PET/MRI and Gemini TF PET/CT data in prostate cancer patients [abstract]. *Eur J Nucl Med Mol Imaging*. 2013;40(suppl2):S164 

Towards multiparametric medical imaging with PET/MRI: current clinical status

D.E. Oprea-Lager, MD¹, J. Löfgren, MD PhD², P.G. Raijmakers, MD PhD¹, I. Law, MD PhD², B.N.M. van Berckel, MD PhD¹, C.J. van der Laken, MD PhD³, I.C. Pieters-van den Bos, MD PhD¹, A. Kjaer, MD PhD²

¹Departments of Radiology & Nuclear Medicine, VU University Medical Centre, Amsterdam, the Netherlands

²Department of Clinical Physiology, Nuclear Medicine & PET, Rigshospitalet, Copenhagen, Denmark

³Departments of Rheumatology, VU University Medical Centre, Amsterdam, the Netherlands

Abstract

Oprea-Lager DE, Löfgren J, Raijmakers PG, Law I, van Berckel BNM, van der Laken CJ, Pieters-van den Bos IC, Kjaer A. Towards multiparametric medical imaging with PET/MRI: current clinical status. Hybrid PET/MRI is the obvious next step towards integration of multiparametric imaging data into clinical medicine and medical research. It provides structural, functional and biochemical information at the same time. To date, a few years after the commercial launch of the first generation of scanners, the technique is in its infancy, and several technical hurdles still need to be dealt with. Efficient workflows eliminating redundant information are required to get the best out of the two worlds without compromising the quality of the individual components. Integration of PET and MRI science requires an additional effort but at the same time this process nicely fits in the current perspective of an integrated imaging profession. In this article, the authors provide an overview of the current clinical data on PET/MRI and a perspective on some potential applications in the near future, with a focus on oncology, neurology, cardiovascular diseases and rheumatology. **Tijdschr Nucl Geneesk 2013; 35(4):1160-1171**

Introduction

Only a decade after the successful introduction of positron emission tomography combined with computed tomography (PET/CT), integration of PET with magnetic resonance imaging (PET/MRI) was introduced clinically as the next hybrid imaging option. Since these two modalities (i.e., PET and MRI) are not easily combined in a single scanner, its design has taken years of technical research. To date, there are two options: an integrated system housing both components in a single gantry, or a geometrically separated PET and MRI on either side of a rotating table. The former has the obvious advantage of truly simultaneous image acquisition, and the latter does not require any concession for either component.

Clinically, the paradigm change towards individualised 'tailored' therapy leads to an increased need for routine diagnosis at a molecular level. Most molecular biology methods mandate tissue sampling for in vitro analysis. In contrast, molecular imaging allows for non-invasive studies at the molecular level in living, intact organisms. Medical imaging can provide anatomical, biological and pharmaceutical information in individual patients, accounting for heterogeneity at each of these levels, non-invasively and at a quantitative level. Therefore medical imaging is a logical link between in vitro sciences and clinical medicine. However, no current imaging modality can cover the full spectrum of data required for personalised medicine by itself: PET only measures a single molecular process at the same time, and MRI has significant limitations with respect to molecular contrast. With respect to PET/MRI systems versus PET alone systems, MRI data adds functional parameters to the PET information (1,2), including cellular density (using diffusion-weighted imaging (DWI)), angiogenic and perfusion characteristics (using intravenous contrast; dynamic contrast-enhanced (DCE)), tractography in cerebral white matter, real-time cardiac contractility and movement, metabolic data by spectroscopy, information on oxygenation (blood-oxygen-level-dependent (BOLD) imaging), etc. Moreover, MRI has some obvious advantages versus CT, including lack of radiation exposure and superior soft-tissue contrast.

Whilst in the case of PET/CT, the merged modality quickly found its way in routine daily practice, PET/MRI is facing a number of technical challenges that never were an issue for PET/CT (3). These issues require a high level of multidisciplinary collaboration in order to capitalise the full multiparametric potential of PET/MRI. However, the current challenge is to make PET/MRI suitable for clinical practice. To some extent, implementing PET/MRI is also challenging for its individual components: for PET to validate new radiotracers demonstrating differences in cancer phenotypes between and within patients, and for MRI to achieve proper platform-independent standardisation. Current clinical applications with PET/MRI are still in their infancy. Here we provide an overview of some of its potential in the clinical domains of oncology, neurology, cardiovascular diseases and rheumatology.

Oncology

CT and PET/CT are the workhorses of current oncological imaging practice. Using either common sense, or co-registered PET and MRI data, several authors have speculated on the potential added value of PET/MRI versus PET/CT, even before the commercial launch of PET/MRI (1, 2, 4-6). Due to its superior soft-tissue contrast in soft-tissue sarcoma, brain -, head and neck -, gynaecological -, breast - and prostate cancer, MRI is the obvious alternative for CT in tumour delineation (T-stage; figure 1) (7-9). Some authors speculated that this improved soft-tissue contrast would be the only advantage of PET/MRI over PET/CT, and that all other indications might remain within the realm of PET/CT (4). In paediatric oncology, the lower radiation dose with PET/MRI is an obvious advantage but it comes with a price if MRI requires anaesthesia during acquisition.

At the same time, several functional MRI techniques are currently under investigation to improve the accuracy of structural MRI (which includes standard T1 and T2-weighted sequences with or without the administration of intravenous contrast). These include e.g. diffusion-weighted imaging (DW-MRI) already shown to improve lesion detection as well as tissue characterisation versus routine MRI sequences

(10,11), 'perfusion-weighted imaging' (PW-MRI) allowing for more exact quantification of inflow, permeability, as well as outflow of contrast agents (12), and MRI spectroscopy. As a consequence, acquisition duration is a common challenge for PET/MRI, and it remains to be settled which MRI procedures really add to the diagnostic interpretation.

As expected in initial phases of innovative technologies, the first published studies actually using PET/MR scanners focused on aspects of *technical feasibility*: PET image quality and the reliability of localising PET findings on MRI instead of CT images (9) and *workflow optimisation* (7), often in a broad spectrum of oncology patients. Previously, some studies had used co-registered MRI and PET/CT with post hoc image fusion as an indication of what might be expected from PET/MRI. Kim et al suggested a potential use for PET/MRI for detection of metastatic lymph nodes in uterine cervical cancer (13). More recently, Nagamachi et al suggested that specificity, and to a lesser extent sensitivity, may be improved by PET/MRI in the diagnosis of solid type pancreatic cancer (14). Recently, Brendle et al reported that hybrid datasets were more accurately aligned than could be achieved with post-hoc image fusion (15). Buchbender et al (5) suggested

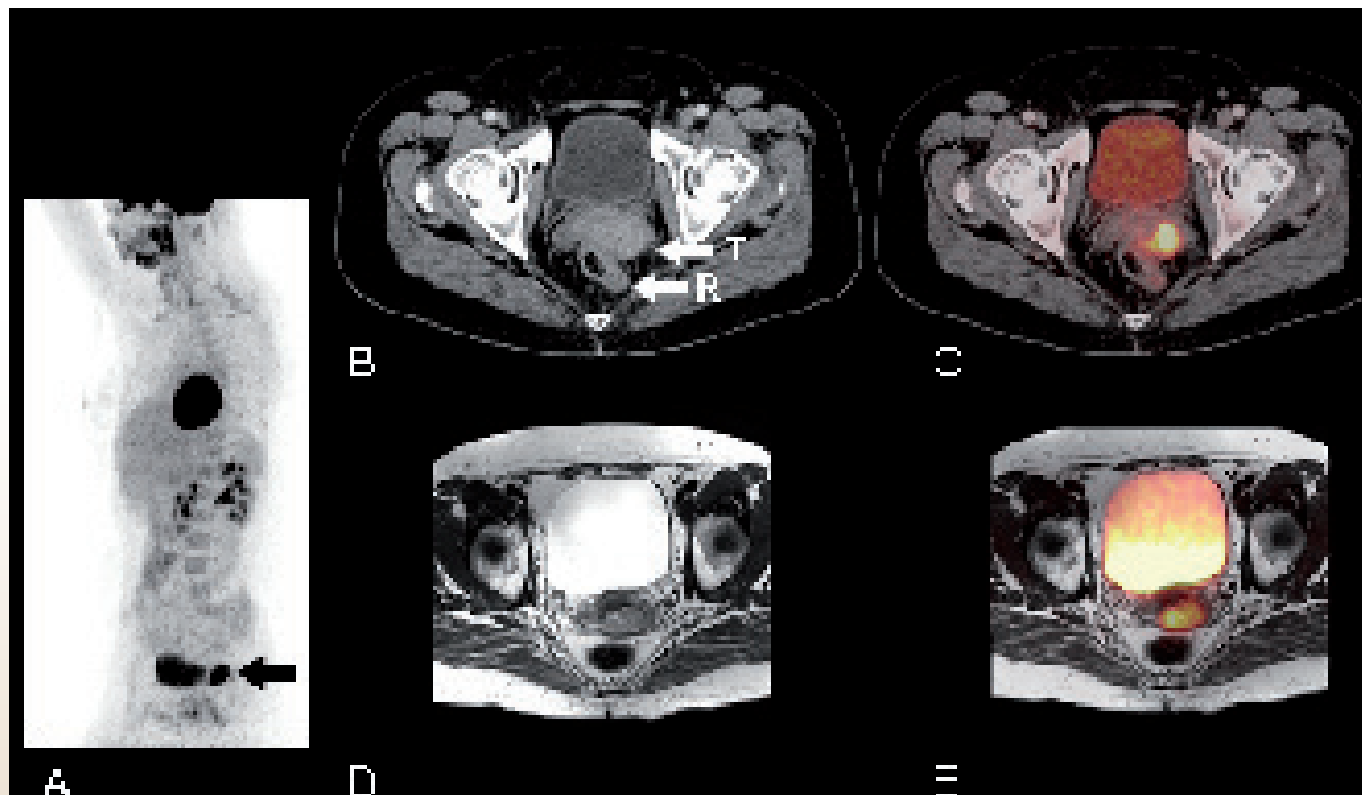


Figure 1. 42-year old female with cervical cancer. ^{18}F -FDG-PET (A) shows increased uptake in the lower pelvis. CT (B) and PET/CT (C) locate hypermetabolism to the cervix with questionable invasion of the rectum. PET/MRI (D, E) in combination with sagittal T2w-MR (F) helps to exclude rectal invasion (illustration with permission reproduced from reference 8).

that the added value of PET/MRI might especially be expected in improved lesion characterisation by MRI in combination with the whole body capability of PET. With primary bone tumours, soft tissue sarcomas and melanoma it was suggested that PET/MRI offers both an accurate one stop TNM staging procedure (added value of PET for biopsy / surgical planning and N- and M-staging) as well as improved assessment of therapy response in the former two diseases and lymphoma. We will briefly discuss some PET/MRI studies that focussed on specific cancer types.

The current clinical indications for hybrid (i.e., PET/CT) ^{18}F -fluorodeoxyglucose (^{18}F -FDG) imaging in *head and neck cancer* mainly consist of detection and staging of unknown primary tumours, screening for distant metastases in high-risk patients, and diagnosis and restaging of recurrence after (chemo)radiotherapy (7-16). There is evidence to suggest that ^{18}F -FDG may predict response during induction therapy of head and neck cancer. However, this requires appropriate PET quantification, but attenuation correction for whole-body PET/MRI is still challenging (3).

At the same time, MRI is the anatomical imaging method of choice in this field, and the diagnostic CT information of PET/CT is considered redundant compared with head and neck MRI. Moreover, accurate image fusion using data from two separately acquired scans is very difficult in head and neck cancer, and it often requires rigorous patient immobilisation during scans (e.g. with radiotherapy masks). Taken together, oncological imaging of head and neck area is an obvious opportunity for PET/MRI clinical research. In a feasibility pilot study of eight patients with head and neck malignancy, ^{18}F -FDG PET/CT was followed by simultaneous PET/MRI (17). The study was performed with a prototype of an integrated PET/MR system (without time-of-flight (TOF) capability). The MRI image quality was excellent without PET-induced artefacts and near-perfect agreement of metabolic ratios (tumour versus cerebellum) obtained from both systems (PET/CT versus PET/MRI). In another feasibility study, Platzeck reported on sequentially acquired TOF PET/MRI (18) in twenty patients with histologically proven squamous cell carcinoma of the head and neck region. Again, PET/MRI acquisitions (40 minutes) were performed after ^{18}F -FDG PET (HR+ scanner in 2D or 3D mode). Image quality was deemed appropriate without MRI-induced artefacts in the PET images. For lymph nodes, any lesion that appeared to have increased ^{18}F -FDG uptake in comparison to salivary glands and muscles were considered malignant. This resulted in 64% higher detection of possible malignant lymph nodes for PET/MRI compared to PET alone. However, there was no histopathological verification, nor any assessment of the interaction of PET and MRI readings. As the authors acknowledge, the PET components of both scanners were different (TOF versus non-TOF, hybrid versus non-hybrid, crystal type) as well as the tracer uptake intervals. The time interval between PET and PET/MRI acquisitions at least partly explains why they found higher SUV values in primary

tumours. One of the challenges in head and neck imaging will be that MRI is quite sensitive to motion artefacts induced by swallowing, coughing etc.

A few PET/MRI studies have been performed in *prostate cancer* (PCa) patients using choline-based radiopharmaceuticals. Choline PET is primarily indicated to diagnose and restage patients with a biochemical relapse of disease (19), as revealed by elevated plasma prostate-specific antigen (PSA) levels (20) or by a PSA doubling time within 6 months and/or PSA increment greater than 1 ng/mL per year (21). At primary presentation, staging with choline PET is not sufficiently reliable. Multiparametric MRI is subject of intensive research and seems to have a role in several clinical PCa problems: in patients with previous negative prostate biopsies and elevated PSA, to assess tumour aggressiveness, local staging and in early identification of local recurrence in patients with biochemical recurrence (22). Hence, current choline PET and MRI applications are only partly overlapping, and it remains to be shown where, when applied in a PET/MRI setting, the two techniques are truly additive or merely redundant. In patients with proven prostate cancer Vargas et al described the problems and limitations common to all examinations as well as the specific prostate imaging difficulties, and proposed optimised protocols for the Philips Ingenuity TOF sequential PET/MRI system (7). In their hands, the optimal PET/MRI protocol consisted of pelvic and total body PET in combination with diagnostic MRI sequences; the trade-off between optimality and efficiency still needs to be established to reduce the scan duration without loss of diagnostic information. Wetter et al reported their initial experience with simultaneous ^{18}F -choline PET/MRI to diagnose prostate cancer (n=15 with suspected or proven prostate cancer). In their hands, PET and diffusion-weighted imaging (DWI) were highly correlated, and they suggested the PET component to add diagnostic confidence to the MRI-based parameters in identifying and localising tumour in the prostate (23). In an attempt to improve prediction of the Gleason score using semiquantitative PET and DW-MRI, Park (24) reported that the ratio of the standardised uptake value (SUV) of ^{11}C -choline PET and DW-MRI's apparent diffusion coefficient (ADC) maps were better correlated with Gleason scores than SUV and ADC individually (n=17). There are similar preliminary findings in lung cancer using ^{18}F -FDG suggesting that ADC and SUV may harbour independent biological information (25). To assess the performance of the integrated Siemens non-TOF PET/MRI scanner with ^{11}C -choline, Souvatzoglou et al studied 32 PCa patients referred for (re)staging. Patients underwent PET/CT (Biograph True-Point 64 PET/CT; 3 min/bed starting 5 min postinjection (p.i.)) followed by PET/MRI (4 min/bed starting 52 min pi) after a single tracer administration (26). The authors observed comparable lesion detectability (95% concordance in eighty lesions); lesion conspicuity tended to be better with PET/CT, but anatomical precision was better with PET/MRI. In many centres, MRI is considered a first-line imaging

modality for the evaluation of patients with potential *colorectal liver metastases* (27). While CT, PET and MRI have a similar sensitivity to detect larger hepatic metastases, DW-MRI outperforms CT in sub-centimetre lesions (28). In a recent meta-analysis, Wu et al reported a pooled sensitivity of DW-MRI of 0.87 (95%CI 0.80-0.91) and a specificity of 0.90 (95%CI 0.86-0.93) (29). Also, preliminary studies suggest potential utility of DWI with ADC quantification in response evaluation (30, 31). The largest series of whole body simultaneous ^{18}F -FDG PET/MRI (Siemens, mMR; head-to-head comparison with PET/CT) in patients with cancer and 'liver lesions' (n=70; e.g. melanoma, breast -, lung -, adenoid-cystic -, colorectal cancer and others; 26 metastases out of a total of 97 lesions) investigated several aspects of diagnostic performance: detection, conspicuity (visual rating of tumour to background contrast) and diagnostic confidence (32). Criteria of test positivity were predefined for (contrast-enhanced) CT and (gadolinium-enhanced and DW-) MRI, and separate readings of hybrid and individual modalities were performed by a team of two radiologists and two nuclear medicine physicians. Acknowledging the probable bias of the longer uptake interval favouring PET/MRI, the authors reported increased diagnostic confidence with PET/MRI versus PET/CT. The same group also recently published a pilot study on the use of ^{68}Ga -DOTATOC PET/MRI in patients with gastroenteropancreatic neuroendocrine tumours. The authors demonstrated the potential of PET/MRI for these lesions, but at the expense of decreased sensitivity for the detection of lung metastases and hypersclerotic bone metastases compared to PET/CT (33).

Vargas et al presented their initial clinical experience with the Ingenuity TOF system in 36 patients with *breast cancer* (7). The indications included locoregional staging of primary and recurrent breast tumours as well as the detection of distant metastases. The optimised protocol (best trade-off between acquisition duration and diagnostic value) consisted of specific MRI sequences (axial T2 FSE and 3D T1 Dixon) performed at predefined time points during image acquisition. Digital subtraction of the water-only Dixon images was also tested using dedicated MRI software. This sequence was used for the (co)interpretation of the images with PET. The authors elaborately discussed the protocol and provided recommendations to improve image quality. Both ^{18}F -FDG PET and MRI have potential to predict locoregional response to neoadjuvant therapy. However, it remains to be shown whether their information is additive or redundant.

Neurology

The main applications of PET/MRI in clinical neurology are to be found in the diagnosis of dementia and brain tumours. However, brain imaging already had the advantage compared to other clinical indications that movement of the brain is restricted by the skull making image fusion between single modality scans, e.g. PET and MRI, already very reliable. An important advantage of PET/MRI imaging above single

modality scanning is the one-stop-shop principle in which the patient conveniently has a PET and MRI in one session (figure 2). A major problem for clinical implementation of PET/MRI in neurology is the attenuation correction with MRI which does not take into account the attenuation from the skull as MRI 'does not see' it. As such the images that are generated by PET/MRI underestimate the real tissue distribution of the radiotracer. It has been estimated that uptake of radiotracers in grey matter just below the skull can therefore be underestimated by approximately 20%. For clinical practice this is a relevant problem especially when subtle changes are relevant (e.g. ^{18}F -FDG in treatment resistant epilepsy or in the diagnosis of frontotemporal dementia where subtle changes in temporal lobes can occur early during the disease). Thus, PET/MRI may have a decreased sensitivity compared to PET/CT, although in general patterns of hypometabolism they are very comparable. To a certain extent, the attenuation artefact with MRI can be circumvented by using a reference tissue approach as it is conceivable that the attenuation artefacts in the region of interest and the reference region are comparable. Indeed, in a pilot study using a ^{18}F -amyloid imaging tracer, PET/MRI (immediately following PET/CT) underestimated PET/CT values with only 5% (range 2-12%) which is acceptable for clinical purposes. In addition, the pattern of an 'amyloid-positive' scan is clearly different from an 'amyloid-negative' one, and this difference is also very clear on the PET-MRI image. As such a promising indication of PET/MRI imaging is in the diagnosis of *dementia* in which MRI is already standard practice in many centres. Adding an amyloid scan to this routine would greatly enhance diagnostic reliability of the neuroimaging part of the diagnostic procedure of dementia. In addition, it can be easily assessed if flow deficits using arterial spin labelling (ASL) can help in the differential diagnosis. Another approach to the problem of attenuation correction with MRI is to use a within-subject design (the patient as his own control), which is already done in research settings. For example, imaging of $\text{D}_{2/3}$ receptors with ^{11}C -raclopride before and after a pharmacological challenge is feasible without any problems on current PET/MRI systems. Finally, another strategy to address attenuation correction is to perform low-dose CT of the head and use this in the PET reconstruction (36). This is particularly important in brain tumours where titanium plugs are used to fixate the craniotomies.

PET/MRI in *brain tumours* may be one of its most obvious applications, since MRI already is the primary tool in routine clinical practice and various PET tracers significantly improve the diagnostic yield. The particular power of PET/MRI will be in the unique tailoring of individual measurements into comprehensive packages that can solve issues related to the particular disease stage. The general clinical question will be to identify active tumour tissue and delineate tumour. In glioma, the best PET tracer of choice will be a radiolabelled amino acid or amino acid analogue, such as ^{18}F -fluoroethyltyrosine (^{18}F -FET; figure 3). This group of

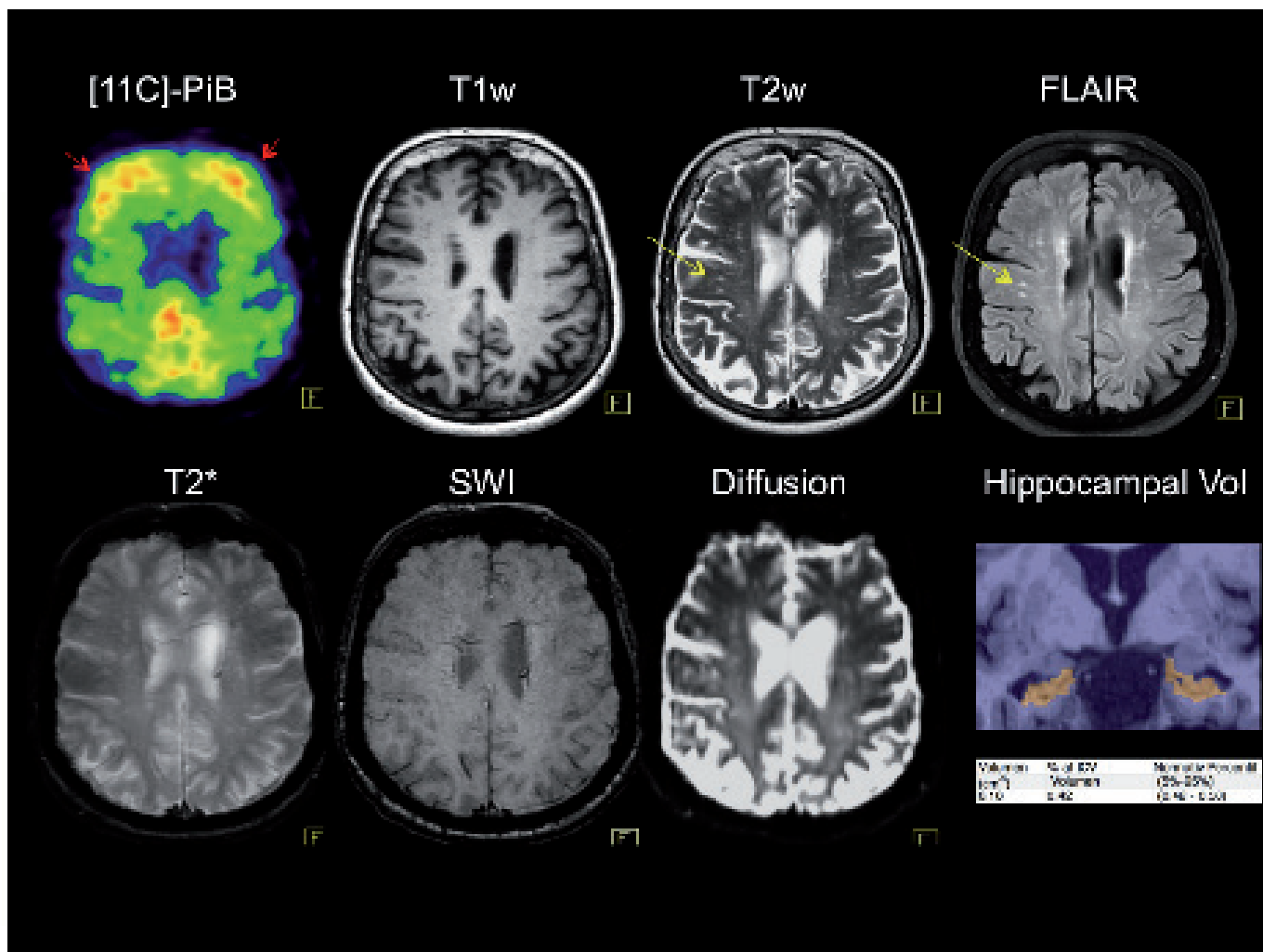


Figure 2. Comprehensive one-stop shopping identifying multiple risk factors for dementia. Patient suspected to suffer from Alzheimer's disease (72-year old female). Single session 30 minute ^{11}C -PiB PET/MR demonstrates significant cortical amyloid uptake (red arrow) with multiple white matter lesions indicative of chronic ischemia (yellow arrow), but without microhaemorrhages. The hippocampal volume is reduced by 2 standard deviations compared to an aged matched normal data.

tracers: 1) supplements conventional MRI by defining the infiltrative tumour components; 2) may improve accuracy of tumour grading, 3) suggests the optimal location for biopsy or resection, and 4) assists in radiotherapy planning (37). Functional MRI may complement this by defining angiogenic activity of the tumour through blood volume and/or vascular permeability measures using DCE T1 weighted imaging, dynamic susceptibility contrast (DSC) T2* (38) weighted imaging, or ASL. DWI-MRI may locate areas of particularly high cellularity. The above diagnostic program can be performed in only 25 minutes in a simultaneously acquiring PET/MRI system. If the study is performed preoperatively it can be supplemented with mapping of eloquent cortex (language, motor function) using BOLD-MRI and mapping of important white matter tracts using tractography (39). Thus, combined use of PET and MRI information may tailor the path for a particular patient, whereby the risks of intervention can be balanced accurately off with the risk of only a partial

resection.

During clinical follow-up, MRI performs less well as post-therapeutic changes accumulate following the mechanical trauma of repeated surgical interventions and the toxic trauma of concomitant radiation-chemotherapy. ^{18}F -FET PET combined with conventional MRI performs better than MRI alone, increasing sensitivity and specificity from 94% and 50% to 100% and 93%, respectively (40). In glioblastoma multiforme anti-angiogenesis treatment (e.g. bevacizumab) is routinely offered as 3rd line therapy in many countries. Some patients may develop a so-called 'pseudo-response', this means that the tumour manifestations on MRI showed marked regression, but with retained metabolic activity indicating viable tumour tissue (41). These patients may also benefit from combined ^{18}F -FET PET/MRI imaging with DCE T1 MRI perfusion (42) or vessel architectural imaging (43). Moreover, MRI spectroscopy can further characterise the tumour and therapy-induced changes (44). Figure 3 shows

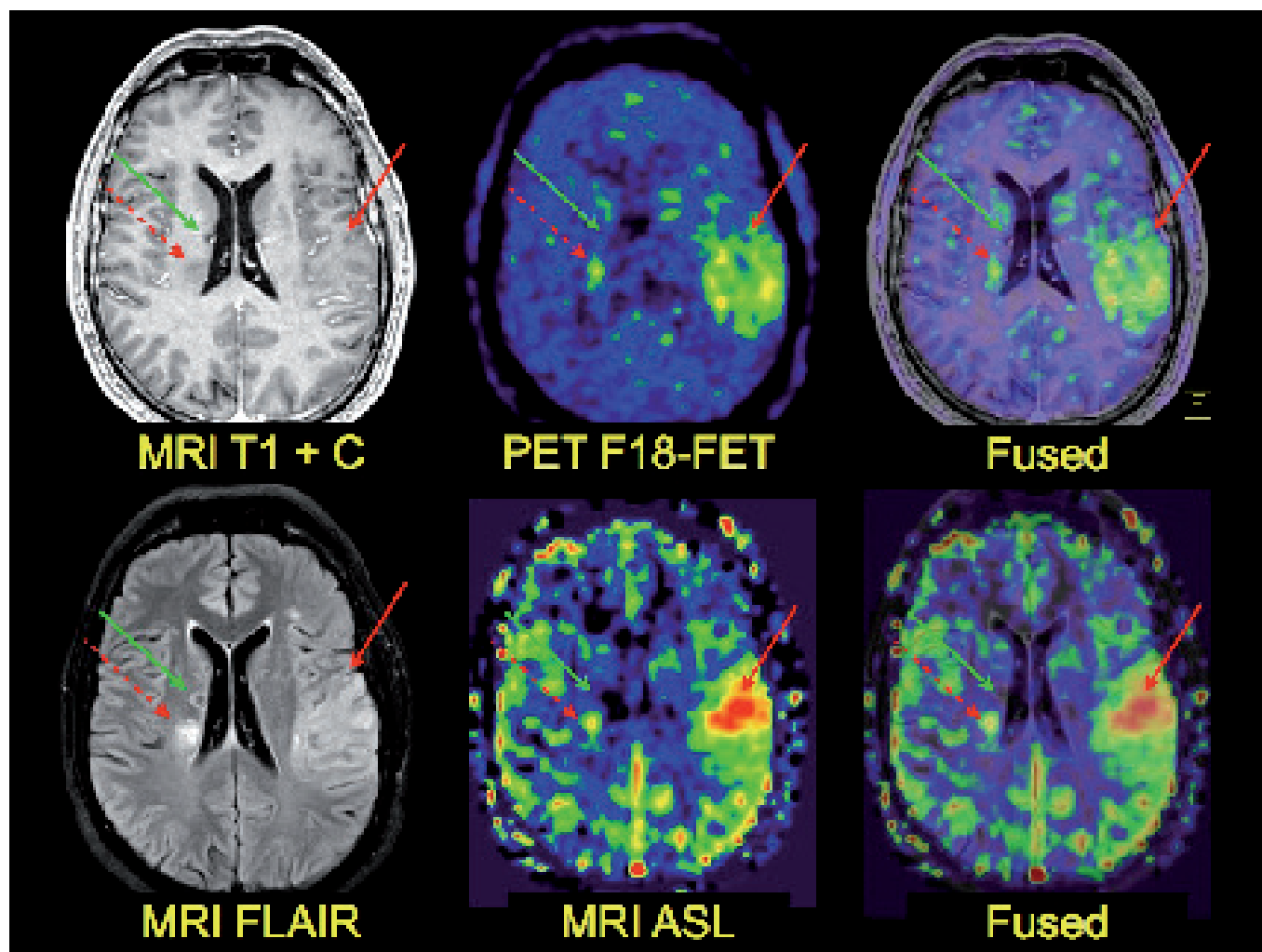


Figure 3. ^{18}F -FET PET/MRI of a 60-year old male patient with glioblastoma multiforme (see text).

a 60-year old male patient investigated preoperatively with simultaneous ^{18}F -FET PET/MRI acquisition including tissue perfusion measures using ASL. The bulk of the tumour is located in the left temporal region (red arrow, solid) and shows diffuse infiltration (MRI FLAIR) and no contrast enhancement (MRI T1+C). The MRI scan without ASL was read independently by a neuroradiologist as a low grade glioma with gliosis (FLAIR, red arrow, broken) in the right central white matter. Particularly the anterior section of the tumour is hyperperfused (MRI ASL) indicating active tumour angiogenesis. However, this area is not the most metabolically active on ^{18}F -FET PET demonstrating intra-tumoural physiological heterogeneity. Although gliosis may lead to increased ^{18}F -FET uptake, increased tissue perfusion indicates neoplastic tissue. Surgical resection showed glioblastoma with malignant vascular proliferation. The lesion in the right hemisphere lesion showed growth on MRI and ^{18}F -FET PET follow-up and was included in the radiation planning field. For comparison, an adjacent ischemic lesion is shown with low perfusion and metabolic signals (green

arrow, solid). Up to 35% of primary tumours that are classified as low grade gliomas on MRI, are in fact high grade tumours (45). Thus, in this case the two physiological modalities can supplement each other to increase the overall diagnostic quality in defining neoplastic tissues.

Cardiovascular

In recent years, PET/CT has been introduced as a hybrid imaging technique to combine PET and CT for diagnostic evaluation of patients with *coronary artery disease* (CAD) (46,47). CT coronary angiography offers rapid assessment of the severity of coronary lesions along with high sensitivity for detection of obstructive CAD (48). Cardiac PET, with either Rubidium-82, ^{13}N -ammonia, or ^{15}O -water, provides functional information about obstructive coronary artery lesions. Furthermore, cardiac PET quantifies myocardial blood flow (MBF) in absolute terms, enabling detection of e.g. 3-vessel - and small vessel disease (48,49). Recent studies have shown that hybrid quantitative ^{15}O -water PET/CT detects obstructive CAD with high accuracy (47,48).

For PET/MRI, the role in cardiac imaging is yet to be defined, and further research is required to elucidate the additional value of the hybrid PET/MRI technique. Compared to CT, cardiac MRI (CMR) offers better tissue characterisation and functional assessment. Combination of PET and CMR is a promising technique that can be used for the assessment of various cardiovascular diseases including cardiomyopathies, metabolic disorders, and inflammatory disorders of the myocardium. It remains to be shown whether hybrid PET/MRI has an advantage over serial CMR and PET. Sequential cardiac PET/MRI using software fusion may be appropriate for certain diagnoses. However, with the introduction of hybrid PET/CT similar concerns have been raised, but currently, PET/CT is the preferred technique for detection of various diseases, such as CAD.

Since to date PET/CT effectively detects CAD, PET/MRI may not increase diagnostic value, but simultaneous assessment of MBF using quantitative PET measurements combined with a detailed evaluation of cardiac function using CMR offers faster evaluation of the cardiac function including ejection fraction (EF), volume analysis, and wall motion. Furthermore, cardiac MRI can be used for regional MBF analysis with better spatial discrimination than with PET, including subendocardial and subepicardial MBF, which may benefit certain groups of patients (50). After myocardial infarction, evaluation of myocardial viability using PET/MRI is a potential area of interest. ^{18}F -FDG PET is a reliable non-invasive tool used for the assessment of myocardial viability (51); viability can also be assessed using CMR. ^{18}F -FDG PET combined with MRI with gadolinium late enhancement might become a patient-friendly and clinically useful tool used for evaluation of regional contractility using MRI data. Furthermore, the high resolution of MRI enables detection of subendocardial scar tissue (52), allowing for simultaneous metabolic and scar evaluation of the myocardium with hybrid PET/MRI. However, it should be noted that recent surgical treatment outcomes of the ischemic heart failure trial have questioned the clinical benefits of the viability assessment on patient outcomes (53). On the other hand, treatment crossovers may have influenced the results of this trial and more studies are necessary to assess the role of viability evaluation in patients with multivessel CAD and left ventricular dysfunction. PET/MRI can also be used for evaluation of *atherosclerosis*, including detection of certain features of the atherosclerotic plaque that is associated with thrombosis and plaque rupture. The high resolution of MRI can provide an anatomical evaluation of the plaque, while PET can provide information on active plaque inflammation using several molecular targets. In a recent study, ^{18}F -FDG uptake by carotid plaques was compared using PET/MRI and PET/CT (54). A strong correlation was observed between ^{18}F -FDG uptake, which was quantified using standardised uptake value (SUV) calculations, in atherosclerotic carotid arteries and PET/MRI and PET/CT, in spite of there being inherent differences in the detection techniques and attenuation correction. An

example of PET/MRI image fusion of carotid vessels is shown as figure 4 (reproduced from reference 54). The advantage of using PET/MRI rather than PET/CT for imaging of atherosclerotic vessels are multiple: first, delineation of area for PET quantification is easier on MRI since it visualises the vessel wall whereas CT with contrast only shows the lumen; secondly, plaque characterisation and composition is possible on MRI but not on CT (except for calcification). Additionally, dynamic contrast-enhanced MRI may allow measurement of the amount of neovascularisation and inflammation caused due to plaque formation. A recent ^{18}F -FDG PET/MRI study (n=40) revealed an inverse relationship between ^{18}F -FDG plaque uptake, representing inflammation, and plaque perfusion indices using DCE-MRI (55). Obviously, further studies are necessary to evaluate the prognostic value of atherosclerotic plaque characterisation with ^{18}F -FDG PET/MRI. Hybrid PET/MRI can also be used for diagnostic evaluation of *cardiomyopathy*, which can result from a variety of underlying disorders. Recently we found, using combined ^{15}O / ^{15}O -water cardiac PET in patients with pulmonary artery hypertension (PAH) and right ventricle failure reduced mechanical efficiency, which implies that more oxygen is used to produce a similar power output (56). Alternatively, ^{11}C -acetate PET can be used as an index for both left and right ventricular oxidative metabolism in patients with ventricular dysfunction (57,58). CMR is used as a reference method for assessment of the right ventricular function in PAH and may be of prognostic importance. Therefore, PET/MRI might be suited for noninvasive evaluation and follow-up of patients with PAH (59). Combined PET/MRI evaluation of patients with cardiomyopathy and/or ventricular failure provides unique data that will provide insight into the pathophysiology of metabolic disorders. It will also provide specific measurements of the functioning of both ventricles, including regional wall motion and volumes.

^{18}F -FDG PET/MRI can be used to identify patients with suspected cardiac sarcoidosis. ^{18}F -FDG PET/MRI can be helpful in identifying extra cardiac sites suitable for biopsy and may be useful for the diagnostic evaluation and monitoring of the activity of the inflammatory cardiac lesions in patients with suspected sarcoidosis (60).

In general, simultaneous use of PET and MRI techniques reduces imaging time compared to sequential PET and MRI and can be performed during a single patient appointment (one-stop shop) with evident advantages for the patient. Further studies are required to ascertain the exact clinical and/or prognostic value using PET/MRI to evaluate cardiovascular disorders.

Rheumatology

There is increasing interest for advanced imaging for early diagnostics and therapy monitoring of inflammatory rheumatic diseases. Early detection of disease activity will enable early and efficient treatment in order to maintain functionality (61). Conventional X-rays do not provide information about soft

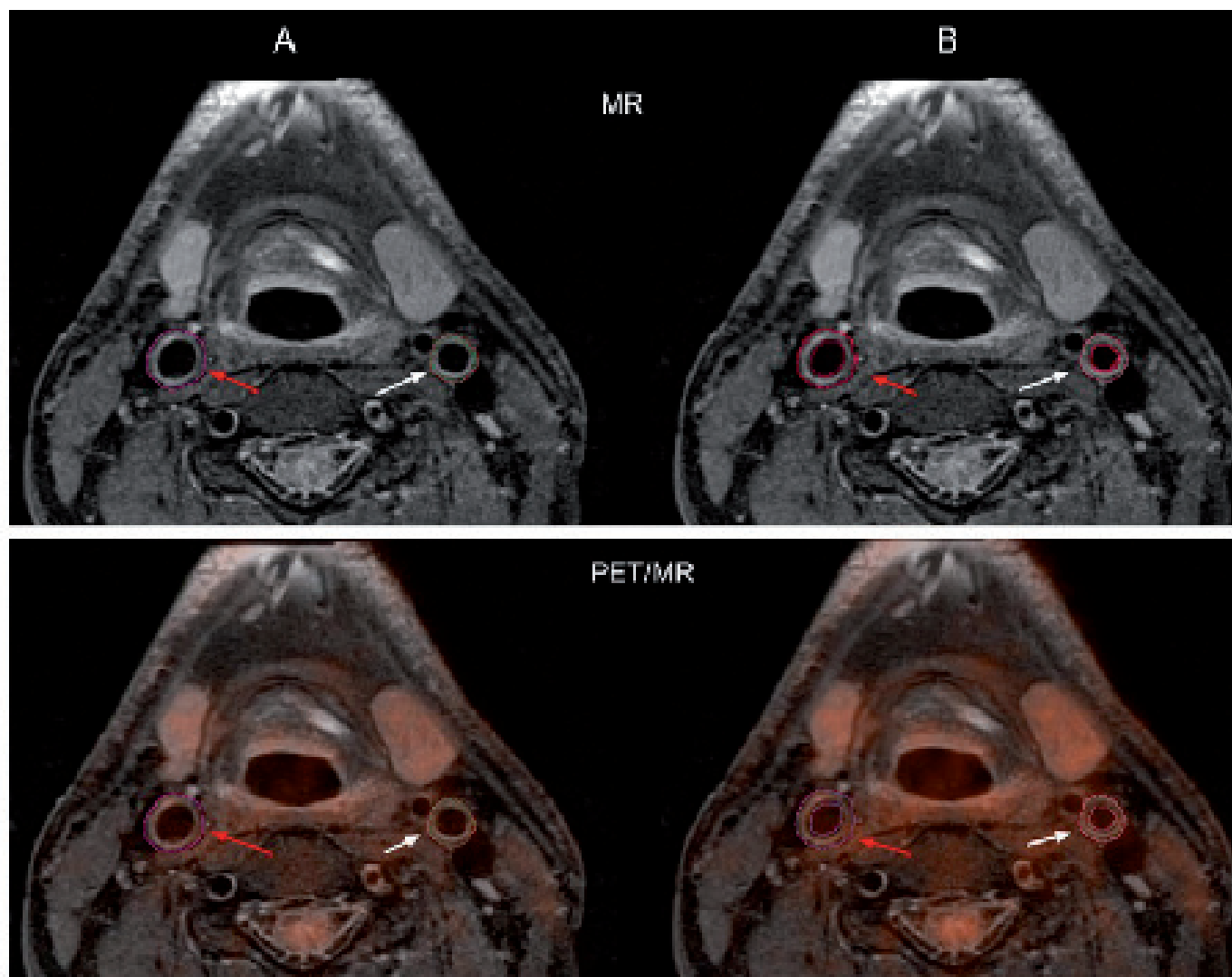


Figure 4. MRI and fused ^{18}F -FDG-PET obtained simultaneously on a hybrid scanner. Note the possibility to delineate the vessel wall for tracer uptake quantification (illustration reproduced from reference 54).

(peri-)articular tissues and only reflect long-term changes of bony structures, and are as such not useful for early diagnostics, prediction of therapeutic outcome and monitoring of short-term therapeutic effects ('tight monitoring'). Ultrasound (US), MRI and PET enable anatomical (US, MRI) and molecular (PET) imaging of both soft tissues and bony structures at a high sensitivity. PET/CT has been investigated in several inflammatory rheumatic diseases. In *rheumatoid arthritis*, most PET studies have been performed with ^{18}F -FDG. Several feasibility studies have demonstrated that it visualises inflamed joints in clinically active rheumatoid arthritis (RA) (62, 63). In a number of studies PET has been compared to MRI. Before and during treatment with NSAIDs, prednisone or methotrexate in RA patients, changes of ^{18}F -FDG joint uptake and synovial volume (MRI) correlated strongly (62,64). The estimated sensitivity of ^{18}F -FDG PET for RA - derived from small-sized study

cohorts - was approximately 90%. With regard to specificity, ^{18}F -FDG PET allows excellent differentiation between inflamed RA- and healthy joints, but absolute joint uptake of ^{18}F -FDG was not different between RA and osteoarthritis (65). This has stimulated the search for more specific PET tracers for RA imaging. ^{11}C -PK11195 is one of the candidates, targeting peripheral benzodiazepine receptors on (activated) macrophages in synovial tissue (66). After successful proof of concept studies in clinically active RA patients, it has also shown promise for imaging of the very first signs of (subclinical) joint inflammation in patients at risk for development of RA (67). PET seems also promising to predict therapeutic outcome early during therapy (68) and to assess persisting (subclinical) joint inflammation in patients clinically assumed to be in remission (69). Such detection of on-going subclinical joint inflammation in clinical remission is relevant since it is associated with increase in-joint damage (70).

The combination of PET with CT led to more accurate localisation of the pathophysiologic PET information in its anatomic surrounding (71). We expect that hybrid PET/MRI will further improve localisation of the PET signal and provide high sensitivity anatomical soft tissue resolution, without extra radiation (CT). Several studies have demonstrated high sensitivity of MRI for imaging of arthritis, in which synovial volume, tenosynovitis and bone oedema seem to have predictive value for development of joint damage (72-75). The first PET/MRI images underline the high potential for imaging of arthritis (activity) (76,77). In a comparative study between PET and MRI in RA patients in clinical remission, MRI seems to strengthen the sensitivity and PET the specificity level of the image signal to depict subclinical arthritis (79). Therefore, PET/MRI might allow for highly sensitive and specific imaging of (subclinical) arthritis offering opportunities for early diagnostics and therapy monitoring as well as prediction of RA.

There is a clinical need for objective diagnostic tests for *ankylopoetic spondylitis* (AS): laboratory tests are usually normal and conventional X-rays do not reveal any abnormalities in the early phase of disease. MRI has been recently accepted as the more or less gold standard for detection of active sacro-iliitis (78), but the precise role of MRI in early AS has not been fully elucidated yet. PET/(CT) may be of additional value: initial reports with ^{18}F -FDG PET/CT showed its potential for imaging of aseptic spondylodiscitis in AS patients as ^{18}F -FDG tracer uptake was demonstrated at the site of discitis with reduced uptake after anti-TNF treatment. There were, however, no correlations between the reduction of ^{18}F -FDG uptake and changes in clinical scores or MRI features (79).

For assessment of sacro-iliitis and spinal inflammation, there are indications that bone targeting with ^{18}F -fluoride PET/(CT) is an interesting approach for imaging of AS activity (80,81). Bone formation (syndesmophyte formation, ankylosis of sacro-iliac joints) is an important clinical hallmark of AS. In the axial skeleton, ^{18}F -fluoride proved to be superior to ^{18}F -FDG and ^{11}C -PK11195, reflected by clearly delineated increased uptake at sites related to AS activity (81). Moreover, ^{18}F -fluoride PET/CT depicted more foci than MRI, which may indicate that this PET technique adds information to MRI. Currently, PET/MRI studies are underway to investigate the value of this hybrid technique in comparison to MRI for assessment of disease activity of AS.

Conclusion

PET/MRI comes with a lot of potential and promise. To date, for daily use of whole body PET/MRI in clinical practice there are still issues to be solved: scanning protocols with optimal trade-offs between scan duration, risk of artefacts and the required level of MRI detail. A typical half-body PET/CT study including contrast-enhanced CT takes about 25-30 minutes, but adding 'full-blown' MRI is often quite time-consuming. The current PET/MRI scanners still compromise either for

scan duration and real-time fusion or for optimal scanner performance. Studies on technical issues and workflow optimisation with PET/MRI are still on-going, and accuracy studies are in their infancy. Currently available comparative studies (^{18}F -FDG PET/CT versus ^{18}F -FDG PET/MRI) typically implement a head-to-head comparison of PET/MRI after the PET/CT study, obviating the need for repeated tracer injection but also introducing uptake interval dependent bias. With head-to-head comparisons of PET/CT and PET/MRI studies in the same patients, recall bias needs to be addressed in the study design. Application of contrast-enhanced CT and MRI-protocols have been quite heterogeneous within and between studies (34,35). Taken together, it cannot be excluded that part of the claimed superiority of PET/MRI is biased due to the ^{18}F -FDG uptake intervals and/or CT- and MRI-protocols. At present, the quantitative strengths of PET cannot yet be exploited due to the inherent problems with attenuation correction (3). In spite of all these considerations and 'to do' items, some groups already addressed the potential impact of PET/MRI on patient management. In a broad spectrum of solid extracerebral malignancies Catalano et al claimed clinical management impact in one out of every five patients referred for ^{18}F -FDG PET/MR (versus PET/CT) (34). Even though this type of information is crucial for clinical acceptance of PET/MRI, the presented data were insufficiently specific to understand the contribution of either component to this perceived added value.

E-mail address for correspondence: d.oprea-lager@vumc.nl

Acknowledgements

The authors are grateful to Dr BMB Fischer (Rigshospitalet, Copenhagen) and Prof OS Hoekstra (VUmc, Amsterdam) for their contribution.

References

1. Balyasnikova S, Löfgren J, de Nijs R et al. PET/MR in oncology: an introduction with focus on MR and future perspectives for hybrid imaging. *Am J Nucl Med Mol Imaging*. 2012;2:458-74
2. Jadvar H, Colletti PM. Competitive advantage of PET/MRI. *Eur J Radiol*. 2013. doi 10.016/j.ejrad.2013.05.028.
3. Yaqub M, D Oprea-Lager, M Hofman, R Boellaard. Methodological aspects of PET/MR imaging. *Tijdschr v Nucl Geneesk* 2013; 35(4):1153-9
4. Buchbender C, Heusner TA, Lauenstein TC, et al. Oncologic PET/MRI. Part 1. Tumors of the brain, head and neck, chest, abdomen, and pelvis. *J Nucl Med*. 2012;53:928-38
5. Buchbender C, Heusner TA, Lauenstein TC, et al. Oncologic PET/MRI. Part 2. Bone tumors, soft-tissue tumors, melanoma, and lymphoma. *J Nucl Med*. 2012;53:1244-52
6. Antoch G, Bockisch A. Combined PET/MRI: a new dimension in whole-body oncology imaging? *Eur J Nucl Med Mol Imaging*. 2009;36:S113-20
7. Vargas MI, Becker M, Garibotto V, et al. Approaches for the optimization of MR protocols in clinical hybrid PET/MRI studies.

- Magn Reson Mater Phys. 2013;26:57–69
8. Kjær A, Loft A, Law J, et al. PET/MRI in cancer patients: first experiences and vision from Copenhagen. *MAGMA*. 2013;26:37–47
 9. Drzezga A, Souvatzoglou M, Eiber M, et al. First clinical experience with integrated wholebody PET/MR: comparison to PET/CT in patients with oncologic diagnoses. *J Nucl Med*. 2012;53:845–55
 10. Laurent V, Trausch G, Bruot O, et al. Comparative study of tow whole-body imaging techniques in the case of melanoma metastases: advantages of multi-contrast MRI examination including a diffusion-weighted sequence in comparison with PET/CT. *Eur J Radiology*. 2012;22:1537–46
 11. Punwani S, Taylor SA, Saad ZZ, et al. Diffusion-weighted MRI of lymphoma: prognostic utility and implications for PET/MRI? *Eur J Nucl Med Mol Imaging*. 2013;40:373–85
 12. Thng CH, Koh TS, Collins DJ, Koh DM. Perfusion magnetic resonance imaging of the liver. *World J Gastroenterol*. 2010;16:1598-1609
 13. Kim SK, Choi HJ, Park SY, et al. Additional value of MR-PET fusion compared with PET/CT in the detection of lymph node metastases in cervical cancer patients. *Eur J Cancer*. 2008;45:2103–9
 14. Nagamachi S, Nishii R, Wakamatsu H, et al. The usefulness of (18)F-FDG PET/MRI fusion image in diagnosing pancreatic tumor: comparison with (18)F-FDG PET/CT. *Ann Nucl Med*. 2013;27:554-63
 15. Brendle CB, Schmidt H, Fleischer S, et al. Simultaneously acquired MR/PET images compared with sequential MR/PET and PET/CT: alignment quality. *Radiology*. 2013;268:190-9
 16. Senft A, de Bree R, Hoekstra OS, et al. Screening for distant metastases in head and neck cancer patients by chest CT or whole body FDG-PET: a prospective multicenter trial. *Radiother Oncol*. 2008;87:221-9
 17. Boss A, Stegger L, Bisdas S, et al. Feasibility of simultaneous PET/MR imaging in the head and upper neck area. *Eur Radiology*. 2011;21:1439–46
 18. Platzek I, Beuthien-Baumann B, Schneider M, et al. PET/MRI in head and neck cancer: initial experience. *Eur J Nucl Med Mol Imaging* 2013;40:6–11
 19. Picchio M, Piert M. Prostate cancer imaging. *Eur J Nucl Med Mol Imaging*. 2013;40:S1–S4
 20. Picchio M, Briganti A, Fanti S, et al. The role of choline positron emission tomography/computed tomography in the management of patients with prostate specific antigen progression after radical treatment of prostate cancer. *Eur Urol*. 2011;59:51–60
 21. Castellucci P, Picchio M. 11C-Choline PET/CT and PSA kinetics. *Eur J Nucl Med Mol Imaging*. 2013;40 Suppl 1:S36-40
 22. Panebianco V, Sciarra A, Cicciariello M, et al. Role of magnetic resonance spectroscopic imaging ((1)HJMRSI) and dynamic contrast-enhanced MRI (DCE-MRI) in identifying prostate cancer foci in patients with negative biopsy and high levels of prostate specific antigen (PSA). *Radiol Med*. 2010. 115:1314–1329
 23. Wetter A, Lipponer C, Nensa F, et al. Simultaneous 18F choline positron emission tomography/magnetic resonance imaging of the prostate: initial results. *Invest Radiol*. 2013;48:256–62
 24. Park H, Wood D, Hussain H, et al. Introducing parametric fusion PET/MRI of primary prostate cancer. *J Nucl Med*. 2012;53:546–51
 25. Schmidt H, Brendle C, Schrami C, et al. Correlation of simultaneously acquired diffusion-weighted imaging and 2-deoxy-[18F]fluoro-2-d-glucosepositron emission tomography of pulmonary lesions in a dedicated whole-body magnetic resonance /positron emission tomography system. *Invest Radiol*. 2013;48:247–55
 26. Souvatzoglou M, Eiber M, Takei T, et al. Comparison of integrated whole-body [11C]choline PET/MR with PET/CT in patients with prostate cancer. *Eur J Nucl Med Mol Imaging*. 2013; 40;1486-99
 27. Niekel MC, Bipat S, Stoker J. Diagnostic imaging of colorectal liver metastases with CT, MR imaging, FDG PET, and/or FDG PET/CT: a meta-analysis of prospective studies including patients who have not previously undergone treatment. *Radiology*. 2010;257:674-84
 28. Frankel TL, Gian RK, Jarnagin WR. Preoperative imaging for hepatic resection of colorectal cancer metastasis. *J Gastrointest Oncol*. 2012;3:11-8
 29. Wu LM, Hu J, Gu HY, et al. Can diffusion-weighted magnetic resonance imaging (DW-MRI) alone be used as a reliable sequence for the preoperative detection and characterisation of hepatic metastases? A meta-analysis. *Eur J Cancer* 2013;49:572-84
 30. Heijmen L, Ter Voert EE, Nagtegaal ID, et al. Diffusion-weighted MR imaging in liver metastases of colorectal cancer: reproducibility and biological validation. *Eur Radiol*. 2013;23:748-56
 31. Tam HH, Collins DJ, Brown G, et al. The role of pre-treatment diffusion-weighted MRI in predicting long-term outcome of colorectal liver metastasis. *Br J Radiol*. 2013;86:20130281
 32. Beiderwellen K, Gomez B, Buchbender C, et al. Depiction and characterization of liver lesions in whole body [(18)F]-FDG PET/ MRI. *Eur J Radiol*. 2013;82:e669-75
 33. Beiderwellen KJ, Poeppel TD, Hartung-Knemeyer V, et al. Simultaneous 68Ga-DOTATOC PET/MRI in patients with gastroenteropancreatic neuroendocrine tumors: initial results. *Invest Radiol*. 2013;48:273-9
 34. Catalano OA, Rosen BR, Sahani DV, et al. Clinical Impact of PET/ MR Imaging in Patients with Cancer Undergoing Same-Day PET/ CT: Initial Experience in 134 Patients—A Hypothesis-generating Exploratory Study. *Radiology* 2013 Sep 5. [Epub ahead of print]
 35. Appenzeller P, Mader C, Huellner MW, et al. PET-CT vs body coil PET-MRI: how low can you go? *Insights into Imaging*. 2013;4:481-90
 36. Andersen FL, Ladefoged CN, Beyer T, et al. Combined PET/ MR imaging in neurology: MR-based attenuation correction implies a strong spatial bias when ignoring bone. *Neuroimage*. 2013;84C:206-16
 37. la Fougere C, Suchorska B, Bartenstein P, Kreth FW, Tonn JC. Molecular imaging of gliomas with PET: opportunities and limitations. *Neuro Oncol*. 2011;13:806-19

38. Law M, Young RJ, Babb JS, et al. Gliomas: predicting time to progression or survival with cerebral blood volume measurements at dynamic susceptibility-weighted contrast-enhanced perfusion MR imaging. *Radiology*. 2008;247:490-8
39. Feigl GC, Safavi-Abbasi S, Gharabaghi A, et al. Real-time 3T fMRI data of brain tumour patients for intra-operative localization of primary motor areas. *Eur J Surg Oncol*. 2008;34:708-15
40. Rachinger W, Goetz C, Popperl G, et al. Positron emission tomography with O-(2-[18F]fluoroethyl)-L-tyrosine versus magnetic resonance imaging in the diagnosis of recurrent gliomas. *Neurosurgery*. 2005;57:505-11
41. Hutterer M, Nowosielski M, Putzer D, et al. O-(2-18F-fluoroethyl)-L-tyrosine PET predicts failure of antiangiogenic treatment in patients with recurrent high-grade glioma. *J Nucl Med*. 2011;52:856-64
42. Larsen VA, Simonsen HJ, Law I, Larsson HB, Hansen AE. Evaluation of dynamic contrast-enhanced T1-weighted perfusion MRI in the differentiation of tumor recurrence from radiation necrosis. *Neuroradiology*. 2013;55:361-9
43. Emblem KE, Mouridsen K, Bjornerud A, et al. Vessel architectural imaging identifies cancer patient responders to anti-angiogenic therapy. *Nat Med*. 2013;19:1178-83
44. Yaman E, Buyukberber S, Benekli M, et al. Radiation induced early necrosis in patients with malignant gliomas receiving temozolomide. *Clin Neurol Neurosurg*. 2010;112:662-7
45. Jansen NL, Graute V, Armbruster L, et al. MRI-suspected low-grade glioma: is there a need to perform dynamic FET PET? *Eur J Nucl Med Mol Imaging*. 2012;39:1021-9
46. Danad I, Rajmakers PG, Appelman YE, et al. Hybrid imaging using quantitative H215O PET and CT-based coronary angiography for the detection of coronary artery disease. *J Nucl Med*. 2013 Jan;54:55-63
47. Kajander S, Joutsiniemi E, Saraste M, et al. Cardiac positron emission tomography/computed tomography imaging accurately detects anatomically and functionally significant coronary artery disease. *Circulation*. 2010 Aug 10;122:603-13
48. Danad I, Rajmakers PG, Knaapen P. Diagnosing coronary artery disease with hybrid PET/CT: It takes two to tango. *J Nucl Cardiol*. 2013;20:874-90
49. Kajander SA, Joutsiniemi E, Saraste M, et al. Clinical value of absolute quantification of myocardial perfusion with (15)O-water in coronary artery disease. *Circ Cardiovasc Imaging*. 2011;4:678-84
50. Vermeltoort IA, Bondarenko O, Rajmakers PG, et al. Is subendocardial ischaemia present in patients with chest pain and normal coronary angiograms? A cardiovascular MR study. *Eur Heart J*. 2007 ;28:1554-8
51. Beanlands RS, Nichol G, Huszti E, et al. F-18-fluorodeoxyglucose positron emission tomography imaging-assisted management of patients with severe left ventricular dysfunction and suspected coronary disease: a randomized, controlled trial (PARR-2). *J Am Coll Cardiol*. 2007;50:2002-12
52. Klein C, Nekolla SG, Bengel FM, et al. Assessment of myocardial viability with contrast-enhanced magnetic resonance imaging: comparison with positron emission tomography. *Circulation*. 2002;105:162-7
53. Bonow RO, Maurer G, Lee KL, et al. Myocardial viability and survival in ischemic left ventricular dysfunction. *N Engl J Med*. 2011;364:1617-25
54. Ripa RS, Knudsen A, Hag AM, et al. Feasibility of simultaneous PET/MR of the carotid artery: first clinical experience and comparison to PET/CT. *Am J Nucl Med Mol Imaging*. 2013;3:361-71
55. Calcagno C, Ramachandran S, Izquierdo-Garcia D, et al. The complementary roles of dynamic contrast-enhanced MRI and F-fluorodeoxyglucose PET/CT for imaging of carotid atherosclerosis. *Eur J Nucl Med Mol Imaging*. 2013 Aug 14.
56. Wong YY, Ruitter G, Lubberink M, et al. Right ventricular failure in idiopathic pulmonary arterial hypertension is associated with inefficient myocardial oxygen utilization. *Circ Heart Fail*. 2011 ;4:700-6
57. Wong YY, Rajmakers P, van Campen J, et al. 11C-Acetate clearance as an index of oxygen consumption of the right myocardium in idiopathic pulmonary arterial hypertension: a validation study using 15O-labeled tracers and PET. *J Nucl Med*. 2013;54:1258-62
58. Klein LJ, Visser FC, Knaapen P, et al. Carbon-11 acetate as a tracer of myocardial oxygen consumption. *Eur J Nucl Med*. 2001;28:651-68
59. Vonk-Noordegraaf A, Souza R. Cardiac magnetic resonance imaging: what can it add to our knowledge of the right ventricle in pulmonary arterial hypertension? *Am J Cardiol*. 2012;110(6 Suppl):25S-31S
60. Schneider S, Batrice A, Rischpler C, et al. Utility of multimodal cardiac imaging with PET/MRI in cardiac sarcoidosis: implications for diagnosis, monitoring and treatment. *Eur Heart J*. 2013 Aug 23.
61. Boers M, Verhoeven AC, Markusse HM, et al. Randomised comparison of combined step-down prednisolone, methotrexate and sulphasalazine with sulphasalazine alone in early rheumatoid arthritis. *Lancet*. 1997;350:309-18
62. Palmer WE, Rosenthal DI, Schoenberg OI, et al. Quantification of inflammation in the wrist with gadolinium-enhanced MR imaging and PET with 2-[F-18]-fluoro-2-deoxy-D-glucose. *Radiology*. 1995;196:647-55
63. Beckers C, Ribbens C, André B, et al. Assessment of disease activity in rheumatoid arthritis with (18)F-FDG PET. *J Nucl Med*. 2004;45:956-64
64. Polisson RP, Schoenberg OI, Fischman A, et al. Use of magnetic resonance imaging and positron emission tomography in the assessment of synovial volume and glucose metabolism in patients with rheumatoid arthritis. *Arthritis Rheum*. 1995;38:819-25
65. Elzinga EH, van der Laken CJ, Comans EF, et al. 2-Deoxy-2-[F-18] fluoro-D-glucose joint uptake on positron emission tomography images: rheumatoid arthritis versus osteoarthritis. *Mol Imaging Biol*. 2007;9:357-60
66. van der Laken CJ, Elzinga EH, Kropholler MA, et al. Noninvasive imaging of macrophages in rheumatoid synovitis using 11C-(R)-PK11195 and positron emission tomography. *Arthritis Rheum*.

- 2008;58:3350-5
67. van der Laken CJ, Elzinga EH, Kropholler MA, et al. Macrophage positron emission tomography imaging as a biomarker for preclinical rheumatoid arthritis: Findings of a prospective pilot study. *Arthritis Rheum.* 2012;64:62-6
 68. Elzinga EH, van der Laken CJ, Comans EF, et al. 18F-FDG PET as a tool to predict the clinical outcome of infliximab treatment of rheumatoid arthritis: an explorative study. *J Nucl Med.* 2011;52:77-80
 69. Gent YY, Voskuyl AE, Ahmadi N, et al. Association between presence of subclinical synovitis on (R)-11C-PK11195 Positron Emission Tomography and clinical outcome in rheumatoid arthritis patients without clinical synovitis. *Ann Rheum Dis.* 2013;72(Suppl3):761
 70. Molenaar ET, Voskuyl AE, Dinant HJ, et al. Progression of radiologic damage in patients with rheumatoid arthritis in clinical remission. *Arthritis Rheum.* 2004;50:36-42
 71. Kubota K, Ito K, Morooka M, et al. FDG PET for rheumatoid arthritis: basic considerations and whole-body PET/CT. *Ann N Y Acad Sci.* 2011;1228:29-38
 72. Conaghan PG, O'Connor P, McGonagle D, et al. Elucidation of the relationship between synovitis and bone damage: a randomized magnetic resonance imaging study of individual joints in patients with early rheumatoid arthritis. *Arthritis Rheum.* 2003;48:64-71
 73. Navalho M, Resende C, Rodrigues AM, et al. Bilateral MR imaging of the hand and wrist in early and very early inflammatory arthritis: tenosynovitis is associated with progression to rheumatoid arthritis. *Radiology.* 2012;264:823-33
 74. Eshed I, Feist E, Althoff CE, et al. Tenosynovitis of the flexor tendons of the hand detected by MRI: an early indicator of rheumatoid arthritis. *Rheumatology.* 2009;48:887-91
 75. Duer-Jensen A, Hørslev-Petersen K, Hetland ML, et al. Bone edema on magnetic resonance imaging is an independent predictor of rheumatoid arthritis development in patients with early undifferentiated arthritis. *Arthritis Rheum.* 2011;63:2192-202
 76. Miese F, Scherer A, Ostendorf B, et al. Hybrid 18F-FDG PET-MRI of the hand in rheumatoid arthritis: initial results. *Clin Rheumatol.* 2011; 30:1247-50
 77. Chaudhari AJ, Bowen SL, Burkett GW, et al. High-resolution (18) F-FDG PET with MRI for monitoring response to treatment in rheumatoid arthritis. *Eur J Nucl Med Mol Imaging.* 2010;37:1047
 78. Maksymowych WP. MRI in ankylosing spondylitis. *Curr Opin Rheumatol.* 2009;21:313-7
 79. Wendling D, Blagosklonov O, Streit G, et al. FDG-PET/CT scan of inflammatory spondylodiscitis lesions in ankylosing spondylitis, and short term evolution during anti-tumour necrosis factor treatment. *Ann Rheum Dis.* 2005;64:1663-5
 80. Strobel K, Fischer DR, Tamborrini G, et al. 18F-fluoride PET/CT for detection of sacroiliitis in ankylosing spondylitis. *Eur J Nucl Med Mol Imaging.* 2010;37:1760-5
 81. Bruijnen ST, van der Weijden MA, Klein JP, et al. Bone formation rather than inflammation reflects Ankylosing Spondylitis activity on PET-CT: a pilot study. *Arthritis Res Ther.* 2012;14:R71 

Baanbrekend

Tijd
voor
meer



De kracht van 'n doelgerichte aanpak van botmetastasen bij CRPC

Combining radioactivity with fluorescence: the first clinical experiences using hybrid tracers

B.M.F. Winkel, BSc¹, J. Kuil, PhD¹, D.D.D. Rietbergen, MD¹, R.A. Valdés Olmos, MD PhD^{1,2}, F.W.B. van Leeuwen, PhD¹

¹ *Interventional Molecular Imaging Laboratory and Nuclear Medicine, Department of Radiology, Leiden University Medical Center, Leiden, the Netherlands.*

² *Nuclear Medicine Department, Netherlands Cancer Institute – Antoni van Leeuwenhoek Hospital, Amsterdam, the Netherlands*

Abstract

Winkel BMF, Kuil J, Rietbergen DDD, Valdés Olmos RA, van Leeuwen FWB. Combining radioactivity with fluorescence: the first clinical experiences using hybrid tracers. With the evolution of imaging technologies and tracers, the applications for nuclear molecular imaging are growing rapidly. To date, radiopharmaceuticals are primarily being applied to diagnose diseases e.g. with single photon emission computed tomography (SPECT) or positron emission tomography (PET). When these nuclear modalities are combined with computed tomography (CT), they can be used to place the disease spread within the anatomical context. At the same time, more accurate diagnosis and localisation of disease may influence the further clinical approach and therapy of patients. For example, these findings may drive surgical resections in more complex anatomical locations. More complex interventions require accurate preoperative planning and intraoperative image guidance. Radio-guided surgery provides a means for surgical identification of radioactive lesions, while fluorescence-guided surgery has been used to accurately demarcate superficial lesions. Unfortunately, both of these techniques have their own drawbacks such as inaccuracy around the injection site (radioactivity) or limited tissue penetration (fluorescence). A compound integrating both techniques as complementary modalities has the potential to overcome the individual drawbacks, thereby advancing the field of image-guided surgery. This review gives a historical overview of radio- and fluorescence-guidance techniques and the logical evolution of these technologies into a fully integrated hybrid approach. Moreover, the current clinical applications of hybrid imaging techniques are outlined, focussing on the first clinical studies in patients undergoing a sentinel lymph node procedure. Finally, some of the exciting future prospects made possible through the use of hybrid tracers are discussed.

Tijdschr Nucl Geneesk 2013; 35(4):1173-1183

Introduction

With the emergence of nuclear molecular imaging techniques such as planar scintigraphy, single photon emission computed tomography (SPECT) and positron emission tomography (PET) in the 1970s, it became possible to visualise, measure and characterise biological processes in the human body (1). These techniques are based on the detection of gamma emission of accumulated radiotracers and allow creation of two- and/or three-dimensional images. As a result of the high sensitivity and specificity of the radiopharmaceuticals, SPECT and PET have proven to be highly valuable diagnostic tools for various disorders. With the addition of computed tomography (CT) scanning in 1999, the 3D anatomical context could be combined with the 3D SPECT or PET images, creating multimodal (or hybrid) modalities (SPECT/CT or PET/CT). The introduction of SPECT/CT and PET/CT halfway the past decade allowed for a precise localisation of lesions of interest and to distinguish between pathological and physiological findings as well as the effective creation of roadmaps for surgical guidance (2,3). Fused modalities also made it possible to correct for attenuation and scatter, thereby reducing errors and improving accuracy (4,5). The above mentioned advances in nuclear medicine also proved to be valuable in the field of radio-guided surgery. A typical example where findings with nuclear medicine are used to drive surgical resections can be found in the sentinel lymph node (SLN) biopsy procedure. The effectiveness of this procedure depends on the ability to surgically identify and localise the lymph nodes in their anatomical context.

Based on the fact that surgeons are used to obtaining real-time optical feedback, fluorescence provides a logical candidate for further expansion of radio-guided surgery. Both radio- and fluorescence-guidance technologies have complementary features, but neither can replace the other. For that reason, strengthening of the synergy between the two approaches is instrumental. To prevent discrepancies in findings, hybrid technologies need to be fully integrated and thus the use of tracers that are both radioactive and fluorescent should be explored. These hybrid tracers allow the use of a single compound for both diagnostics and surgical (fluorescence) guidance. In this review a historical overview of radio- and fluorescence-guidance techniques is provided

and the value of the novel hybrid approach that is based on combination of the two modalities is illustrated. In addition, the clinical applications of hybrid imaging agents within the current clinical logistics are outlined, using the SLN procedure as an example. Based on the first clinical experiences future prospects are discussed.

Radio-guided surgery

First described by Selverstone in 1949, radio-guided surgery utilises the accumulation of preoperatively injected radioactive tracers to identify lesions during surgery by using a gamma ray detector (6). The major advantage of radiopharmaceuticals is their deep tissue penetration as a result of the limited attenuation of gamma rays by tissue. This feature facilitates the localisation of regions of interest even before the first incision is made.

The radiopharmaceuticals used in the clinic are mostly based on low energy photon emitters. For example, ^{99m}Tc is a widely used isotope that emits gammas typically at 140 keV. Radiotracers can be injected either intravenously or locally, depending on the kind of tumour and the type of tracer to be used. Following preoperative imaging and surgical planning, the radioactive signal can be used to guide the surgeon to the area of accumulation. The first detectors to be used were handheld gamma probes. These probes convert gamma counts into acoustic signals in real-time, allowing surgeons to navigate by ear. The sensitivity of this approach is high, however, spatial resolution is poor. This is especially problematic in areas where lesions are located in close proximity to sites with a high background signal such as the injection site. In addition to this, it remains difficult to correlate intraoperative findings with the preoperative findings, mainly because of changes in patient positioning. Differences in patient positioning triggered the development of portable gamma cameras (e.g. Sentinella, Oncovision, Spain) that can provide surgical imaging data. Over the years the quality of these portable cameras has improved significantly; these devices are now able to generate images with a resolution up to 5 mm within 30 seconds (7). For example, recently a SLN detection rate of 90% was described, compared to 97% with conventional cameras (8,9). In line with this, Kerrou et al showed that identification and localisation of SLNs with the portable gamma camera was not inferior to that using standard lymphoscintigraphy (10). Various studies also suggest a higher efficiency of gamma camera surgical guidance over the acoustic gamma probe. Additionally, the portable gamma camera was shown to detect lesions initially not identified with SPECT/CT or lymphoscintigraphy, when these nodes were located in difficult areas (11-13). Limitations of the portable gamma camera include the lack of anatomical detail, sometimes difficulties in differentiating lesions from (deeper lying) background signals, and the lack of in-depth information.

To further advance the radio-guided surgery concept, the freehand SPECT technology was introduced (declipseSPECT

SurgicEye, Munich). Although its sensitivity and resolution are similar to a conventional gamma probe this system enables intraoperative generation of a 3D reconstruction based on gamma signal intensities. Fiducial markers fixed on both the patient and the gamma probe are tracked by an overhead camera, thereby constantly recording the position of the gamma probe relative to the patient. Reconstruction of gamma counts results in a 3D image that can be overlaid on the patient position (mixed reality) or can be used for virtual navigation of surgical tools. Navigation through the 3D reconstruction provides accurate real-time monitoring of the 'distance to hotspot' (figure 1). A pilot study including 44 breast cancer patients showed an accuracy of 77.8% compared to SPECT/CT when good quality images were used. The quality of a freehand SPECT scanner is determined by the amount of gamma counts per surface area in three or more scanning directions. When images were of intermediate and poor quality, freehand accuracy was reduced to 34.3 and 12.8%, respectively. In the same study, a sensitivity of 83.3% was found (detection of 35/42 nodes) after careful definition of the scanning protocol (7). Freehand SPECT has successfully been used as a surgical navigation guide in small scale studies of patients with head and neck cancer, breast cancer and melanoma (14-18).

In summary, many valuable advances have been made in the field of radio-guided surgery, however, the physics behind the technology is limiting for some indications.

Fluorescence guided surgery

Optical techniques are potential candidates to enhance the degree of real-time feedback and detail during surgery. Next to blue dye, fluorescent dyes were introduced to optically localise a variety of lesion types (19).

The term fluorescence is used to describe the emission of light by a dye, a fluorophore, after excitation with an external light source. In fluorescence-guided surgery, generally fluorophores are used that emit in the near-infrared (NIR) range (750-1000 nm); photons in the 750-1000 nm range benefit from the tissue transparency window (20). As the human eye cannot detect light in the NIR range, dedicated camera systems are required to detect the emitted signals. Three types of fluorophores have been most widely explored in a clinical setting; protoporphyrin IX (PpIX) precursors, fluorescein and indocyanine green (ICG). Where PpIX and fluorescein either excite or emit in the visual spectrum, (PpIX: excitation at 400 nm and emission at 635 nm, fluorescein: excitation at 494 nm and emission at 520 nm), ICG emits in the 820-830 nm range after excitation at 780 nm, making it potentially more suitable for surgical applications. This said, the conversion of excitation light into a fluorescent signal is relatively inefficient for ICG (21). After intravenous injection, ICG binds to albumin, a blood plasma protein. Clearance from the body occurs exclusively via the liver (bile), with a biological half-life of 3-4 minutes. ICG has clinically proven to be safe; very few serious side effects have been described.

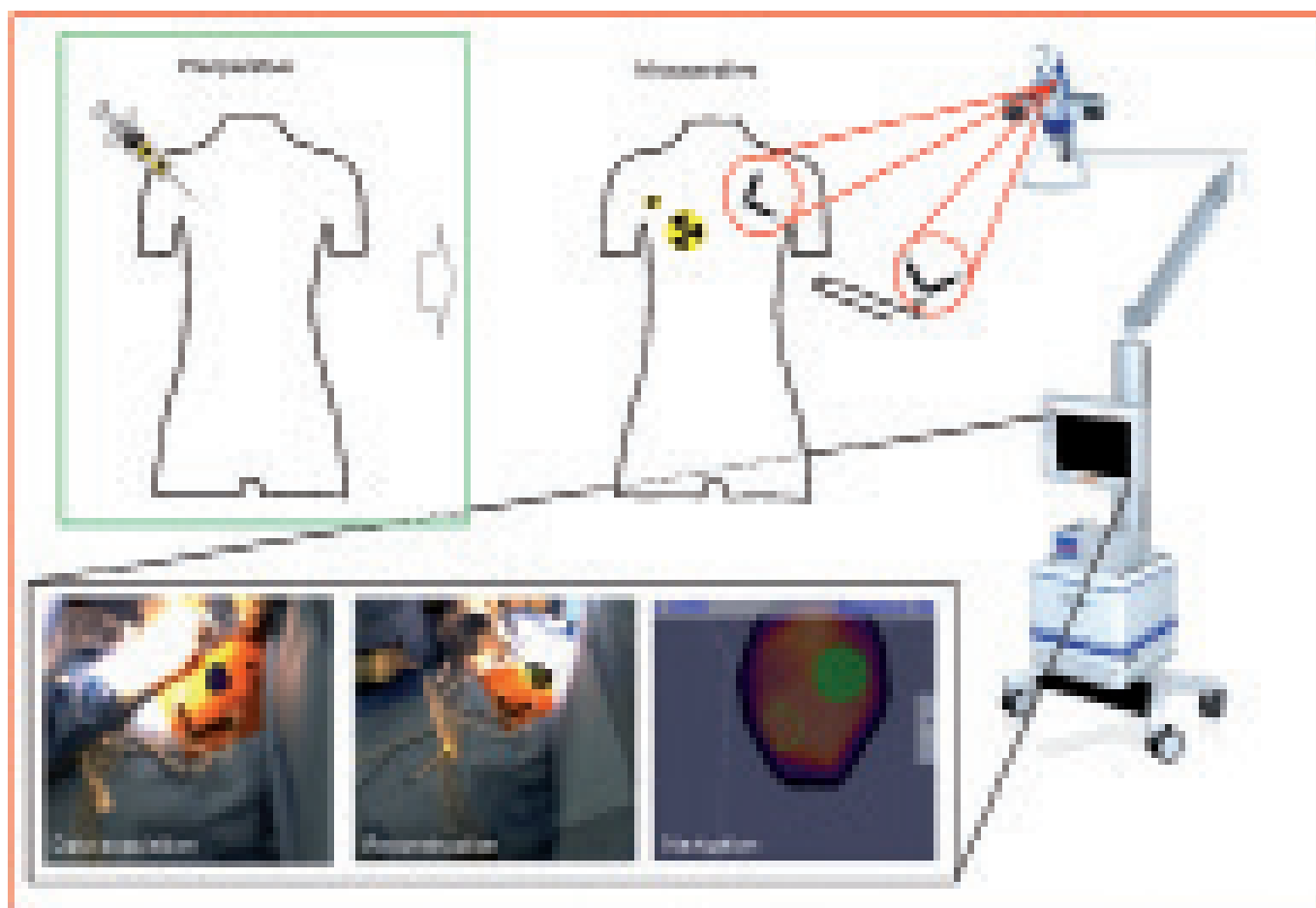


Figure 1. Intraoperative navigation using freehand SPECT technology (declipseSPECT). Following preoperative tracer injection and preoperative imaging, the patient is transferred to the operating theatre. By fixing a fiducial marker on the body of the patient, and a second one on the navigation tool (gamma probe), a 3D freehand SPECT scan can be generated using a navigation system (declipseSPECT, SurgicEye, Munich, Germany). For this the tracked gamma probe is used to scan an area of interest thereby collecting gamma counts of this area (bottom left image). After reconstruction of this scan (middle image on the bottom), a freehand SPECT scan is generated in which the gamma probe can be navigated to the lesion of interest. The navigation system provides the estimated distance from the tip of the gamma probe to the center of activity.

In the clinic, the NIR dye ICG is used in oncologic surgery for tumour detection (22), in the field of urology for the visualisation of the urologic tract (23,24), and for angiography (25-27). Furthermore, ICG is used intraoperatively during SLN procedures for identification of LNs and visualisation of lymphatic vessels (28). Other than with radio-guidance approaches, the use of fluorescence allows real-time visualisation of the SLNs during the resection and the sensitivity of this technique is superior to the use of blue dye. Recently, the use of methylene blue as a fluorescent alternative to ^{99m}Tc -sestamibi has been explored in patients with parathyroid adenoma (29), and as a method to visualise the ureters in abdominal surgery (30). After early preclinical experiments (31), a fluorescent tracer targeting the folate receptor has recently been used to study the clinical ability to visualise metastatic ovarian cancer (32). The latter study really exemplifies the level of detail that can be provided

by fluorescence. It should also be noted that the same fluorescent dye is commonly used during microscopic fluorescence imaging approaches, meaning a subcellular resolution can be obtained when the right modality is used. When fluorophores were initially applied during surgical guidance procedures, it was hypothesised that these fluorescent dyes could overcome the need for radioactive tracers, thereby improving logistics and decreasing the radiation exposure to the surgical personnel. However, though they proved highly effective in mouse models, the tissue penetration of even NIR fluorescent dyes (<1 cm) proved suboptimal for the detection of lesions of interest in humans (20). Hence, fluorescence alone does not enable accurate in-depth diagnostics. These drawbacks restrict the use of fluorescent tracers to superficially located lymph nodes such as those in the axilla. In summary, fluorescence can be used effectively as a

surgical guidance tool. However, due to its drawbacks, such as low tissue penetration, its use in the clinic is limited to a use in superficial tissues.

Combining radio- and fluorescence-guidance, a hybrid approach

To overcome the limitations of the separate use of radiotracers and fluorophores, a novel imaging method was designed combining both radioactivity and fluorescence in a 'best of both worlds' model. Considering the different drawbacks of radioactive and fluorescent tracers (detailed in table 1), it was hypothesised that a combination of the two would yield complementary results. The term 'multimodal' or 'hybrid' tracer describes this fusion of techniques through the generation of imaging tracers that contain both a radio- and a fluorescent-label.

Because radioactive signals penetrate deep through tissue they can be used to improve preoperative diagnostic (molecular) imaging and thus the ability to identify disease spread. Additionally, such imaging may improve surgical planning and help select the least invasive surgical approach, resulting in a shorter exploration time. Fluorescent signals, however, can accurately demarcate a superficial lesion in real-time. Moreover, due to its limited tissue penetration, in patients, fluorescence imaging only marginally suffers from background noise caused by e.g. an injection site or non-specific accumulation in an organ. A full overlap of pre- and intraoperative imaging findings improves translation of imaging to the operating room, validation of the resection accuracy (33). Finally, increasing anatomical detail in both pre- and intraoperatively generated images may reduce complications associated with surgery.

Despite the fact that efforts are ongoing to improve the clinical value of both radio- and fluorescence-guidance technologies, we have hypothesised that integration of the individual strong points of these two surgical guidance technologies is a logical route to benefit healthcare. The first clinical indication where these features have been studied is the widely applied SLN procedure described below.

Sentinel Lymph Node biopsy procedure

The SLN biopsy procedure is based on the concept of sequential lymphatic dissemination; the assumption that lymphatic metastasis occurs in stages. Lymph nodes receiving direct lymphatic drainage from the tumour are called SLNs. Second or higher echelon nodes are lymph nodes that receive drainage in a later phase. The SLN is generally considered to be the site most likely to contain the first (micro) metastases when they occur within the lymphatic system (34). It is now clinical practice in most hospitals to identify and surgically remove the SLNs after diagnosis with a lymphatically spreading tumour type such as breast cancer or melanoma. Indication for the SLN procedure includes only patients without evidence of regional lymph node involvement (N0). Histopathological evaluation of the SLNs is used to stage the tumour, after which further therapy is decided on. Cabañas was the first to describe the significance of sentinel node status for the prognosis and treatment of cancer in 1977 (35). Currently, nodal status is considered the most important prognostic parameter of breast cancer and melanoma (36,37). Traditionally, SLN detection is performed preoperatively using lymphoscintigraphy and intraoperatively by gamma ray detection complemented by injecting a blue dye (e.g. patent or methylene blue). For preoperative lymphoscintigraphy, a radioactive colloid (in the Netherlands ^{99m}Tc-nanocolloid) is generally injected in or around the tumour. This radiocolloid is retained in the lymph nodes, thereby enabling SLN visualisation using a gamma camera, and subsequently, without additional tracer injection, SN identification in the operating room. Intraoperatively, the blue dye is injected and transported through the lymphatic system, directly visualising the lymphatic drainage over time. In some hospitals (not in the Netherlands) where nuclear medicine facilities are unavailable, surgeons still rely solely on blue dye for SLN identification (38). However, studies have shown that combined detection of SLNs using both blue dye and radioactive materials is superior to blue dye alone (39-42). Even using optimal protocols, planar lymphoscintigraphy creates only a 2D map of the lymphatic vessels and drainage patterns (figure 2; panels a,b). The introduction of SPECT/CT

Table 1. The complementary properties of fluorescence and radioactivity combined in the hybrid tracer.

property	fluorescence	radioactivity	hybrid
short range <1 cm	+	-	+
accuracy of margins	+	-	+
deep tissue penetration	-	+	+
preoperative imaging	-	+	+
excitation source necessary	+	n.a.	+, compensated by nuclear component
autofluorescence	+	n.a.	+, compensated by nuclear component

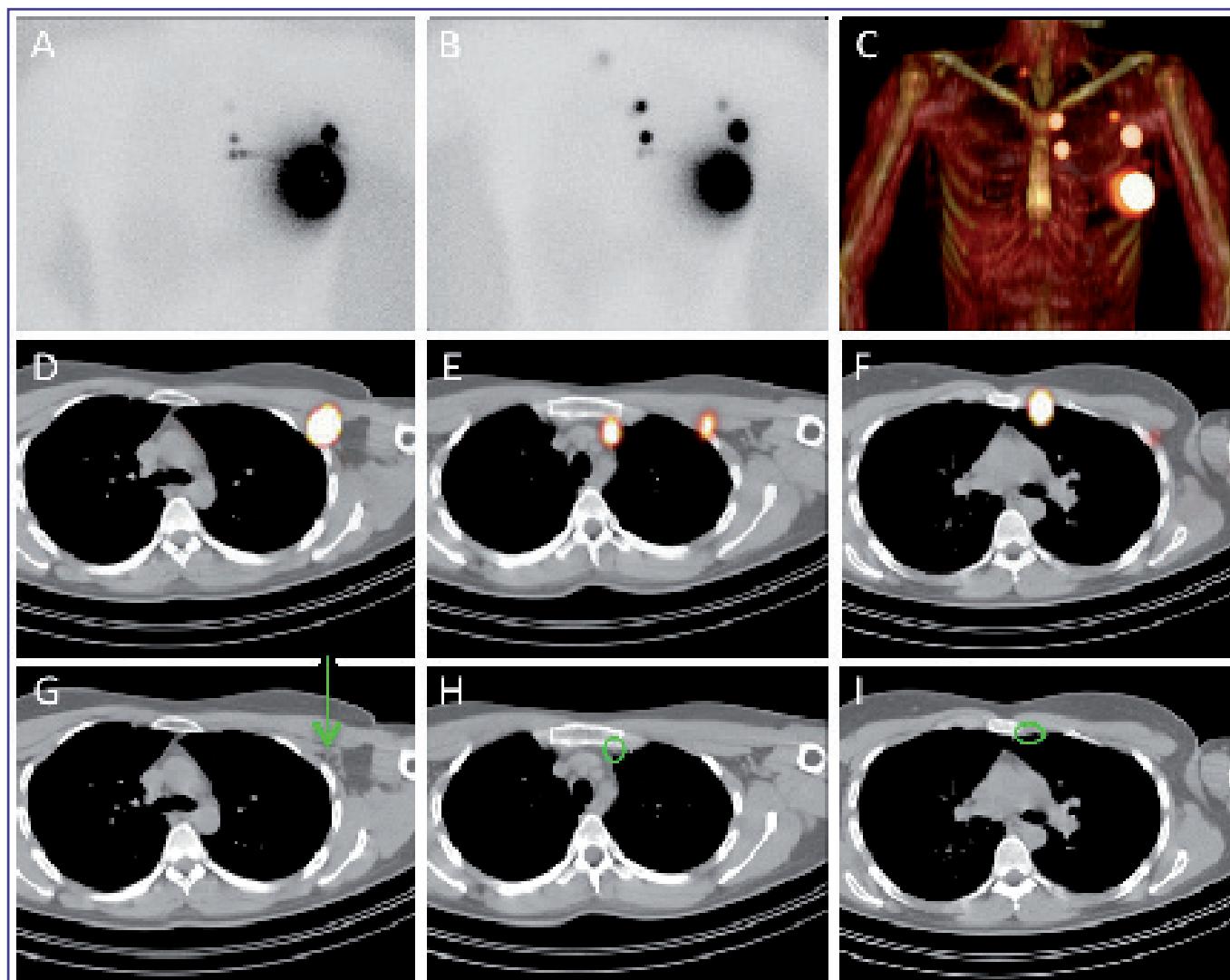


Figure 2. The additional value of SPECT/CT imaging during sentinel lymph node biopsy. Immediately after radiotracer (e.g. radiocolloid or a hybrid tracer) injection, dynamic lymphoscintigraphy is performed followed by static anterior (A) and lateral images. At our institute, late images are acquired 2-4 hours after tracer injection, depending on the indication studied. Static anterior (B) and lateral images are acquired. Thereafter SPECT imaging and low-dose CT imaging is performed. Fusion of the SPECT and CT images allows the generation of a 3D volume rendering image (C) showing the overview image of the location of the sentinel lymph node(s) (arrows) (Osirix Medical Imaging software was used to generate this image). Fused SPECT and CT images (D, E, F) with the corresponding CT images (G, H, I) showing the anatomical location of the radioactive lymph nodes. Sentinel lymph nodes were found in the axilla (D, G), in the mediastinal (E, H) and intercostal (F, I) area.

added a new dimension for a more accurate anatomical SLN localisation and allowed for better preoperative planning in difficult anatomic areas, obese patients, as well as in patients with non-visualisation on planar lymphoscintigraphy (figure 2; panels c-f) (43,44). However, to date, an important part of the effectiveness of the SLN biopsy procedure still depends heavily on the experience of the surgical team and this is probably related to the considerable range in overall success rate (45,46). It is expected that the improvement of surgical guidance procedures may have a positive effect on the success rates of these procedures.

Clinical implementation of the hybrid tracer ICG-^{99m}Tc-nanocolloid

In 2001, Motomura et al showed that SLN detection rates could be improved from 83.9% to 94.9% by combining fluorescence and radioactivity in two separate injections (42). While separate injection of both nuclear and fluorescent tracers may appear a simple strategy, co-administration of these compounds proved complex due to alterations in their pharmacokinetics. Recently, ICG-^{99m}Tc-nanocolloid was developed to integrate the radioactive and fluorescence signatures without altering the pharmacokinetics of the

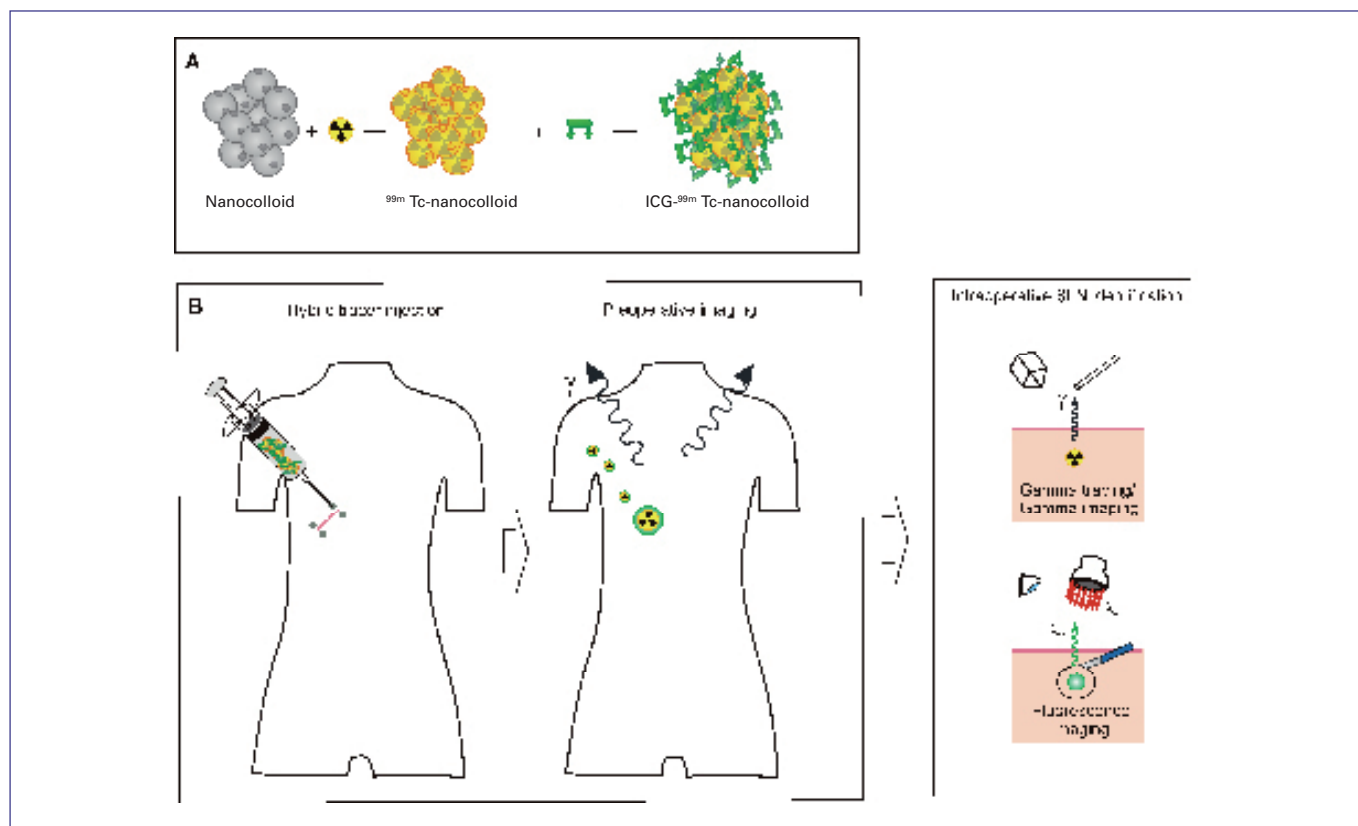


Figure 3. Schematic overview of sentinel lymph node biopsy using the hybrid tracer. The hybrid tracer ICG-^{99m}Tc-nanocolloid is formed via non-covalent self-assembly of ^{99m}Tc-nanocolloid and indocyanine green (ICG) (A). Following formation of the hybrid tracer, the tracer is injected in 3-4 deposits surrounding the lesion (B). Thereafter preoperative imaging is performed (e.g. lymphoscintigrams and SPECT/CT) to determine the number and location of the sentinel lymph node(s). Intraoperatively, sentinel lymph nodes can be acoustically traced using a gamma probe and/or a portable gamma camera. Using a dedicated near-infrared handheld camera the fluorescence signature of the hybrid tracer can be visualised allowing identification of the node and its radical resection.

parental radiocolloid (47,48). Hence the lymphatic drainage patterns of ICG-^{99m}Tc-nanocolloid are identical to those using ^{99m}Tc-nanocolloid, the standard radiopharmaceutical in the Netherlands and other European countries. Currently ICG-^{99m}Tc-nanocolloid is being evaluated in clinic setting and is commercially available in the Netherlands via GE Healthcare. Since ICG alone is a small dye with short lymph node retention, it does not reside in the SLNs. Coupling of ICG to an albumin based radiocolloid, ^{99m}Tc-nanocolloid, creates the larger, non-covalent complex ICG-^{99m}Tc-nanocolloid (figure 3). The albumin based nanocolloid enhances the kinetic and fluorescent properties of ICG, increasing the signal to background ratio (SBR), and improving retention of the compound in SLNs. Due to the improved retention, the surgical window is expanded and the optical discrimination of first and second echelon nodes improves. The radioactive component of the hybrid complex allows surgical planning through identification and localisation of SLNs up to 30 hours prior to surgery by using SPECT/CT and lymphoscintigraphy. Gamma tracing of the radioactive component enables the surgeon to localise the region of interest even in the case of

deeply situated lesions, thereby overcoming the limitations of fluorescence in surgical guidance. After zooming in on the region of interest, the fluorescent component allows precise and detailed optical localisation of the SLN and its margins, enabling its radical resection (figures 3 and 4).

In a clinical feasibility study by Van der Poel et al, eleven patients with prostate cancer, three hours before (laparoscopic) surgery, ICG-^{99m}Tc-nanocolloid was injected in the peripheral zone of the prostate. Prostate and SLNs detected with SPECT/CT were surgically removed and examined for radioactivity and fluorescence. All patients subsequently underwent a standard pelvic lymph node dissection (total amount of resected lymph nodes was 112). Twenty-seven SLNs were detected preoperatively with SPECT/CT. One SLN identified using SPECT/CT could not be localised during surgery and four SLNs could not be found with the fluorescent laparoscope alone, but were detected using the gamma probe. All fluorescent SLNs were found to be radioactive. Finally, 5 out of 27 SLNs (2 tumour positive) were located outside the standard dissection field and would not have been resected if the patient had received standard care (49).

This successful initial study has been followed by a number of other studies, highlighted in table 2. As the initial steps to implement hybrid tracers in the clinic have been made, the advantages of the hybrid approach over solely fluorescence- or radio-guided surgery could be studied in detail. Based on these studies we have been able to determine a number of beneficial features from the hybrid tracer:

- the hybrid tracer allows both preoperative lymphatic

imaging as well as intraoperative guidance without the need for multiple injections;

- the radioactive component indicates distant and aberrant SLN sites, while the fluorescent component also allows for identification of lesions/SLNs in the proximity of the injection site; in the case of near-the-injection-site SLNs conventional gamma probe detection suffers from the high background signal;

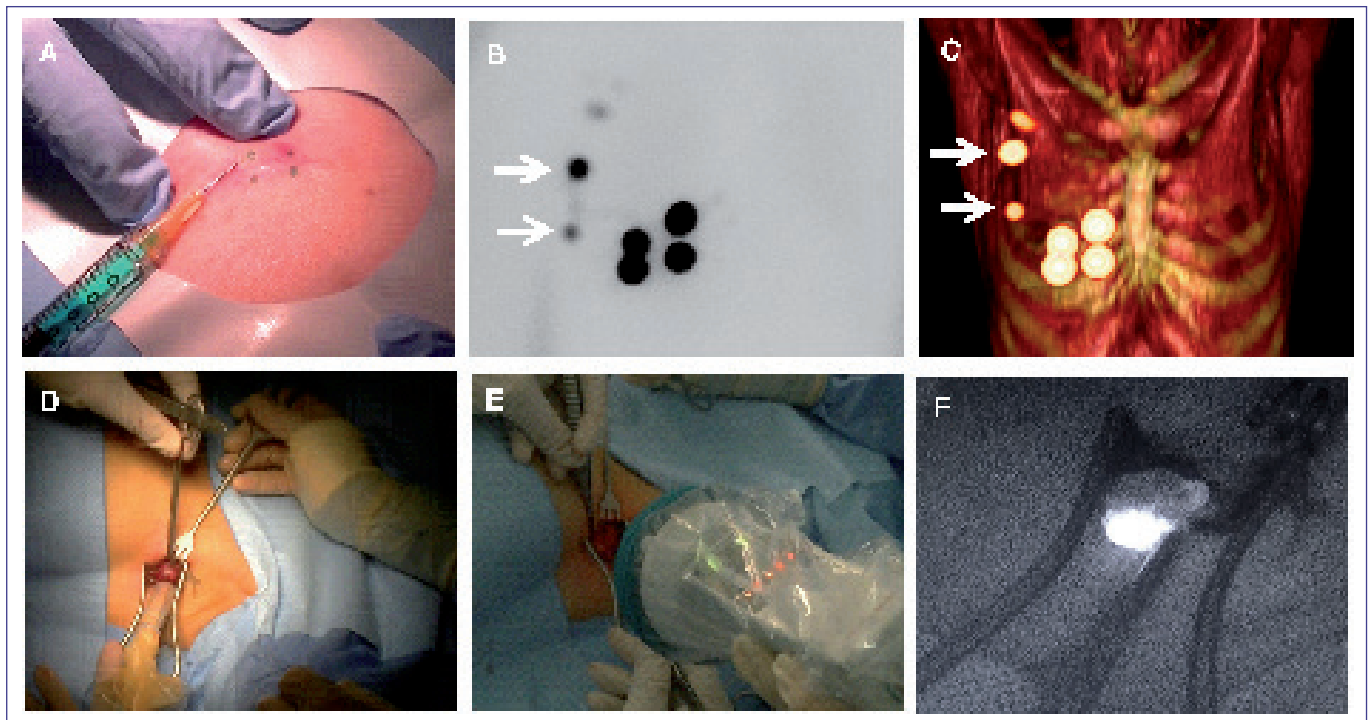


Figure 4. Sentinel lymph node biopsy using the hybrid tracer. The hybrid tracer is injected in 3-4 deposits surrounding the lesion (A). Subsequently, preoperative sentinel lymph node mapping is performed with lymphoscintigrams (B) and SPECT/CT imaging (C) to determine the number and location of the sentinel lymph node(s). Intraoperatively, sentinel lymph nodes can be acoustically traced using a gamma probe (D). Using a dedicated near-infrared handheld or laparoscopic camera (E; PhotoDynamic Eye, Hamamatsu Photonics, Hamamatsu, Japan) the fluorescence signature of the hybrid tracer can be visualised allowing optical identification of the node (F).

Table 2. Clinical studies using ICG-^{99m}Tc-nanocolloid.

tumour type (ref)	n° of patients	^{99m} Tc mean (range) (MBq)	volume (ml)	time injection-surgery; mean (range)	open/laparoscopic	total nodes resected	intraoperative detection rate using blue dye (%)	intraoperative detection rate using radioactivity (%)	intraoperative detection rate using fluorescence (%)
prostate (49)	11	280	4x 0.1	3h	laparoscopic	112	not used	96	96
breast (50)	32	100	0.2	23h (19-29)	open	48	88	100	100
SCC ¹ oral cavity (52)	14	41	4x 0.1	7h (3-19)	open	47	not used	88	96
melanoma (12)	11	70	4x 0.1	5h (4-6)	open	29	43	93	93
vulva (51)	15	87 (67-110)	3-4 x 0.1 (0.4 total)	13h (4-24)	open	46	65	98	96
melanoma + penile carcinoma (47)	25	71 (54-88)	3-4x 0.1 (0.4 total)	6h (4-23)	open	79	54	94	95

¹SCC = Squamous Cell Carcinoma

- similar to the blue dye, fluorescence imaging can also be used to surgically visualise the lymphatic ducts leading to the SLNs (50);
- in a direct comparison, the fluorescent component of the hybrid tracer outperforms the ability to optically identify the SLNs compared to blue dye (51);
- in complex anatomical areas the addition of a fluorescent signal improves both resolution and the in depth interpretation of the surgical field (12,52);
- an important additional beneficial aspect of hybrid tracers is that it reduces the oversampling of SLNs;
- in addition to the radioactive signature fluorescence can be used to surgically validate accurate removal of the SLNs;
- the fluorescent signal remains visual in pathological specimens and therefore can be used to study the placement of tracer deposits (53) and/or the (microscopic) accumulation of the radiocolloids within SLNs.

Future prospects

Clinical studies using the hybrid tracer have prompted technological advances. Recently, gamma probes have been developed that can detect fluorescence (Opto-Nuclear probe, Eurorad) and progress is made in the development of handheld gamma cameras that include an optical component (11,54,55). In addition, surgical navigation tools are being assessed. Conceptualising that nuclear images can be used to provide a basis for the navigation of the surgical tools, while real-time gamma tracing and/or fluorescence imaging is used to validate the navigation accuracy (56). In addition to the generation of the freehand SPECT, the declipseSPECT system is able to load preoperatively acquired SPECT/CT images, provided that they are constructed with a positional tracker fixed to the patient. The declipseSPECT program recognises the tracker in the CT scan and copies the positional information of the tracker to the scan. Intraoperatively a similar, sterile tracker can be fixed to the patient in the exact position as during the preoperative scan. The system can then create a mixed reality overlay of the preoperative imaging data with a real-time video feed of the patient. Subsequently, images can be rendered in the perspective of a gamma probe or a fluorescence laparoscope (KARL STORZ Endoscope, Germany), allowing navigation towards the lesion. Although clinical studies on the identification of SLNs have shown the added value of hybrid tracers over radiotracers, hybrid tracers have not yet been clinically applied in tumour-targeted imaging. Targeted hybrid imaging agents have been widely evaluated in preclinical studies. For most hybrid imaging agents the combination of radioactivity and fluorescence is used (57,58). However, also other imaging techniques such as MR, ultrasound, photoacoustic tomography, Raman and Cerenkov imaging have been applied in hybrid imaging, especially using nanoparticles (21,59,60). The tracers studied can be divided in antibodies, peptides, small molecules and nanoparticles. Antibodies generally have high receptor affinity and specificity

and the (random) functionalisation of antibodies with imaging labels is well validated (57,61). A disadvantage of antibodies is their liver accumulation and long in vivo half-life time, which requires long waiting times between the injection and the scan. The most straightforward method for hybrid labelling of an antibody is to separately couple two different labels. Using this method antibodies directed against epidermal growth factor receptor (cetuximab) and vascular endothelial growth factor (bevacizumab) have been labelled with near infrared dye IRDye800CW and the chelate desferrioxamine (DFO), which can bind ^{89}Zr for PET imaging (62). Alternatively, antibodies can be labelled with a single hybrid label consisting of a chelate and a dye, which results in less alteration of the antibody, and therefore, minimises the loss in receptor affinity (63). Although this has been done for labelling of the HER-2 antibody trastuzumab (64), this concept should receive more attention.

Peptides have been extensively used in preclinical receptor-targeted hybrid imaging (65). Peptides are significantly smaller than antibodies, generally resulting in a better pharmacokinetic profile (i.e. shorter half-life and less liver uptake). The attachment of a hybrid label to a peptide can alter the receptor affinity and the biodistribution. However, this effect can be minimised by coupling the label further from the pharmacophore, thereby optimising its chemical properties. Hybrid peptides have been developed for the visualisation of e.g. $\alpha_v\beta_3$ integrin (RGD), somatostatin receptor (octreotide), GRPR (bombesin) and CXCR4 (Ac-TZ14011) (65). We have demonstrated for $\alpha_v\beta_3$ integrin and CXCR4 that hybrid peptides can be used for pre-, intra- and post-operative imaging in the same manner ICG- $^{99\text{m}}\text{Tc}$ -nanocolloid is used in the clinic (33,66,67).

Small organic compounds cannot easily be functionalised with a relatively large hybrid label without significant reduction of receptor affinity (68). An exception of this rule of thumb is the PSMA-binding compound Glu-urea-Lys, which consists of two amino acids that are linked to each other via a urea bond. This compound has been labelled with IRDye800CW and ^{111}In -DOTA (69). The SPECT/CT and optical imaging results in mice appear promising.

Nanoparticles, such as quantum dots, iron oxide, gold nanorods and liposomes, have also been functionalised with targeting moieties for hybrid imaging (60). These targeting moieties are generally antibodies or peptides. The clinical potential of nanoparticles for tumor-targeted imaging is lower than that of antibodies and peptides, mainly because of toxicity problems (e.g. the heavy metals in quantum dots) and unfavourable biodistribution due to their (large) size. A more promising application for nanoparticles seems the sentinel lymph node procedure, as was demonstrated for quantum dots (70).

Although the work on hybrid modalities is currently limited to proof of concept studies and the studies with tumour-targeted hybrid tracers still remain confined to the preclinical setting, we are convinced that these studies lay the groundwork for future exploration of the hybrid surgical guidance concept.

Conclusions

With the emergence of hybrid tracers that facilitate both nuclear and fluorescent imaging, a first step has been made in the integration of these powerful technologies; fluorescence and radioactivity have the potential to complement each other as interventional molecular imaging methods, even acting in synergy. Clinical SLN studies have already demonstrated that hybrid tracers can preserve nuclear medicine imaging while improving surgical guidance. The current evolution in the field of hybrid imaging technologies and tumour-targeted hybrid tracers open up exciting possibilities for future research and development.

E-mail address for correspondence: f.w.b.van_leeuwen@lumc.nl

References

- Histed SN, Lindenberg ML, Mena E, et al. Review of functional/anatomical imaging in oncology. *Nucl Med Comm.* 2012;33:349–61
- Ploeg IMC, Valdés Olmos RA, Kroon BBR, Nieweg OE. The hybrid SPECT/CT as an additional lymphatic mapping tool in patients with breast cancer. *World J Surg.* 2008;32:1930–4
- Mariani G, Bruselli L, Kuwert T, et al. A review on the clinical uses of SPECT/CT. *Eur J Nucl Med Mol Imaging.* 2010;37:1959–85
- O'Connor MK, Kemp BJ. Single-Photon Emission Computed Tomography/Computed Tomography: basic instrumentation and innovations. *Semin Nucl Med.* 2006;36:258–66
- Hutton BF, Buvat I, Beekman FJ. Review and current status of SPECT scatter correction. *Phys Med Biol.* 2011;56:R85–R112
- Selverstone B, Sweet W, Robinson C. The clinical use of radioactive phosphorus in the surgery of brain tumors. *Ann Surg.* 1949;130: 643-50
- Wendler T, Herrmann K, Schnelzer A, et al. First demonstration of 3-D lymphatic mapping in breast cancer using freehand SPECT. *Eur J Nucl Med Mol Imaging.* 2010;37:1452–61
- Dengel LT, More MJ, Judy PG, et al. Intraoperative imaging guidance for sentinel node biopsy in melanoma using a mobile gamma camera. *Ann Surg.* 2011;253:774–8
- Vidal-Sicart S, Vermeeren L, Solà O, Paredes P, Valdés Olmos RA. The use of a portable gamma camera for preoperative lymphatic mapping: a comparison with a conventional gamma camera. *Eur J Nucl Med Mol Imaging.* 2010;38:636–41
- Kerrou K, Pitre S, Coutant C, et al. The usefulness of a preoperative compact imager, a hand-held -camera for breast cancer sentinel node biopsy: final results of a prospective double-blind, clinical study. *J Nucl Med.* 2011;52:1346–53
- Vermeeren L, Valdés-Olmos RA, Klop WMC, Balm AJM, van den Brekel MWM. A portable -camera for intraoperative detection of sentinel nodes in the head and neck region. *J Nucl Med.* 2010;51:700–3
- Brouwer OR, Klop WMC, Buckle T, et al. Feasibility of sentinel node biopsy in head and neck melanoma using a hybrid radioactive and fluorescent tracer. *Ann Surg Oncol.* 2011;19:1988–94
- Vidal-Sicart S, Brouwer OR, Matheron HM, Bing Tan I, Valdés-Olmos RA. Sentinel node identification with a portable gamma camera in a case without visualisation on conventional lymphoscintigraphy and SPECT/CT. *Revista española de medicina nuclear e imagen molecular.* 2013;32:203-4
- Heuveling DA, Karagozoglou KH, van Schie A, et al. Sentinel node biopsy using 3D lymphatic mapping by freehand SPECT in early stage oral cancer: a new technique. *Clin Otolaryngol.* 2012;37:89–90
- Naji S, Tadros A, Traub J, Healy C. Case report: Improving the speed and accuracy of melanoma sentinel node biopsy with 3D intra-operative imaging. *Br J Plast Surg.* 2011;64:1712–5
- Bluemel C, Schnelzer A, Okur A, et al. Freehand SPECT for image-guided sentinel lymph node biopsy in breast cancer. *Eur J Nucl Med Mol Imaging.* 2013;40:1656-61
- Rieger A, Saeckl J, Belloni B, et al. First experiences with navigated radio-guided surgery using freehand SPECT. *Case Rep Oncol.* 2011;4:420–5
- Rahbar K, Colombo-Benkmann M, Haane C, et al. Intraoperative 3-D mapping of parathyroid adenoma using freehand SPECT. *EJNMMI Research.* 2012;2:51
- Van den Berg NS, van Leeuwen FWB, van der Poel HG. Fluorescence guidance in urologic surgery. *Curr Opin Urol.* 2012;22:109–20
- Keereweer S, Van Driel PBAA, Snoeks TJA, et al. Optical image-guided cancer surgery: challenges and limitations. *Clin Cancer Res.* 2013;19:3745–54
- Chin PTK, Welling MM, Meskers SCJ, et al. Optical imaging as an expansion of nuclear medicine: Cerenkov-based luminescence vs fluorescence-based luminescence. *Eur J Nucl Med Mol Imaging.* 2013;40:1283–91
- Schaafsma BE, Mieog JSD, Hutteman M, et al. The clinical use of indocyanine green as a near-infrared fluorescent contrast agent for image-guided oncologic surgery. *J Surg Oncol.* 2011;104:323–32
- Tanaka E, Ohnishi S, Laurence RG, et al. Real-time intraoperative ureteral guidance using invisible near-infrared fluorescence. *J Urol.* 2007;178:2197–202
- Nguyen NQ, Biankin AV, Leong RWL, et al. Real time intraoperative confocal laser microscopy-guided surgery. *Ann Surg.* 2009;249:735–7
- Sekijima M, Tojimbara T, Sato S, et al. An intraoperative fluorescent imaging system in organ transplantation. *Transplant Proc.* 2004;36:2188–90
- Taggart DP, Choudhary B, Anastasiadis K, et al. Preliminary experience with a novel intraoperative fluorescence imaging technique to evaluate the patency of bypass grafts in total arterial revascularization. *Ann Thorac Surg.* 2003;75:870–3
- Walsh DC, Zebian B, Toliás CM, Gullan RW. Intraoperative

- indocyanine green video-angiography as an aid to the microsurgical treatment of spinal vascular malformations. *Br J Neurosurg.* 2013; in press
28. Polom K, Murawa D, Rho YS, et al. Current trends and emerging future of indocyanine green usage in surgery and oncology. *Cancer.* 2011;117:4812–22
 29. Van der Vorst JR, Schaafsma BE, Verbeek FPR, et al. Intraoperative near-infrared fluorescence imaging of parathyroid adenomas using low-dose methylene blue. *Head Neck.* 2013; in press
 30. Verbeek FPR, van der Vorst JR, Schaafsma BE, et al. Intraoperative near infrared fluorescence guided identification of the ureters using low dose methylene blue: A first in human experience. *JURO.* 2013;190:574–9
 31. Lu Y. Folate receptor-targeted immunotherapy of cancer: mechanism and therapeutic potential. *Adv Drug Deliv Rev.* 2004;56:1161–76
 32. van Dam GM, Themelis G, Crane LMA, et al. Intraoperative tumor-specific fluorescence imaging in ovarian cancer by folate receptor- targeting: first in-human results. *Nat Med.* 2011;17:1315–9
 33. Buckle T, Kuil J, van den Berg NS, et al. Use of a single hybrid imaging agent for integration of target validation with in vivo and ex vivo imaging of mouse tumor lesions resembling human DCIS. *PLoS ONE.* 2013;8:e48324
 34. Leong SP. Paradigm of metastasis for melanoma and breast cancer based on the sentinel lymph node experience. *Ann Surg Oncol.* 2004;11(3 suppl):192S–7S
 35. Cabanas RM. An approach for the treatment of penile carcinoma. *Cancer.* 1977;39:456–66
 36. Nieweg OE, Tanis PJ, Kroon BB. The definition of a sentinel node. *Ann Surg Oncol.* 2001;8:538–41
 37. Morton D, Wen DR, Wong JH, et al. Technical details of intraoperative lymphatic mapping for early stage melanoma. *Arch Surg.* 1992;127:392–9
 38. Rietbergen DD, van den Berg NS, van Leeuwen FW, Valdés Olmos RA. Hybrid techniques for intraoperative sentinel lymph node imaging: early experiences and future prospects. *Imaging in Medicine.* 2013;5:147–59
 39. Varghese P, Mostafa A, Abdel-Rahman AT, et al. Methylene blue dye versus combined dye-radioactive tracer technique for sentinel lymph node localisation in early breast cancer. *Eur J Surg Oncol.* 2007;33:147–52
 40. Radovanovic Z, Golubovic A, Plzak A, Stojiljkovic B, Radovanovic D. Blue dye versus combined blue dye—radioactive tracer technique in detection of sentinel lymph node in breast cancer. *Eur J Surg Oncol.* 2004;30:913–7
 41. Kapteijn BA, Nieweg OE, Liem I, et al. Localizing the sentinel node in cutaneous melanoma: gamma probe detection versus blue dye. *Ann Surg Oncol.* 1997;4:156–60
 42. Motomura K, Inaji H, Komoike Y, et al. Combination technique is superior to dye alone in identification of the sentinel node in breast cancer patients. *J Surg Oncol* 2001; 76:95–9
 43. Lerman H, Lievshitz G, Zak O, et al. Improved sentinel node identification by SPECT/CT in overweight patients with breast cancer. *J Nucl Med.* 2007;48:201–6
 44. Ploeg IMC, Nieweg OE, Kroon BBR, et al. The yield of SPECT/CT for anatomical lymphatic mapping in patients with breast cancer. *Eur J Nucl Med Mol Imaging.* 2009;36:903–9
 45. Kim T, Giuliano AE, Lyman GH. Lymphatic mapping and sentinel lymph node biopsy in early-stage breast carcinoma: a metaanalysis. *Cancer.* 2006;106:4–16
 46. Schirrmester H, Kotzerke J, Vogl F, et al. Prospective evaluation of factors influencing success rates of sentinel node biopsy in 814 breast cancer patients. *Cancer Biother Radiopharm.* 2004;19: 784–90
 47. Brouwer OR, Buckle T, Vermeeren L, et al. Comparing the hybrid fluorescent-radioactive tracer indocyanine green-99mTc-nanocolloid with 99mTc-nanocolloid for sentinel node identification: a validation study using lymphoscintigraphy and SPECT/CT. *J Nucl Med.* 2012;53:1034–40
 48. Van Leeuwen AC, Buckle T, Bendle G, et al. Tracer-cocktail injections for combined pre and intraoperative multimodal imaging of lymph nodes in a spontaneous mouse prostate tumor model. *J Biomed Opt.* 2011;16:016004
 49. Van der Poel HG, Buckle T, Brouwer OR, Valdés Olmos RA, van Leeuwen FWB. Intraoperative laparoscopic fluorescence guidance to the sentinel lymph node in prostate cancer patients: clinical proof of concept of an integrated functional imaging approach using a multimodal tracer. *Eur Urol.* 2011;60:826–33
 50. Schaafsma BE, Verbeek FPR, Rietbergen DDD, et al. Clinical trial of combined radio- and fluorescence-guided sentinel lymph node biopsy in breast cancer. *Br J Surg.* 2013;100:1037–44
 51. Mathéron HM, van den Berg NS, Brouwer OR, et al. Multimodal surgical guidance towards the sentinel node in vulvar cancer. *Gynecol Oncol.* 2013;131(3):720–5
 52. Berg NS, Brouwer OR, Klop WMC, et al. Concomitant radio- and fluorescence-guided sentinel lymph node biopsy in squamous cell carcinoma of the oral cavity using ICG-99mTc-nanocolloid. *Eur J Nucl Med Mol Imaging.* 2012;39:1128–36
 53. Buckle T, Brouwer OR, Valdes-Olmos RA, van der Poel HG, van Leeuwen FWB. Relationship between intraprostatic tracer deposits and sentinel lymph node mapping in prostate cancer patients. *J Nucl Med.* 2012;53:1026–33
 54. Vermeeren L, Valdes-Olmos RA, Meinhardt W, Horenblas S. Intraoperative imaging for sentinel node identification in prostate carcinoma: its use in combination with other techniques. *J Nucl Med.* 2011;52:741–4
 55. Valdes Olmos R, Vidal-Sicart S, Giammarile F, et al. The GOSST concept and hybrid mixed/virtual/augmented reality environment radioguided surgery. *Q J Nucl Med Mol Imaging.* 2014; in press
 56. Brouwer OR, Buckle T, Bunschoten A, et al. Image navigation as a means to expand the boundaries of fluorescence -guided surgery. *Phys Med Biol.* 2012;57:3123–36
 57. Azhdarinia A, Ghosh P, Ghosh S, Wilganowski N, Sevick-Muraca EM. Dual-labeling strategies for nuclear and fluorescence molecular imaging: a review and analysis. *Mol Imaging Biol.* 2012;14:261–76
 58. Culver J, Akers W, Achilefu S. Multimodality molecular imaging with combined optical and SPECT/PET modalities. *J Nucl Med.*

- 2008;49:169–72
59. Kobayashi H, Longmire MR, Ogawa M, Choyke PL. Rational chemical design of the next generation of molecular imaging probes based on physics and biology: mixing modalities, colors and signals. *Chem Soc Rev.* 2011;40:4626
 60. Lee DE, Koo H, Sun IC, et al. Multifunctional nanoparticles for multimodal imaging and theragnosis. *Chem Soc Rev.* 2012;41:2656
 61. Kaur S, Venktaraman G, Jain M, et al. Recent trends in antibody-based oncologic imaging. *Cancer Lett.* 2012;315:97–111
 62. Cohen R, Vugts DJ, Stigter-van Walsum M, Visser GWM, van Dongen GAMS. Inert coupling of IRDye800CW and zirconium-89 to monoclonal antibodies for single- or dual-mode fluorescence and PET imaging. *Nat Protoc.* 2013;8:1010–8
 63. Wängler C, Moldenhauer G, Eisenhut M, Haberkorn U, Mier W. Antibody–dendrimer conjugates: the number, not the size of the dendrimers, determines the immunoreactivity. *Bioconjugate Chem.* 2008;19:813–20
 64. Xu H, Baidoo K, Gunn Y AJ, Boswell CA, et al. Design, synthesis, and characterization of a dual modality positron emission tomography fluorescence imaging agent for monoclonal antibody tumor-targeted imaging. *J Med Chem.* 2007;50:4759–65
 65. Kuil J, Velders AH, van Leeuwen FWB. Multimodal tumor-targeting peptides functionalized with both a radio- and a fluorescent label. *Bioconjugate Chem.* 2010;21:1709–19
 66. Bunschoten A, Buckle T, Visser NL, et al. Multimodal interventional molecular imaging of tumor margins and distant metastases by targeting $\alpha_v\beta_3$ integrin. *ChemBiochem.* 2012;13:1039–45
 67. Kuil J, Buckle T, Yuan H, et al. Synthesis and evaluation of a bimodal CXCR4 antagonistic peptide. *Bioconjugate Chem.* 2011;22:859–64
 68. Knight JC, Hallett AJ, Brancale A, et al. Evaluation of a fluorescent derivative of AMD3100 and its interaction with the CXCR4 chemokine receptor. *ChemBiochem.* 2011;12:2692–8
 69. Banerjee SR, Pullambhatla M, Byun Y, et al. Sequential SPECT and optical imaging of experimental models of prostate cancer with a dual modality inhibitor of the prostate-specific membrane antigen. *Angew Chem Int Ed.* 2011;50:9167–70
 70. Chin PTK, Buckle T, de Miguel AA, et al. Dual-emissive quantum dots for multispectral intraoperative fluorescence imaging. *Biomaterials.* 2010;31:6823–32 

LOVE IT...
MET AL JE
VRIENDEN IN
ACTIE KOMEN

KOM OOK IN ACTIE
 CHECK FIGHTCANCER.NL



Fight
 FIGHT CANCER IS PART OF
 KWF KANKERBESTRIJDING

Love life. Fight cancer.

VANDERWILT

techniques



VANDERWILT techniques is a development and manufacturing company, specialised in products for nuclear medicine

T +31 (0)411 68 60 19 | www.for-med.nl



The use of SPECT/CT in daily practice

B.L.F. van Eck-Smit, MD PhD

Department of Nuclear Medicine, Academic Medical Center, University of Amsterdam, Amsterdam, the Netherlands

Abstract

Van Eck-Smit BLF. The use of SPECT/CT in daily practice. Hybrid imaging has become an important tool in the armamentarium of nuclear medicine physicians. Matching anatomical images with 3D representation of radiopharmaceutical biodistribution by single photon emission computed tomography (SPECT) and positron emission tomography (PET) has supported the interpretation of nuclear medicine studies tremendously. In this article the role of SPECT/CT in various clinical conditions are discussed. **Tijdschr Nucl Geneesk 2013; 35(4):1184-1193**

Introduction

Hybrid imaging has become an important tool in our armamentarium as nuclear medicine physicians. Matching structural images with our 3D representation of the biodistribution of radiopharmaceuticals with techniques such as single photon emission computed tomography (SPECT) and positron emission tomography (PET) has supported the interpretation of our nuclear studies tremendously, especially when the biodistribution of the radiopharmaceutical leaves room for multiple interpretations. In the past two decades hybrid imaging has developed from correlative image fusion by soft-ware co-registration to a fully hybrid analysis of molecular and morphological aspects of disease (1). Integration of molecular and morphological imaging is not only a technological development, but also an evolution in the minds of physicians. Imaging specialists as well as our referring colleagues had to learn, and are still learning, the incremental value of hybrid imaging and its role in the diagnostic work-up and follow-up of patients.

The first publication in PubMed on SPECT/CT originates from 1989 in the American Journal of Roentgenology (2), but it took another ten years before the first commercial SPECT/CT system was available.

For PET imaging, hybrid acquisition, image reconstruction and image interpretation became standard of care. Stand alone PET cameras are no longer on the market and standardisation of quality control and scan protocols is on its way to be implemented in daily patient care.

For SPECT the additional clinical value of hybrid imaging has yet to be established, but evidence of the incremental value of hybrid SPECT/CT is increasing fast. One explanation for lagging implementation of SPECT/CT as the standard of care compared to PET/CT is that in contrast to PET, SPECT is not a

whole body technology. Usually, 3D imaging of single photon radiopharmaceuticals by SPECT is limited to a specific region of interest of the body selected after planar imaging. Moreover, the additional radiation exposure caused by CT feeds the reluctance of nuclear medicine physicians to add SPECT/CT routinely to planar imaging, especially in young patients and benign disease. On the other hand we all have the experience of the beneficial additional value of SPECT/CT in specific cases. In this article some of the most striking examples from my own institution will be shown, and some of the evidence on the additional value of SPECT/CT will be quoted. The article does not claim to be a complete review on this subject.

SPECT/CT in bone scintigraphy

Figure 1 shows a 64-years old patient treated for breast carcinoma (pT1N1M0), one year before she was referred for bone scanning because of newly developed pain in the left hip region. Planar images show intense ^{99m}Tc-hydroxymethane diphosphonate (HDP) accumulation in the region of the left ramus of the pubic bone and less intense accumulation in what was interpreted as activity in the bladder. Realising that evidence or exclusion of a solitary bone metastasis was crucial for treatment planning and prognosis, SPECT/CT was performed. The intense ^{99m}Tc-HDP accumulation could be assigned to activity in the urine in a displaced bladder due to a calcified uterus myoma. The uterus myoma accumulates the radiopharmaceutical as well, and could therefore easily be mistaken for activity in the bladder on planar imaging. Based on these additional images, bone metastasis of the left ramus of the pubis could be excluded.

Figure 2 shows the bone scan of a 55-years old female patient, known with osseous metastases of breast cancer. She recently developed radiating pain to the left arm. Bone scanning was performed to evaluate the evolution of bone metastases and especially the presence of cervical spine metastases. The whole body scan revealed multiple abnormalities in the skull, spine, ribs, and pelvis. In the cervical spine there was no evidence of bone metastases. However, in this region sensitivity of planar imaging is suboptimal. Therefore SPECT/CT was performed. On the maximum intensity projection (MIP) representation (figure 2b), apart from the clear delineation of abnormalities in cervical region, the overall higher number of abnormalities is striking. Moreover, combining SPECT with CT (figure 2c) revealed that the cervical abnormalities are located in the vertebral bodies and partly coincide with sclerotic alterations on low dose CT, confirming the presence of osteoblastic cervical bone metastases.



Figure 1a. Whole body scintigraphy of a 64-years old woman with known breast carcinoma and pain in the left hip region. Note the increased ^{99m}Tc -HDP uptake in the region of the left ramus superior of the pubis and mild uptake in the bladder region.

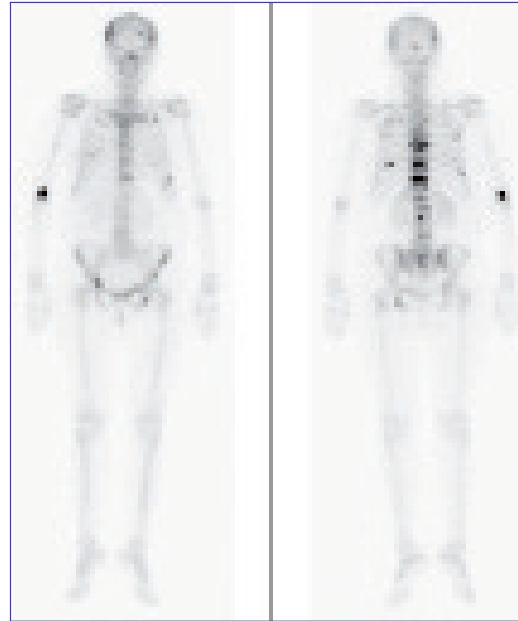


Figure 2a. Whole body scintigraphy of a 55-years old female with known osseous metastases of breast cancer.

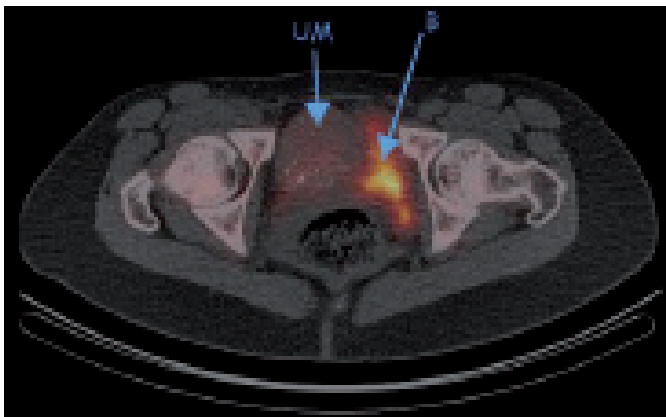


Figure 1b. Transverse fused SPECT/CT image showing uptake of ^{99m}Tc -HDP in a calcified uterus myoma (UM) and excretion in a displaced bladder (B).

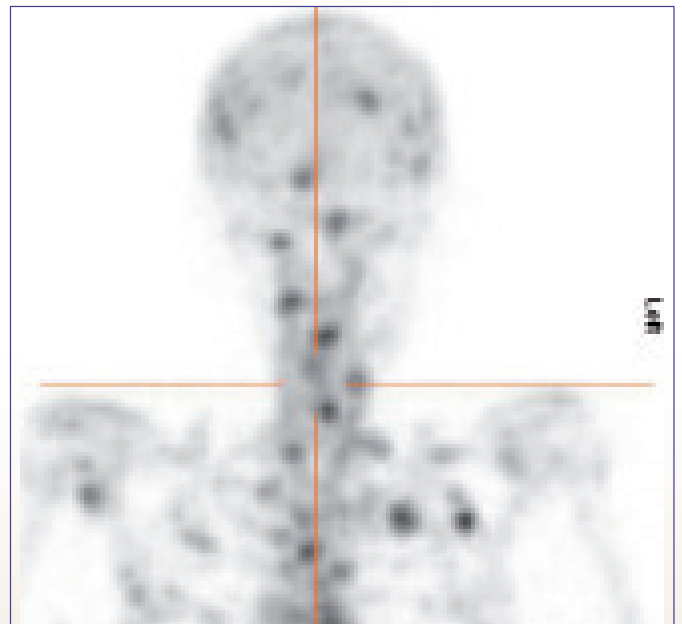


Figure 2b. Maximum Intensity Projection (MIP) showing far more lesions than on planar imaging.

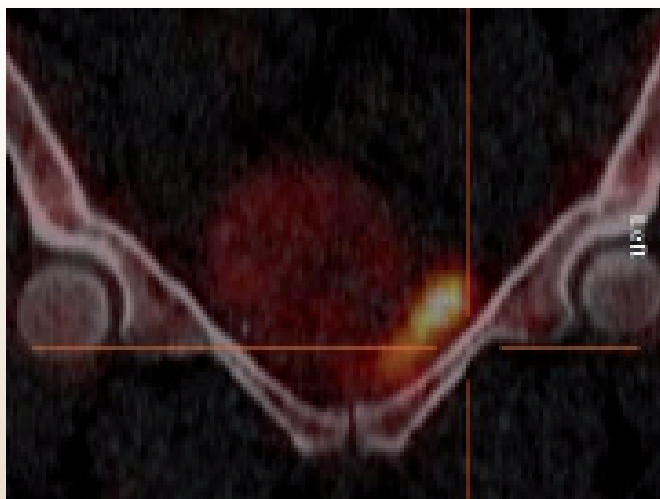


Figure 1c. Coronal fused SPECT/CT image showing normal uptake of ^{99m}Tc -HDP uptake in the left ramus superior of the pubis.

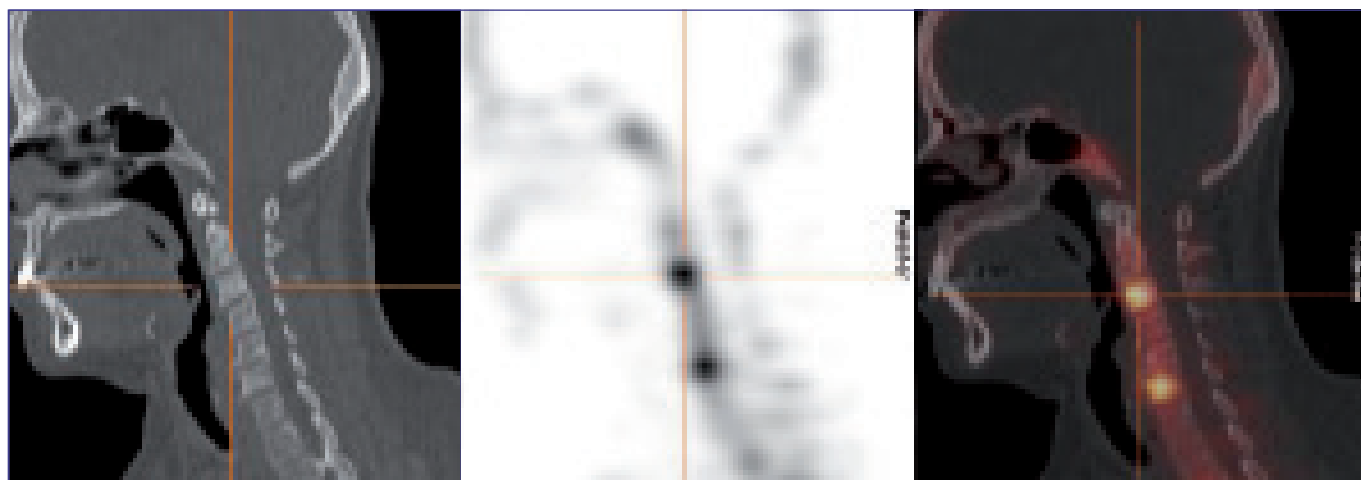


Figure 2c. Sagittal SPECT, SPECT/CT and CT images showing increased ^{99m}Tc -HDP and sclerotic lesions in vertebral bodies of the cervical spine compatible with bone metastases.

What are the reasons to perform SPECT/CT in bone scanning?

In patients with known malignant disease, symptoms of pain or rising tumour markers may raise the question of bone metastases. However, many of these patients also have a high pre-test likelihood of benign, degenerative bone disease. Combining SPECT/CT with whole body planar imaging may have two different results; revealing the precise localisation and characterisation of a known abnormality or detection of a non-visualised abnormality. In a recently published prospective study Palmedo *et al* showed that the addition of SPECT/CT to planar imaging in patients with known breast or prostate cancer increased the specificity of bone scanning from 78% to 94%, the positive predictive value from 59% to 88%, and down staged metastatic disease in approximately one third of the patients (3). Upstaging was only found in 2.1% of patients. Downstaging was the result of eliminating benign alterations, such as degenerative disease.

Another important group of patients in which bone SPECT/CT seems advantageous is the orthopaedic patient group, especially patients after arthroplasty or osteosynthesis. In these patients, the interpretation of conventional radiographs is often insufficient and MR imaging is hampered by implants. On the other hand, bone scintigraphy is a sensitive but non-specific tool for the assessment of increased bone turnover such as in conditions of trauma, loosening of the prosthesis, inflammation, infection and degeneration. In patients with persistent or recurrent pain after arthroplasty or osteosynthesis neither of these imaging techniques alone can differentiate between the various causes of symptoms. Combined SPECT/CT can often reveal the origin of complaints by identifying the culprit by the increased bone turnover and specifying the culprit by the combined morphologic imaging. Pathology specific patterns are increasingly recognised and described. In 2010 Hirschmann *et al* proposed a standardised analysis of SPECT/CT images in patients after knee

arthroplasty and even supporting soft-ware was presented, but evidence of its applicability is still lacking (4). In 2013 the same group used the standardised analysis to correlate tracer distribution with the stability and laxity of the knee joint and the position and orientation of the tibial and femoral tunnels in patients after anterior cruciate ligament reconstruction. SPECT/CT tracer uptake intensity and distribution showed a significant correlation with the femoral and tibial tunnel position and orientation (5).

In complex regions of the skeleton such as joints, SPECT/CT provides exact anatomical correlation with pathological bone turnover. In many cases, SPECT increases the sensitivity and CT the specificity of the study, increasing confidence in the final diagnosis compared to planar images alone (6). In contrast to other regions of the skeleton, high resolution CT images are often required to identify the morphologic abnormalities underlying the increased bone metabolism. Close collaboration with the (orthopaedic) surgeon and radiologist to optimise the yield of SPECT/CT for these complex regions is warranted. Figure 3a shows planar and SPECT/CT images of a 50-years old male ultra-runner, frequently running 50-100 km per day. Since one year, his right foot was transiently painful with redness and swelling after running. Three-phase planar imaging showed diffuse hyperaemia of the right foot (images not shown) and focally increased bone turnover laterally in the right ankle. On SPECT/CT focal bone turn-over is located laterally in the talus. Important is to notice that bone turnover is restricted to the talus and does not include the calcaneal side of the talo-calcaneal joint. Close examination of the CT images showed discrete sclerosis in the same region (figure 3b). Although the CT images were suboptimal for a definite radiological diagnosis, it was concluded in consensus with an experienced radiologist that the images were compatible with a stress fracture.

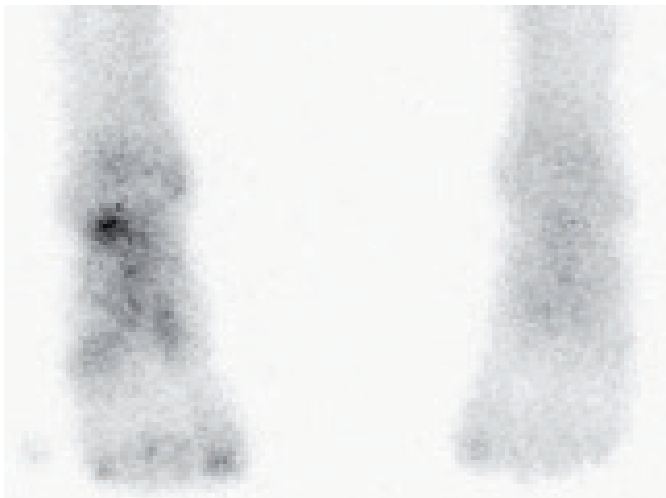


Figure 3a. Planar image of the feet of a 50-years old ultra-runner, with focally increased bone turnover laterally in the right ankle.

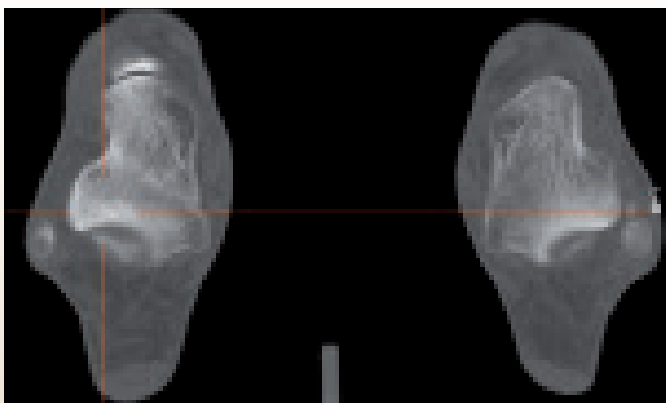
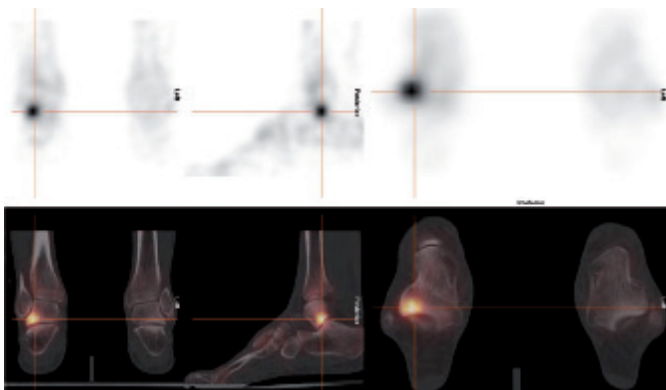


Figure 3b. SPECT/CT (upper and middle panel) focal bone turn-over located laterally in the talus, without involvement of the talo-calcaneal joint or calcaneus. CT images show discrete sclerosis in the same region (lower panel).

The additional value of SPECT/CT in complex regions such as the ankle is illustrated by a recent paper by Singh *et al.* The authors reported a change in treatment planning after SPECT/CT scanning compared to triple-phase planar bone scanning in 39/50 (78%) patients where definitive diagnosis could not be achieved after clinical examination and plain radiography (7).

It has also been shown that the combined evaluation of morphology and bone turnover by SPECT/CT in complex regions decreased the inter- and intra-observer variability significantly compared to separate evaluation of CT and bone scanning (8).

SPECT/CT for localising sentinel nodes

Pre-surgical mapping of sentinel nodes followed by surgical biopsy has become a cornerstone in nodal staging of several types of carcinoma. Although planar images combined with the use of an intra-operative probe may guide the surgeon adequately, in some patients sentinel nodes remain undetected or turn out to be located outside the usual compartment of the body, prolonging and complicating the surgical procedure. As sentinel node scintigraphy is associated with poor anatomical landmarks, SPECT/CT, being a true 3D modality including morphologic information, can be expected to be extremely helpful. Breast carcinoma was the first malignancy in which sentinel lymph node mapping was implemented routinely. In several other malignancies sentinel lymph node procedures have nowadays been proven to be valuable for staging purposes. In melanoma, gynaecological cancers, head & neck, bladder, prostate, and penile cancer, for example, sentinel node detection has been applied on a large scale. The use of SPECT/CT in all of these patient groups is less clear, but evidence of the additional value is growing fast.

Figure 4 shows the imaging results of a 66-years old woman with a non-palpable mass in the lateral upper quadrant of the left breast. Four hours after ultra-sound guided injection of the radiopharmaceutical there was still non-visualisation of the sentinel node (early and 2 hour post-injection images are not shown). Additional SPECT/CT shows faint but clear uptake in a non-enlarged axillary lymph node, which was successfully removed at surgery.

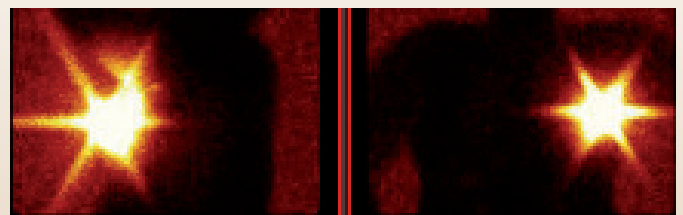


Figure 4a. Anterior and lateral planar images 4 h after injection of ^{99m}Tc -nanocolloid.



Figure 4b. Fused SPECT/CT images with identification of the sentinel node in the left axilla.

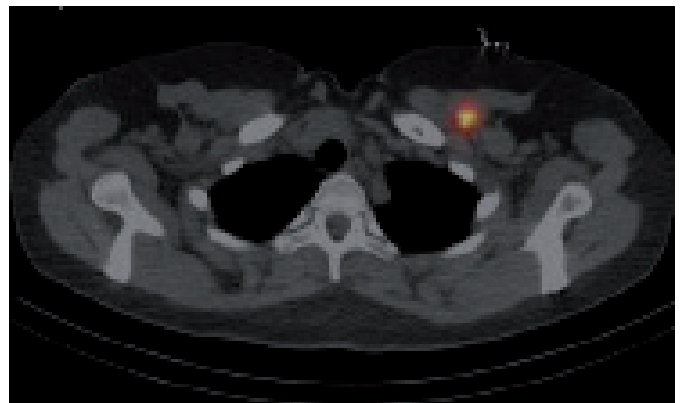


Figure 5b. Fused SPECT/CT images with identification of the sentinel node posterior of the left musculus pectoralis major.

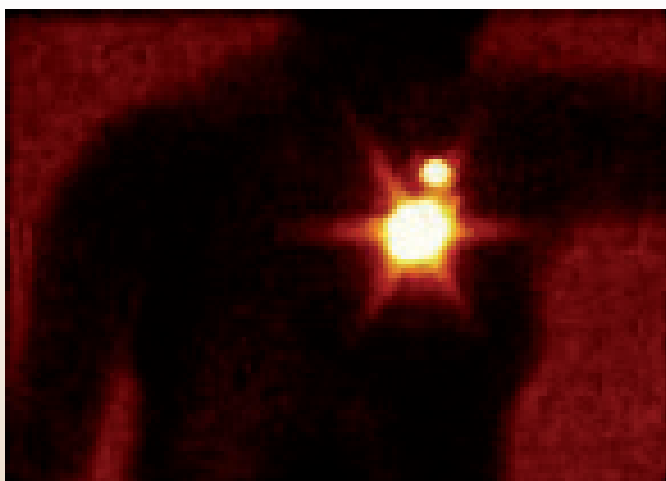
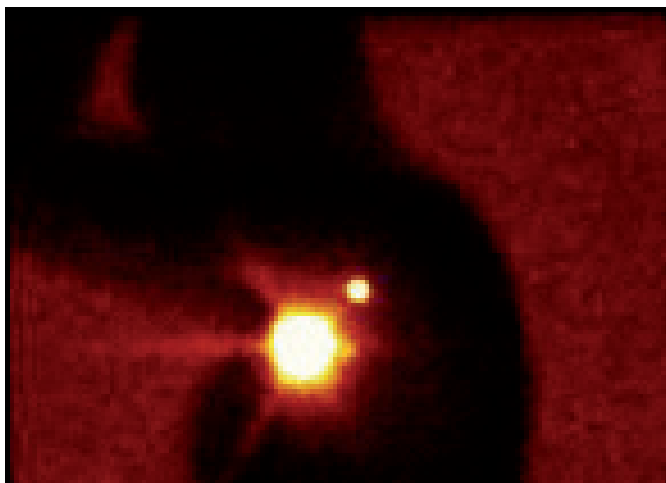


Figure 5a. Anterior and lateral planar images 4 h after injection of ^{99m}Tc -nanocolloid.

Figure 5 shows planar and SPECT/CT images of a 72-years old breast cancer patient. The radiopharmaceutical was administered in the two cm large tumour in the medial upper quadrant of the left breast. As the sentinel node seemed to be located more medially than usual, additional SPECT/CT was performed. In this patient, the sentinel node was located posterior from the pectoral muscle.

In 2009 van der Ploeg *et al* from the Dutch Cancer Center reported that in 8/15 (53%) patients without visualisation of any sentinel node and 2/13 (15%) of patients with only extra-axillary sentinel node visualisation on planar imaging, SPECT/CT revealed a sentinel node in the axilla without reinjection of a second dose of ^{99m}Tc -nanocolloid (9). In 2007 Lerman *et al* already reported improved detection of sentinel nodes using SPECT/CT in overweight patients. Sentinel node detection rose from 72% to 89% in a group of 122 breast carcinoma patients with a body mass index (BMI) of $29.2 \pm 6.6 \text{ kg/m}^2$ (10).

Also in melanoma patients sentinel node mapping provides important information on the drainage of the primary tumour. The lymphatic drainage of this kind of malignancy is often unpredictable and complex, increasing the need for 3D representation and anatomical matching. In a prospective study in 32 melanoma patients, Farbairn *et al* showed that although SPECT/CT did not change the accuracy of the detection of sentinel nodes compared to planar scintigraphy, for the surgeon it was judged to provide useful anatomical information in all cases and even altered the surgical approach in 12 out of 32 patients (11). In contrast to the findings of Farbairn *et al*, Stoffels and co-workers reported improved staging for SPECT/CT compared to planar scintigraphy in a large cohort of melanoma patients (12). In 403 melanoma patients the accuracy of staging using SPECT/CT (149 patients) was compared to planar scintigraphy (254 patients). In the SPECT/CT cohort, more sentinel lymph nodes/patient were detected than in the standard cohort (2.40 vs 1.87).

The number of positive sentinel lymph nodes/patient was significantly higher in the SPECT/CT cohort than in the standard cohort (0.34 vs 0.21). The local relapse rate in the SPECT/CT cohort was lower than in the standard cohort (6.8% vs 23.8%), which prolonged 4-years disease-free survival (93.9% vs 79.2%). Moreover, SPECT/CT more often showed sentinel nodes in the head and neck area (12).

There is also evidence on the added value of SPECT/CT for sentinel node scintigraphy in gynaecological cancer. In a recently published meta-analysis of the literature on the accuracy of sentinel node mapping in vulvar squamous cell cancer, the pooled patient and groin basis sentinel node detection rates were 94.4% and 84.6%, respectively (13). Although sentinel node procedures are frequently performed in patients with gynaecological cancers, the evidence of the additional value of SPECT/CT is scarce. One of the few studies (64 consecutive women with gynaecologic tumours; cervical, endometrial and vulvar cancer) reported non visualisation of sentinel nodes in seven patients on planar imaging and in four patients on SPECT/CT. In 35 patients SPECT/CT detected more lymph nodes than planar imaging (14). An interesting study from the University Medical Center Utrecht describes the reduction in operating time as well as the improved diagnostic accuracy in 7

patients with cervical cancer and 7 patients with vulvar cancer. A historical case control group was used as reference. The average bilateral sentinel node retrieval time was 75.4 ± 33.5 min after planar sentinel node mapping and 50.1 ± 15.6 min after SPECT/CT (15).

SPECT/CT in parathyroid imaging

At a first glance, SPECT/CT does not seem rational for superficially located structures, such as the thyroid or parathyroid. As the pathologically enlarged or hyperfunctioning parathyroid may still be of sub-centimetre diameter and will most likely be located in the direct vicinity of the thyroid its detection is challenging. Moreover, the lack of a tissue-specific tracer for the parathyroid hampers contrast between the parathyroids and the thyroid. Dual phase imaging using ^{99m}Tc -sestamibi or dual-isotope subtraction scintigraphy using a ^{99m}Tc -sestamibi or ^{99m}Tc -tetrofosmin combined with ^{123}I -NaI often results in the identification of the pathologically enlarged or hyperfunctioning parathyroid, but the reported sensitivity is still sub-optimal, varying from 56 to 91%, depending on patient selection, underlying pathology, size of the parathyroid gland and imaging protocol (16-18). The additional value of SPECT/CT is most prominent for precise localisation of the parathyroid gland, which has been proven to lead to a

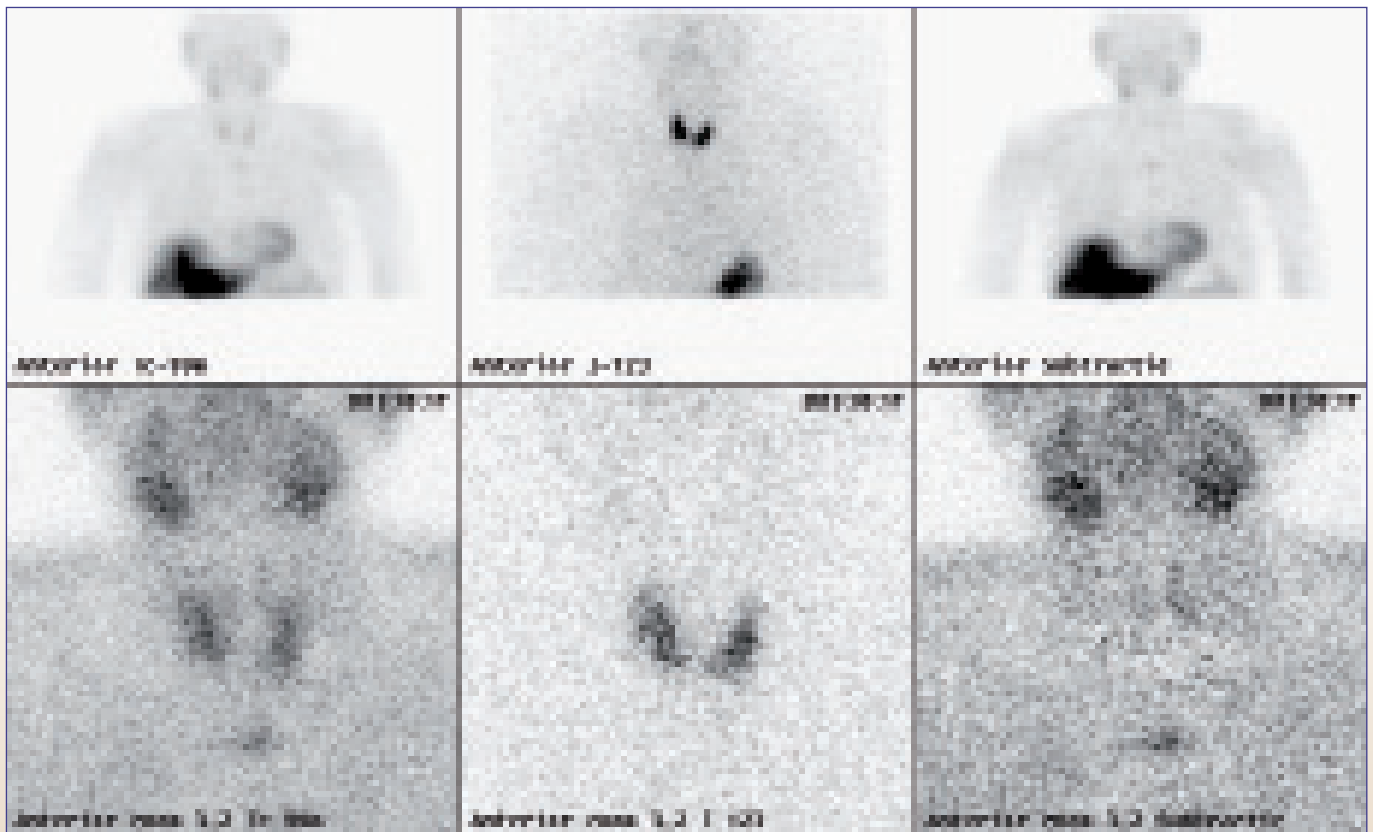


Figure 6a. Dual isotope, single acquisition planar scintigraphy. From left to right; ^{99m}Tc -tetrofosmin, ^{123}I -NaI, ^{99m}Tc - ^{123}I subtraction. Focal uptake of ^{99m}Tc -tetrofosmin, caudally from the thyroid.

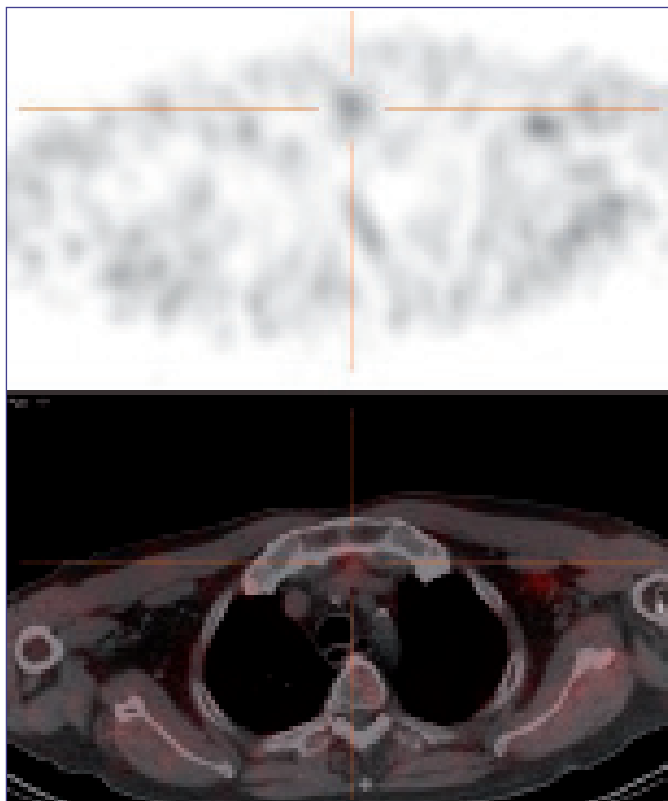


Figure 6b. Transverse SPECT/CT image at the level of the manubrium sterni. At the site of ^{99m}Tc -tetrofosmin accumulation, CT revealed a mass with a diameter < 1 cm compatible with ectopic parathyroid localisation.

reduction of operation time and costs (19). In our institution, we use dual isotope single acquisition planar subtraction imaging followed by dual isotope subtraction SPECT/CT, 3.5 hours after administration of ^{123}I -NaI and 15 minutes after administration of ^{99m}Tc -tetrofosmin. Figure 6 shows a 52-years old male patient with primary hyperparathyroidism. On planar imaging ectopic location of parathyroid tissue is already appreciated. SPECT/CT images revealed a small retrosternal mass correlating with tracer uptake. Although SPECT/CT did not add any new knowledge to the diagnosis, the visualisation of the morphologic substrate was extremely important for the surgeon as this localisation increases the operative risk significantly.

SPECT/CT and tumour imaging

Whole body tumour imaging using tissue specific SPECT radiopharmaceuticals is a very sensitive modality in cancer patients. Draw-backs of planar imaging are the limited sensitivity for the detection of small lesions, especially when located deeply in the body, and the lack of morphologic correlation. The use of SPECT/CT in these patients should be standard of care not only to optimise sensitivity, but also to correlate morphological aspects of the disease with the distribution of the tumour marker. In figure 7, planar ^{123}I -metaiodobenzylguanidine (MIBG) imaging of a 6-years old girl suspected for neuroblastoma

showed pathological accumulation of the radiopharmaceutical in the upper part of the right hemi-thorax extending caudally, all the way down to the liver/adrenal region. On SPECT/CT, one can not only appreciate that the tumour is restricted to the thorax, but also that the distribution of the radiopharmaceutical within the tumour mass is inhomogeneous. Both findings influenced the therapeutic options markedly. Due to the inhomogeneous distribution of ^{123}I -MIBG within the tumour, up-front treatment with ^{131}I -MIBG was withheld. The sole localisation in the thorax influenced surgical planning.

In figure 8 the results of ^{111}In -octreotide imaging of a 75-years old woman with a long history of a metastasised neuro-endocrine tumour of the small intestine (grade 2) is shown. As symptoms slowly aggravated, treatment with ^{177}Lu -labeled somatostatin analogues was considered. On previously performed CT- and MRI imaging multiple and slowly growing metastases were visualised. ^{111}In -octreotide SPECT/CT images show variable uptake of the tracer in the known liver lesions, toning down the expectations of ^{177}Lu -somatostatin analogue therapy. In the literature there is an abundance of studies reporting on the favourable effect of SPECT/CT on the identification of unexpected metastases, improvement of the localisation of tumour sites, and the effect of these findings on patient management (20-22).

SPECT/CT in cardiology

There is a lot of debate on the use of imaging in cardiology. In the abundance of imaging modalities available and the rapid technological developments, it becomes extremely difficult to obtain evidence based algorithms for the use of old and new imaging modalities before the technology tested becomes outdated (23). Myocardial perfusion imaging is by far the best established modality for the assessment of myocardial perfusion and therefore a valuable tool for the evaluation of patients with stable anginal complaints. Major drawbacks are the lack of absolute quantitative assessment of perfusion, limited specificity due to artefacts and lack of correlation with vessel morphology. Except for quantification, SPECT/CT overcomes or ameliorates these drawbacks.

Using fractional flow reserve as the gold standard, Schaap *et al* found significantly improved overall performance of hybrid imaging compared to SPECT or cardiac computed tomography angiography (CCTA) alone, with a sensitivity and specificity of 96% and 95%, respectively (24). However, one should realise that for the state-of-the-art CCTA at least a 64 slice MDCT is necessary and the population of patients for which hybrid imaging is essential needs to be further evaluated in large multi-centre studies. Moreover, direct comparison with other modalities measuring perfusion, such as magnetic resonance imaging (MRI), should be included in these studies.

SPECT/CT does it pay off?

Although the evidence of the clinical advantages of SPECT/CT is growing, costs of integrated SPECT/CT systems are relatively high due to the low degree of utilisation of the

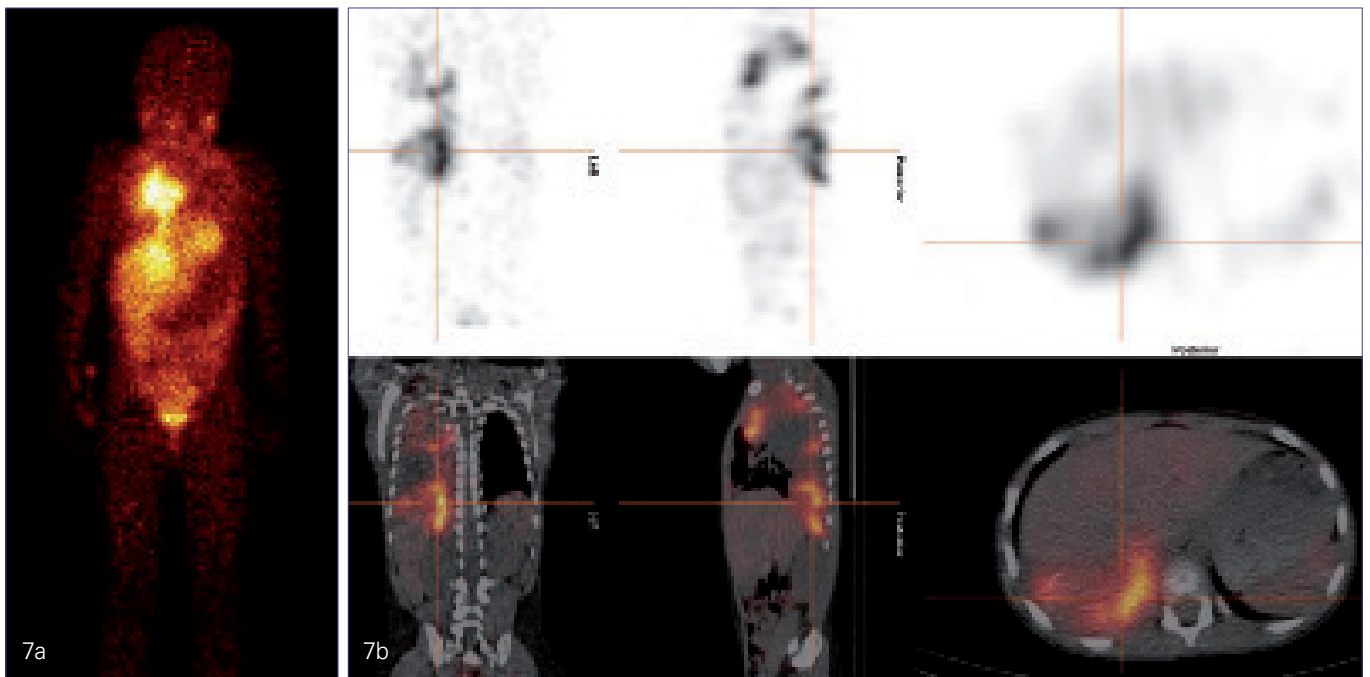


Figure 7a. Anterior ^{123}I -MIBG whole body imaging (24 h) of a 6-years old girl with a known mass in the upper part of the right hemi-thorax suspect for neuroblastoma. Abnormal ^{123}I -MIBG accumulation in the upper part of the right hemi-thorax with caudal extension to the level of the liver.

Figure 7b. Fused SPECT/CT images reveal a paravertabral mass, limited to the thorax with irregular distribution of ^{123}I -MIBG within the tumour.

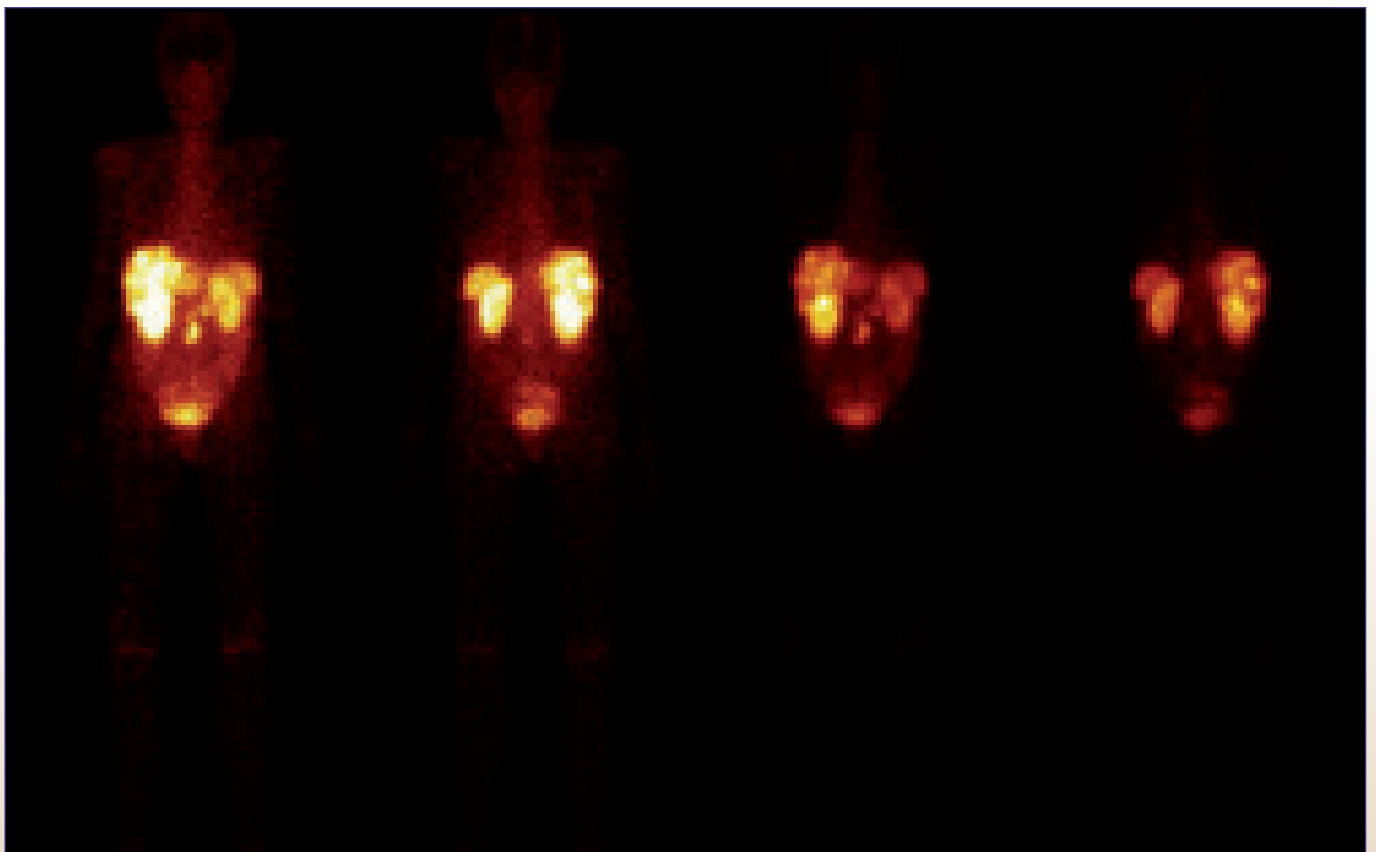


Figure 8a. Whole body ^{111}In -Octreotide scintigraphy, 24 h after injection, with multiple ^{111}In -Octreotide-avid lesions in the liver and in the umbilical region.

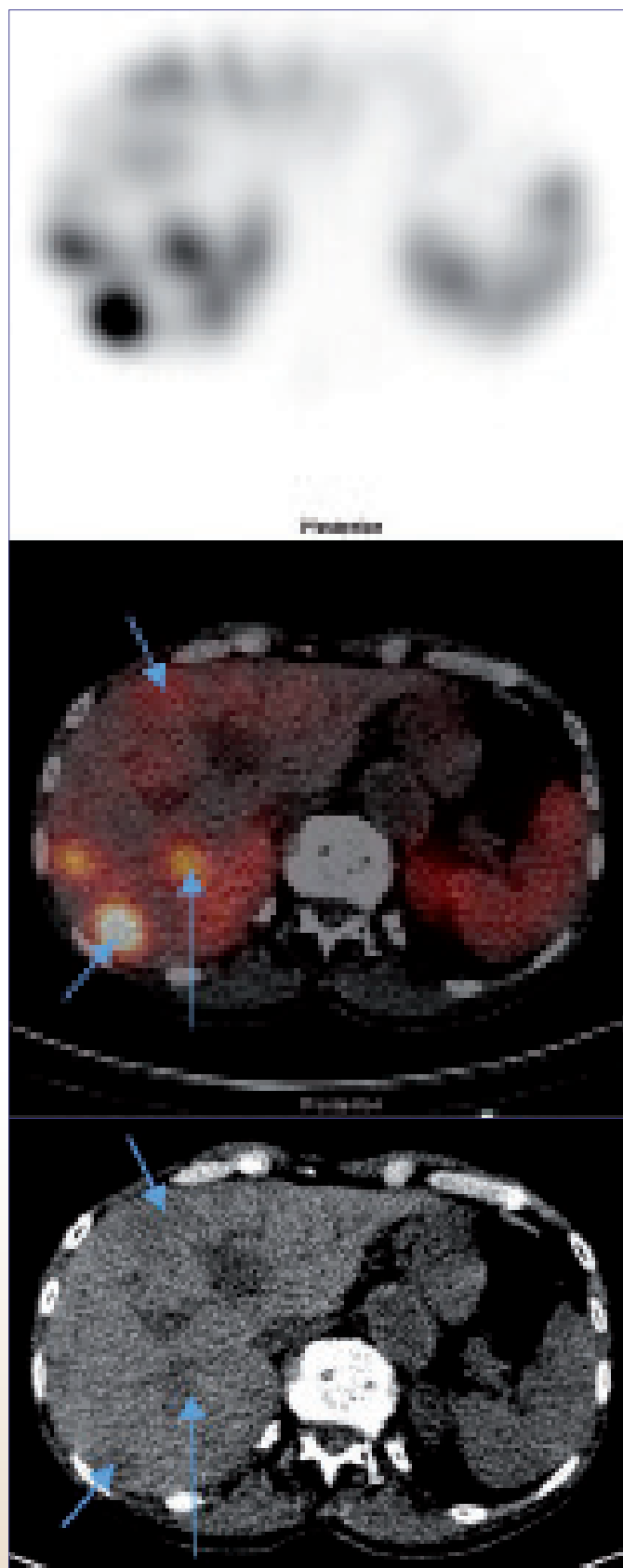


Figure 8b. On transversal images (SPECT, SPECT/CT and CT) at the level of the liver a highly variable uptake of ^{111}In -octreotide in liver metastases (arrows) is seen.

diagnostic capabilities of the CT in the SPECT/CT context. This raises questions about the cost-benefit of investing in high-end CT for SPECT/CT applications. Moreover, with the increasing availability of tracers, PET-CT as a 3D whole body imaging modality and advantageous image quality, takes over some of the best proven indications, increasing the costs of SPECT/CT per study (25,26). Nevertheless, at this moment the wide availability of SPECT/CT systems, the high number of different SPECT tracers and the existing evidence of cost-effectiveness or cost-benefit are in favour of the use of SPECT/CT in selected patient populations (19,27). To further establish the role of SPECT/CT the nuclear medicine community should provide more and prospectively collected evidence of the incremental value of SPECT/CT imaging in close cooperation with radiologists and relevant clinicians.

E-mail address for correspondence: b.l.vaneck-smit@amc.uva.nl

References:

1. Levin DN, Pelizzari CA, Chen GT, Chen CT, Cooper MD. Retrospective geometric correlation of MR, CT, and PET images. *Radiology*. 1988;169:817-23
2. Kaplan IL, Swayne LC. Composite SPECT/CT images: technique and potential applications in chest and abdominal imaging. *AM J Roentgenol*. 1989;152:865-66
3. Palmedo H, C. Marx, Ebert A, et al. Whole-body SPECT/CT for bone scintigraphy: diagnostic value and effect on patient management in oncological patients. *Eur J Nucl Med Mol Imaging*. 2013;40:2532-6
4. Hirschmann MT, Iranpur F, Konala P, et al. A novel standardised algorithm for evaluating patients with painful total knee arthroplasty using combined single photon emission computerised tomography and conventional computerised tomography. *Knee Surg Sports Traumatol Arthrosc*. 2010;18:939-44
5. Hirschmann MT, Mathis D, Rasch H, Amsler F, Friederich NF, Arnold MP. SPECT/CT tracer uptake is influenced by tunnel orientation and position of the femoral and tibial ACL graft insertion site. *International Orthopaedics (SICOT)*. 2013;37:301-9
6. Huellner MW, Strobel K. Clinical applications of SPECT/CT in imaging the extremities. *Eur J Nucl Med Mol Imaging*. 2013;40:2533-5
7. Singh VK, Javed S, Parthipun A, Sott AH. The diagnostic value of single photon-emission computed tomography bone scans combined with CT (SPECT/CT) in diseases of the foot and ankle. *Foot Ankle Surg*. 2013;19:80-3
8. Pagenstert GI, Barg A, Leumann AG, et al. SPECT/CT imaging in degenerative joint disease of the foot and ankle. *J Bone Joint Surg Br*. 2009;91:1191-6
9. van der Ploeg IMC, Valdés Olmos RA, Kroon BBR, Rutgers EJT, Nieweg OE. The hidden sentinel node and SPECT/CT in breast cancer patients. *Eur J Nucl Med Mol Imaging*. 2009;36:6-11
10. Lerman H, Lievshitz G, Zak O, Metser U, Schneebaum S, Even-Sapir E. Improved sentinel node identification by SPECT/CT in overweight patients with breast cancer. *J Nucl Med*. 2007;48:201-6
11. Fairbairn N, Munson C, Ali Khan Z, Butterworth M. The role

- of hybrid SPECT/CT for lymphatic mapping in patients with melanoma. *J Plast Reconstr Aesthet Surg.* 2013;66:1248-55
12. Stoffels I, Boy C, Pöppel T, et al. Association Between Sentinel Lymph Node Excision With or Without Preoperative SPECT/CT and Metastatic Node Detection and Disease-Free Survival in Melanoma. *JAMA.* 2012;308:1007-14
 13. Hassanzade M, Attaran M, Treglia G, Yousefi Z, Sadeghi R. Lymphatic mapping and sentinel node biopsy in squamous cell carcinoma of the vulva: systematic review and meta-analysis of the literature. *Gynecol Oncol.* 2013;130:237-45
 14. Kraft O, Havel M. Detection of Sentinel Lymph Nodes in Gynecologic Tumours by Planar Scintigraphy and SPECT/CT. *Mol Imaging Radionucl Ther.* 2012;21:47-55
 15. Hoogendam JP, Hobbelen MGG, Veldhuis WB, Verheijen RHM, van Diest PJ, Zweemer RP. Preoperative sentinel node mapping with ^{99m}Tc-nanocolloid SPECT-CT significantly reduces the intraoperative sentinel node retrieval time in robot assisted laparoscopic cervical cancer surgery. *Gynecol Oncol.* 2013;129:389-94
 16. Keane DF, Roberts G, Smith R, et al. Planar parathyroid localization scintigraphy: a comparison of subtraction and 1-, 2- and 3-h washout protocols. *Nucl Med Commun.* 2013;34:582-9
 17. Patel CN, Salahudeen HM, Lansdown M, Scarsbrook AF. Clinical utility of ultrasound and ^{99m}Tc sestamibi SPECT/CT for preoperative localization of parathyroid adenoma in patients with primary hyperparathyroidism. *Clin Radiol.* 2010;65:278-87
 18. Lavelly WC, Goetze S, Friedman KP, et al. Comparison of SPECT/CT, SPECT, and Planar Imaging with Single- and Dual-Phase ^{99m}Tc-Sestamibi Parathyroid Scintigraphy. *J Nucl Med.* 2007;48:1084-9
 19. Pata G, Casella C, Magri GC, et al. Financial and clinical implications of low-energy CT Combined with ^{99m}Technetium-Sestamibi SPECT for primary hyperparathyroidism. *Ann Surg Oncol.* 2011;18:2555-63
 20. Fukuoka M, Taki J, Mochizuki T, Kinuya S. Comparison of diagnostic value of I-123 MIBG and high-dose I-131 MIBG scintigraphy including incremental value of SPECT/CT over planar image in patients with malignant pheochromocytoma/paraganglioma and neuroblastoma. *Clin Nucl Med.* 2011;36:1-7
 21. Castaldi P, Rufini V, Treglia G, et al. Impact of ¹¹¹In-DTPA-octreotide SPECT/CT fusion images in the management of neuroendocrine tumours. *Radiol Med.* 2008;113:1056-67
 22. Wong KK, Cahill JM, Frey KA, Avram AM. Incremental value of ¹¹¹In pentetreotide SPECT/CT fusion imaging of neuroendocrine tumors. *Acad Radiol.* 2010;17:291-7
 23. Flotats A, Knuuti J, Gutberlet M, et al. Hybrid cardiac imaging: SPECT/CT and PET/CT. A joint position statement by the European Association of Nuclear Medicine (EANM), the European Society of Cardiac Radiology (ESCR) and the European Council of Nuclear Cardiology (ECNC). *Eur J Nucl Med Mol Imaging.* 2011;38:201-12
 24. Schaap J, Kauling RM, Boekholdt MS, et al. Incremental diagnostic accuracy of hybrid SPECT/CT coronary angiography in a population with an intermediate to high pre-test likelihood of coronary artery disease. *Eur Heart J Cardiovasc Imaging.* 2013;14:642-9
 25. Von Schulthess GK, Burger C. Integrating imaging modalities: what makes sense from a workflow perspective? *Eur J Nucl Med Mol Imaging.* 2010;37:980-90
 26. Hicks RJ, Hofman MS. Is there still a role for SPECT-CT in oncology in the PET-CT era? *Nat Rev Clin Oncol.* 2012;9:712-20
 27. Klode J, Poeppel T, Boy C, et al. Advantages of preoperative hybrid SPECT/CT in detection of sentinel lymph nodes in cutaneous head and neck malignancies. *J Eur Acad Dermatol Venereol.* 2011;25:1213-21 

Tijdschrift voor Nucleaire Geneeskunde
ISSN 1381-4842, nr. 4, december 2013
Uitgever



KLOOSTERHOF
ACQUISITIE SERVICES - UITGEVERIJ

Kloosterhof acquisitie services - uitgeverij
Napoleonsweg 128a
6086 AJ Neer
T 0475 59 71 51
F 0475 59 71 53
E info@kloosterhof.nl
I www.kloosterhof.nl

Hoofdredacteur

prof. dr. J. Booij
j.booij@amc.uva.nl

Redactie

mw. drs. B. Bosveld
mw. drs. F. Celik
dr. J. van Dalen
dr. E.M.W. van de Garde
drs. A.W.J.M. Glaudemans
mw. dr.C.J. Hoekstra
dr. P. Laverman
A. Reniers
dr. H.J. Verberne
dr. O. de Winter

Bureau redactie

Yvonne van Pol-Houben
T 0475 60 09 44
E nucleaire@kloosterhof.nl

Advertentie-exploitatie

Kloosterhof Neer B.V.
acquisitie services - uitgeverij
Eric Vullers
T 0475 597151
E eric@kloosterhof.nl

Vormgeving

Kloosterhof Vormgeving
Marie-José Verstappen
Sandra Geraedts

Abonnementen

Leden en donateurs van de aangesloten Leden en donateurs van de aangesloten beroepsverenigingen ontvangen het Tijdschrift voor Nucleaire Geneeskunde kosteloos. Voor anderen geldt een abonnementsprijs van € 45,00 per jaar; studenten betalen € 29,00 per jaar (incl. BTW en verzendkosten). Voor buitenlandse abonnementen gelden andere tarieven. Opgave en informatie over (buitenlandse) abonnementen en losse nummers (€ 13,50) bij Kloosterhof acquisitie services - uitgeverij, telefoon 0475 59 71 51. www.tijdschriftvoornucleairegeneeskunde.nl

Verschijningsdata, jaargang 35
Nummer 4: 24 december 2013

Verschijningsdata, jaargang 36
Nummer 1: 1 april 2014
Nummer 2: 1 juli 2014
Nummer 3: 30 september 2014
Nummer 4: 23 december 2014

Aanleveren kopij, jaargang 36
Nummer 1: 1 januari 2014
Nummer 2: 1 april 2014
Nummer 3: 1 juli 2014
Nummer 4: 1 oktober 2014

Aanleveren kopij, jaargang 37
Nummer 1: 1 januari 2015

Kloosterhof acquisitie services - uitgeverij

Het verlenen van toestemming tot publicatie in dit tijdschrift houdt in dat de auteur aan de uitgever onvoorwaardelijk de aanspraak overdraagt op de door derden verschuldigde vergoeding voor kopiëren, als bedoeld in Artikel 17, lid 2, der Auteurswet 1912 en in het KB van 20-7-1974 (stb. 351) en artikel 16b der Auteurswet 1912, teneinde deze te doen exploiteren door en overeenkomstig de Reglementen van de Stichting Reprorrecht te Hoofddorp, een en ander behoudend uitdrukkelijk voorbehoud van de kant van de auteur.

Cursus- en Congresagenda

2014

NKRV Workshop

17 January, 2014. Groningen, the Netherlands. www.nkrv.nl

TOPIM 2014 – ESMI Winter Conference

19 – 24 January, 2014. Les Houches, France. www.e-smi.eu

Oncologiedag “Kanker in Beeld / Imaging in Oncology”

5 February, 2014. Utrecht, the Netherlands. www.nvvoncologie.nl/

3rd Tübingen PET/MR Workshop

17 – 21 February, 2014. Tübingen, Germany. www.pet-mr-tuebingen.de

NuklearMedizin 2014

26 – 29 March, 2014. Hannover, Germany. www.eanm.org

Beyond FDG: International Symposium on PET Tracers in Oncology

3 - 4 April, 2014. Groningen, the Netherlands. symposiumngmb@umcg.nl

Symposium “Coronary Imaging”

11 April, 2014. Zwolle, the Netherlands.

NVKF-congres

18 - 19 April, 2014. Woudschoten, the Netherlands. www.nvkf.nl

voorjaarsbijeenkomst NVNG

23 May, 2014. Amersfoort, the Netherlands. www.nvng.nl

EMIM 2014 – European Molecular Imaging Meeting

4 – 6 June, 2014. Antwerp, Belgium. www.e-smi.eu

AVL symposium ‘Oncologie in perspectief’

5 June, 2014. Amsterdam, the Netherlands. www.avl.nl/oncologieinperspectief

SNMMI Annual Meeting

7– 11 June, 2014. St. Louis, Missouri, USA. www.snmmi.org/am2014

EANM’14 - 27th Annual Congress of the European Association of Nuclear Medicine

18 – 22 October, 2014. Gothenburg, Sweden. www.eanm.org

100th RSNA annual meeting,

30 November – 5 December, 2014. Chicago IL, USA. www.rsna.org

Adreswijzigingen

Regelmatig komt het voor dat wijzigingen in het bezorgadres voor het Tijdschrift voor Nucleaire Geneeskunde op de verkeerde plaats terecht komen. Adreswijzigingen moeten altijd aan de betreffende verenigingssecretariaten worden doorgegeven. Dus voor de medisch nucleair werkers bij de NVMBR, en voor de leden van de NVNG en het Belgisch Genootschap voor Nucleaire Geneeskunde aan hun respectievelijke secretariaten. De verenigingssecretariaten zorgen dan voor het doorgeven van de wijzigingen aan de Tijdschrift adresadministratie. Alleen adreswijzigingen van betaalde abonnementen moeten met ingang van 1 januari 2011 rechtstreeks aan de abonnementenadministratie van Kloosterhof Neer B.V. worden doorgegeven: Kloosterhof Neer B.V., t.a.v. administratie TvNG, Napoleonsweg 128a | 6086 AJ Neer of per E-mail: nucleaire@kloosterhof.nl

Oldelft Benelux Medical Solutions

Mediso AnyScan: de eerste klinische SPECT-CT-PET scanner...



...een unieke oplossing binnen de nucleaire geneeskunde.

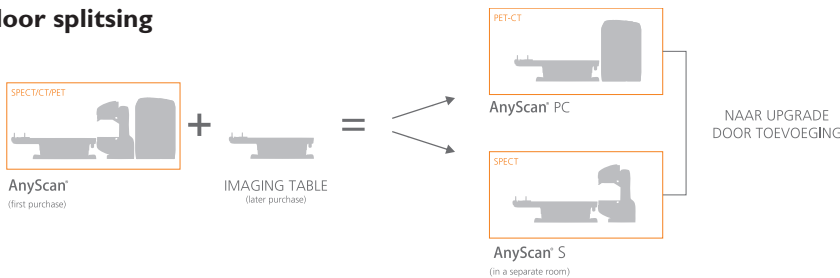
Basis configuraties



Upgrade door toevoeging



Upgrade door splitsing



Oldelft Benelux heeft reeds meer dan 80 jaar ervaring in de verkoop en service van diagnostische apparatuur en innovatieve healthcare ICT systemen. Zij heeft zich ontwikkeld van producent van apparatuur naar System Integrator en Service Provider voor ziekenhuizen en zorginstellingen.

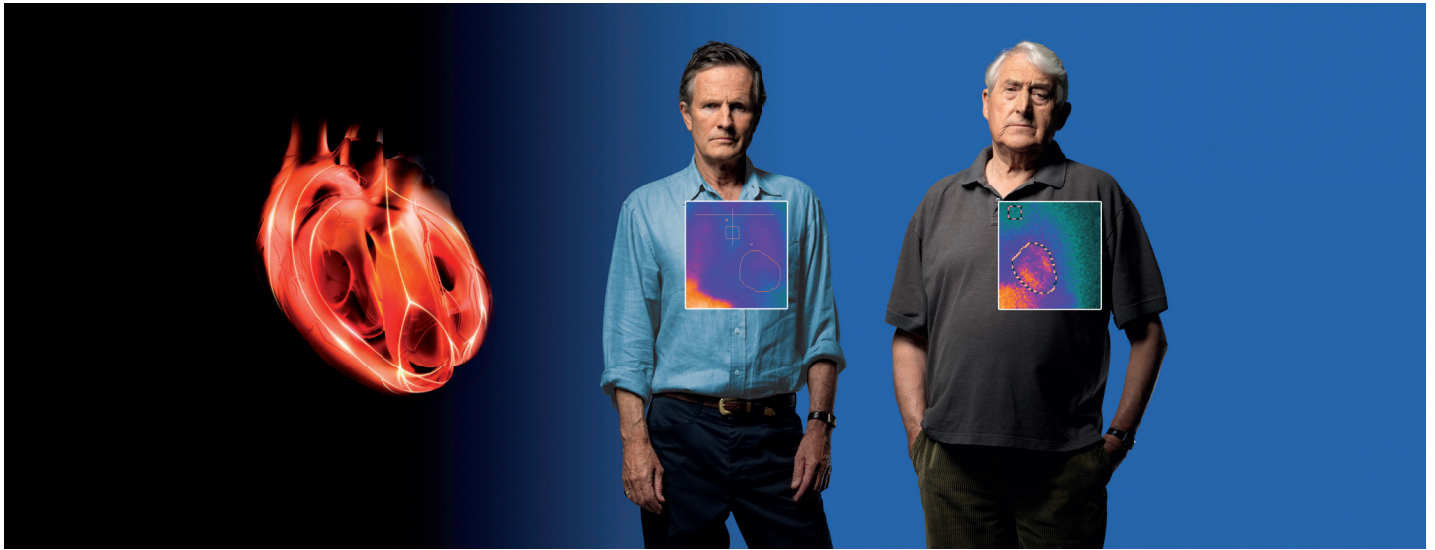
Met Mediso levert Oldelft Benelux het hele spectrum aan gamma camera's; van kleine enkelkops, tot geavanceerde SPECT-CT-PET combinaties.

Voor meer informatie omtrent de Mediso oplossingen kunt u contact opnemen met uw accountmanager; of stuur een e-mail naar info@oldelftbenelux.nl.



Oldelft Benelux B.V. Wiltonstraat 41 3905 KW Veenendaal The Netherlands
T +31 318 583 400 F +31 318 583 401 E info@oldelftbenelux.nl I www.oldelftbenelux.nl

Improving Heart Failure Risk Assessment



AdreView is a diagnostic agent providing a powerful prognostic insight into heart failure¹

- Assesses cardiac sympathetic innervation¹
- Helps predict patients who are at greater or lower risk of heart failure progression, arrhythmias & cardiac death¹
- Provides a Negative Predictive Value (NPV) of 96% for arrhythmia likelihood & an NPV of 98% for cardiac death likelihood over 2 years¹
- Provides superior prognostic information in combination with LVEF or BNP compared to LVEF or BNP alone¹
- Improves heart failure patients' risk assessment and may help clinicians' management decisions¹



GE imagination at work

AdreView™
Iobenguane I 123 Injection

AdreView is authorised for marketing in the following European countries: Germany, France, Spain, Italy, the United Kingdom, Denmark, Norway, The Netherlands and Belgium.

PRESCRIBING INFORMATION AdreView, Iobenguane [¹²³I] Injection 74 MBq/ml solution for injection

Please refer to full national Summary of Product Characteristics (SPC) before prescribing. Indications and approvals may vary in different countries. Further information available on request.

PRESENTATION Vials containing 74 MBq/ml [¹²³I]Iobenguane at calibration date and hour. Available pack size: 37 to 740 MBq. **DIAGNOSTIC INDICATIONS**

• Assessment of sympathetic innervation of the myocardium as a prognostic indicator of risk for progression of symptomatic heart failure, potentially fatal arrhythmic events, or cardiac death in patients with NYHA class II or class III heart failure and LV dysfunction. • Diagnostic scintigraphic localisation of tumours originating in tissue that embryologically stems from the neural crest. These are pheochromocytomas, paragangliomas, chemodectomas and ganglioneuromas. • Detection, staging and follow-up on therapy of neuroblastomas. • Evaluation of the uptake of Iobenguane. The sensitivity to diagnostic visualisation is different for the listed pathological entities. The sensitivity is approximately 90% for the detection of pheochromocytoma and neuroblastoma, 70% in case of carcinoid and only 35% in case of medullary thyroid carcinoma (MTC). • Functional studies of the adrenal medulla (hyperplasia).

DOSAGE AND METHOD OF ADMINISTRATION Cardiology: For adults the recommended dosage is 370MBq. Children under 6 months: 4 MBq per kg body weight (max. 40 MBq), the product must not be given to premature babies or neonates. Children between 6 months and 2 years: 4 MBq per kg body weight (min. 40 MBq). Children over 2 years: a fraction of the adult dosage should be chosen, dependent on body weight (see SPC for scheme). No special dosage scheme required for elderly patients. Oncology: For adults the recommended dosage is 80-200 MBq, higher activities may be justifiable. For children see cardiology. No special dosage scheme required for elderly patients. Administer dose by slow intravenous injection or infusion over several minutes. **CONTRAINDICATIONS** Hypersensitivity to the active substance or to any of the excipients. The product contains benzyl alcohol 10.4 mg/ml and must not be given to premature

babies or neonates **WARNINGS AND PRECAUTIONS** Drugs known or expected to reduce the Iobenguane(123-I) uptake should be stopped before administration of AdreView (usually 4 biological half-lives). At least 1 hour before the AdreView dose administer a thyroid blocking agent (Potassium Iodide Oral Solution or Lugol's Solution equivalent to 100 mg iodine or potassium perchlorate 400 mg). Ensure emergency cardiac and anti-hypertensive treatments are readily available. In theory, Iobenguane uptake in the chromaffin granules may induce a hypertensive crisis due to noradrenaline secretion; the likelihood of such an occurrence is believed to be extremely low. Consider assessing pulse and blood pressure before and shortly after AdreView administration and initiate appropriate anti-hypertensive treatment if needed. This medicinal product contains benzyl alcohol. Benzyl alcohol may cause toxic reactions and anaphylactoid reactions in infants and children up to 3 years old. **INTERACTIONS** Nifedipine (a Ca-channel blocker) is reported to prolong retention of Iobenguane. Decreased uptake was observed under therapeutic regimens involving the administration of antihypertensives that deplete norepinephrine stores or reuptake (reserpine, labetalol), calcium-channel blockers (diltiazem, nifedipine, verapamil), tricyclic antidepressives that inhibit norepinephrine transporter function (amitriptyline and derivatives, imipramine and derivatives), sympathomimetic agents (present in nasal decongestants, such as phenylephrine, ephedrine, pseudoephedrine or phenylpropranolamine), cocaine and phenothiazine. These drugs should be stopped before administration of [¹²³I]Iobenguane (usually for four biological half-lives to allow complete washout). **PREGNANCY AND LACTATION** Only imperative investigation should be carried out during pregnancy when likely benefit exceeds the risk to mother and foetus. Radionuclide procedures carried out on pregnant women also involve radiation doses to the foetus. Any woman who has missed a period should be assumed to be pregnant until proven otherwise. If uncertain, radiation exposure should be kept to the minimum needed for clinical information. Consider alternative techniques. If administration to a breast feeding woman is necessary, breast-feeding should be interrupted for three days and the expressed feeds discarded. Breast-feeding can be restarted when the level in the milk will not result in a radiation dose to a child greater than 1 mSv. **UNDESIRABLE EFFECTS** In rare cases the following undesirable effects have occurred: blushes, urticaria, nausea,

cold chills and other symptoms of anaphylactoid reactions. When the drug is administered too fast palpitations, dyspnoea, heat sensations, transient hypertension and abdominal cramps may occur during or immediately after administration. Within one hour these symptoms disappear. Exposure to ionising radiation is linked with cancer induction and a potential for development of hereditary defects. For diagnostic nuclear medicine investigations the current evidence suggests that these adverse effects will occur with low frequency because of the low radiation doses incurred. **DOSIMETRY** The effective dose equivalent resulting from an administered activity amount of 200 MBq is 2.6 mSv in adults. The effective dose equivalent resulting from an administered activity amount of 370 MBq is 4.8 mSv in adults. **OVERDOSE** The effect of an overdose of Iobenguane is due to the release of adrenaline. This effect is of short duration and requires supportive measures aimed at lowering the blood pressure. Prompt injection of phentolamine followed by propranolol is needed. Maintain a high urine flow to reduce the influence of radiation. **CLASSIFICATION FOR SUPPLY** Subject to medical prescription (POM). **MARKETING AUTHORISATION HOLDERS.** DE: GE Healthcare Buchler GmbH & Co. KG, 18974.00.00. DK: GE Healthcare B.V., DK R. 1013. FR: GE Healthcare SA, NL 18599. NL: GE Healthcare B.V., RVG 57689. NO: GE Healthcare B.V., MTrn. 94-191. **DATE OF REVISION OF TEXT** 9 August 2010.

GE Healthcare Limited, Amersham Place, Little Chalfont, Buckinghamshire, England HP7 9NA
www.gehealthcare.com

© 2010 General Electric Company – All rights reserved.
GE and GE Monogram are trademarks of General Electric Company.
GE Healthcare, a division of General Electric Company.

AdreView is a trademark of GE Healthcare Limited.

References: 1. Jacobson AF et al. Myocardial Iodine-123 Meta-Iodo-benzylguanidine Imaging and Cardiac Events in Heart Failure. Results of the Prospective ADMIRE-HF (AdreView Myocardial Imaging for Risk Evaluation in Heart Failure) Study. J Am Coll Cardiol 2010;55.